Title
END REGIONS IN THE STEADY STATE OF MIRROR-CONFINED PLASMAS

Author
Guillory, John U.

Publication Date
1971-02-01

UCRL-20615

END REGIONS IN THE STEADY STATE OF MIRROR-CONFINED PLASMAS

John U. Guillory, Jr.
(Ph. D. Thesis)

February 24, 1971

AEC Contract No. W-7405-eng-48

LAWRENCE RADIATION LABORATORY
UNIVERSITY of CALIFORNIA BERKELEY

UCRL-20615

DISCLAIMER

END REGIONS IN THE STEADY STATE OF MIRROR-CONFINED PLASMAS

Contents

END REGIONS IN THE STEADY STATE OF MIRROR-CONFINED PLASMAS

John U. Guillory, Jr.

Lawrence Radiation Laboratory
University of California
Berkeley, California 94720

February 24, 1971

ABSTRACT

Previous calculations of steady-state mirror confinement give no estimate of the density in the region between the mirror and the wall of the vacuum vessel. In this paper, realistic models for the ion and electron distribution functions in the confinement region are used to estimate the external density and external plasma potential. It is found that this density is usually sufficient for plasma in the external region (a fact of importance to instability studies). The external ion density due to losses from the confinement region depends on the scattering rate (Coulomb or other scattering) in a simple way, through the flux of escaping ions and the width of the "tail" of the ion distribution function. Because of their small mass, most of the electrons in the external region must usually be trapped in order to preserve quasi-neutrality; i.e., they must have turning points in the external region but stream through the confinement region as part of the confined electron distribution. This is brought about by a "shoulder" on the electrostatic potential profile; ϕ continues to decrease with distance outside the mirror. There is, in general, a plasma sheath at the vessel wall.

The external density may be enhanced by production of plasma near the walls or by electron emission from the walls, but two-stream instability sets in at some critical production rate (which is very low in the case of emitting walls). In the presence of such an "external" source, the plasma reaches a new steady state, which is described for the stable and the unstable case. As a corollary to the instability problem, it is shown that the plasma density cannot ordinarily increase outward from the mirrors. Finally, the hot-electron plasma is discussed, and it is shown that the availability of cold electrons outside the mirror "clamps" the potential there and neutralizes the slow escaping ions.

SYNOPSIS OF CHAPTER I

The usual "loss cone" in midplane velocity space is generalized to a "loss region" when ambipolar electrostatic potential is present. And in fact, with each spatial point $\underline{s}$ along a field line, there is associated a curve in midplane velocity space ($v_{\|0} \equiv x$, $v_{\perp 0} = y$) which is the locus of ions with turning points at $\underline{s}$, assuming collisionless dynamics. The electrons also have such a turning-point locus (different from that for ions) for each point $\underline{s}$. If there are no particles constrained away from the midplane, then in the collisionless approximation all the particles at $\underline{s}$ are represented in the midplane velocity distribution, and the particle density at $\underline{s}$ comes from those particles which have not been turned back toward the midplane at some smaller $\underline{s}$. The density $n(s)$ then is calculable by integrating over the region of midplane velocity space "outside" all the curves for points $\underline{s}'$ less than $\underline{s}$ [Eq. (5)]. We discuss these matters quantitatively in part B of this chapter. Exact and approximate loss boundaries for the device, as compared with turning-point loci for various turning points $\underline{s}$, may be seen in Figs 2 (p. 8) and B6 (p. 129). It is also instructive to look at the ion phase space (Fig. 7, p. 31).

In part C of this chapter we discuss how the midplane velocity distributions of ions, and the plasma potential, have been computed from Fokker-Planck equations by various authors in the limit of short bounce times; the ion and electron distributions go to zero at the boundaries of their respective loss regions in midplane velocity space. We show that with the simplifications made by these authors upon the loss boundaries and distribution functions, the density would be zero outside the mirrors ($s > L$) and vary as $(L - s)^3$ just inside the mirrors ($s < L$).

I. INTRODUCTION

A. General Remarks

Classical analyses of the steady state in mirror-confinement systems ignore the density of ions outside the mirrors,[1,2] and often treat the electron distribution as nearly Maxwellian (a Maxwellian distribution implies nonzero electron density outside the mirror).

The aim of this work is to estimate roughly the actual densities and potential drop in this external region. This information should be useful in the study of end effects on, e.g., flutelike and loss-cone-driven instabilities.

Studies of "line-tying" stabilization of flute instabilities[3-5] have shown the importance of the parameters of the electrical path connecting unstably growing regions of opposite polarity, through the end regions. If the end regions are reasonably short, conduction takes place through the end walls and their associated sheath boundary layer; two magnetic-field lines are "short circuited" together to the extent that the total external impedance is low. This impedance is very high and capacitive if a vacuum separates the plasma from the end walls, but can be fairly small (and sheath-dependent) if the intervening medium is a plasma, because of the high conductivity along the magnetic field lines.

Preliminary studies have also been made[6] on the coupling between unstable loss-cone modes and plasma waves in a magnetic mirror geometry (with zero plasma potential and no external plasma), and the general question of reflection or absorption of convectively unstable waves[7,8] at the ends of a plasma is an important one for the feasi-

bility of open ended fusion reactors.

In this paper, rather than attempting to solve exactly a well-defined problem of limited applicability, we attempt to give order-of-magnitude estimates and point out qualitative features without assuming any specific magnetic field shape, particle source mechanism, scattering mechanism, etc. It is still necessary to make fairly lengthy model calculations in order to get these results, but their approximate validity is wide. Results are expressed wherever possible in terms of experimentally measurable quantities, e.g., plasma potential and particle loss rates. It was felt that rough analytical formulas could be of wider utility than computer solutions for a few special cases. This paper is a first step in analyzing a large problem of rather amorphous scope, rather than a complete examination of a simpler soluble problem.

Nonrelativistic equations are used to describe the adiabatic motion of particles in a time-independent plasma which is nearly collisionless, i.e., the larger of the rates ν (loss rate, inverse of time required to diffuse in velocity to an untrapped state) and ν_0 (collision rate, inverse time for cumulative 90-deg scattering) must be slower than a typical bounce frequency (along the magnetic field, from turning point to opposite turning point). Bounce times of a few barely trapped (or barely untrapped) particles will be long, as is the period of a pendulum with nearly enough energy to rotate over the top, but these particles spend most of their bounce period very near the turning points, where scattering is usually negligible because of low density; so the spatially averaged ν need not be zero for validity of

wall itself grounded. Steady-state[9] particle-loss rates maintain the mirror-confined plasma at a positive potential, ϕ_0, at the midplane, decreasing to ϕ_L at $s = \pm L$ and ϕ_W at $s = \pm W^-$, a Debye length or so away from the wall. We call the magnetic field at $s = 0, L, W$ respectively B_0, B_L, B_W, and define the mirror ratios $R_L \equiv B_L/B_0$ and $R_W \equiv B_W/B_0$. Generalizing, we define $R_s \equiv B(s)/B_0$ for any s, and for convenience we write ϕ_s in place of $\phi(s)$.

2. Effect of Particle Drifts

We will examine properties of a relatively steady state plasma in this geometry. Because this steady state is established over a time long compared with typical bounce periods on the field line, we must say a few words about the effects of the slow drift of guiding centers across the field lines. As the guiding centers of the bouncing particles move across the field lines, they sweep out a "drift surface", which we will assume to be closed[10] in the sense of having finite area. As the guiding centers drift along this surface, they encounter, in general,

(a) different lengths L from the reference surface $s = 0$ to the maxima of B, and different lengths W to the walls outside,

(b) different mirror ratios at the maxima of B, and thus different criteria separating trapped orbits from untrapped ones, and

(c) different central densities and velocity distributions, and thus different scattering rates and loss fluxes due to plasma interactions.

If the "collision" or scattering times are long compared with drift times around the drift surface, one can see that the effective

mirror ratio for the drift surface, i.e., the one most effective in determining the boundary between trapped and untrapped orbits, is the smallest maximum of B on the surface; and the field lines in the neighborhood of this one on which B_{max} has its smallest value will play a dominant role in the ion loss. (Electron loss will be seen to be relatively insensitive to B except as ϕ may be determined by B.)

In the classical mirror device there is azimuthal symmetry: all field lines on a drift surface are identical and none of these difficulties is present. For simplicity, we do the analysis for this case, although small deviations from this symmetric geometry are within the scope of the theory[11] if we use the average values of L and W on the drift surface, but the minimum value of R_L. Likewise if the geometry is asymmetric in $\pm$ s, the smaller R_L is the one determining the loss boundary (trapping boundary) in phase space.

3. Subdivision of Midplane Velocity Space

For each point s along a field line, one can draw a curve in $\epsilon_\parallel$, $\epsilon_\perp$ space (midplane energy space) such that particles with $\epsilon_\parallel$, $\epsilon_\perp$ on the curve will have zero parallel velocity at the spatial point s (if they can get to s). This curve is just the line

$$\epsilon_\parallel = \epsilon_s(\epsilon_\perp) \equiv (R_s - 1)\epsilon_\perp - q(\phi_0 - \phi_s) \qquad (2)$$

in midplane energy space. If a particle at the midplane has

$$\epsilon_\parallel > \sup_{0<s'\leq s} \epsilon_{s'}(\epsilon_\perp),$$

(where Sup indicates the supremum, or maximum value), then in the

absence of collisions its turning point is beyond s. (This will be proved shortly.) Of course, for those particles with $U(s',\mu) = \mu B(s') + q\phi(s')$ monotonically increasing for $s' < s$, we have

$$\sup_{0<s'<s} \epsilon_{s'} \equiv \epsilon_s \quad .$$

We consider only $s > 0$ in what follows, since there is symmetry in s. If we assume $\phi(s)$ monotonically decreasing for all $s > 0$ (as indicated by the results of section C for $s > L$, and by previous studies[1,13] for $s < L$, then for the electrons $U(s,\mu)$ is always increasing when $0 < s < L$, but decreases for large μ and increases for small μ when $s > L$. Figure 1 shows $U(s,\mu)$ for the electrons. Figure 2 shows the lines $\epsilon_s(\epsilon_\perp)$ of the electrons, for $s \geq L$. The crossing of these lines reflects the fact that U decreases for large μ but is still increasing for small μ.

For the ions, $U(s,\mu)$ is monotonically decreasing for $s > L$, so that all ions passing $s = L$ are lost. Figure 3 shows $U(s,\mu)$ for the ions, and Fig. 4 shows the line $\epsilon_L(\epsilon_\perp)$ for the ions and the corresponding line $\epsilon_L(\epsilon_\perp)$ for the electrons. Because the ϵ's are energies at the midplane, $\epsilon_\perp \equiv \mu B_0$, so that the vertical axis of Figs. 2 and 4 is the magnetic moment invariant, except for a constant scale factor.

The maximum of $U(s,\mu) = \mu B(s) + q\phi(s)$ will be at some $s = M(\mu)$, different for ions and electrons. As $\mu \to \infty$, $M(\mu) \to L$, but $M(\mu) = L$ for all μ only if $d\phi/ds = 0$ at $s = L$ (where $dB/ds = 0$). If $d\phi/ds < 0$ at L, then $M(\mu) < L$ for the ions and $M(\mu) > L$ for the electrons. Below some critical μ_c there will usually be no maximum of U except

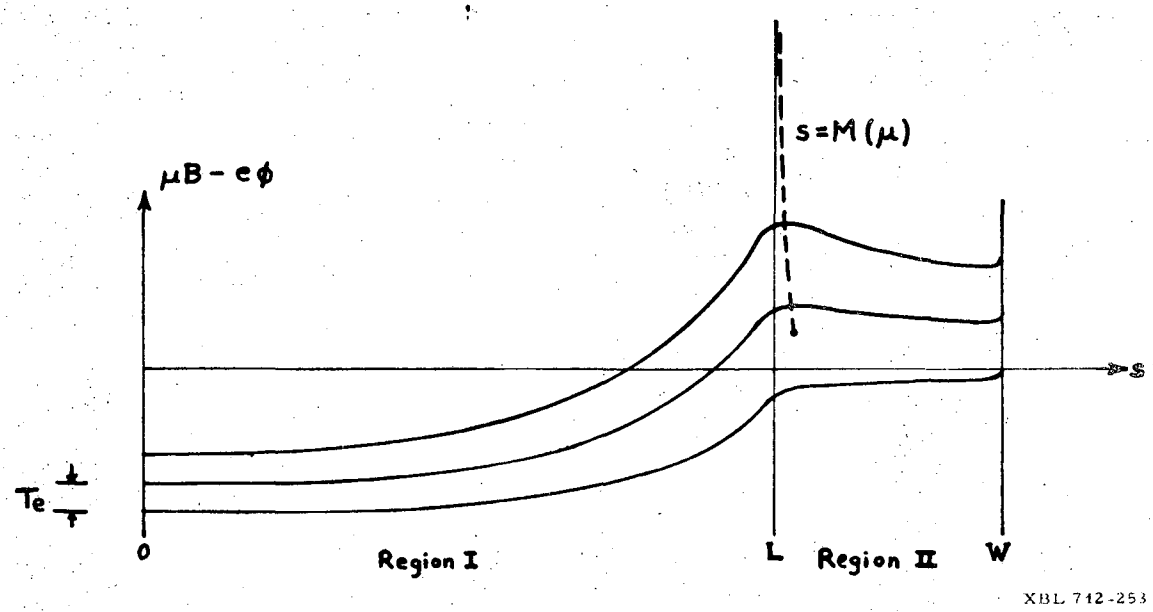

Fig. 1. Electron potential energy $\mu B(s) - e\phi(s)$ vs s, for $\mu B_0/T_e = 0, 1, 2$. Midplane is at $s = 0$, end wall at $s = W$.

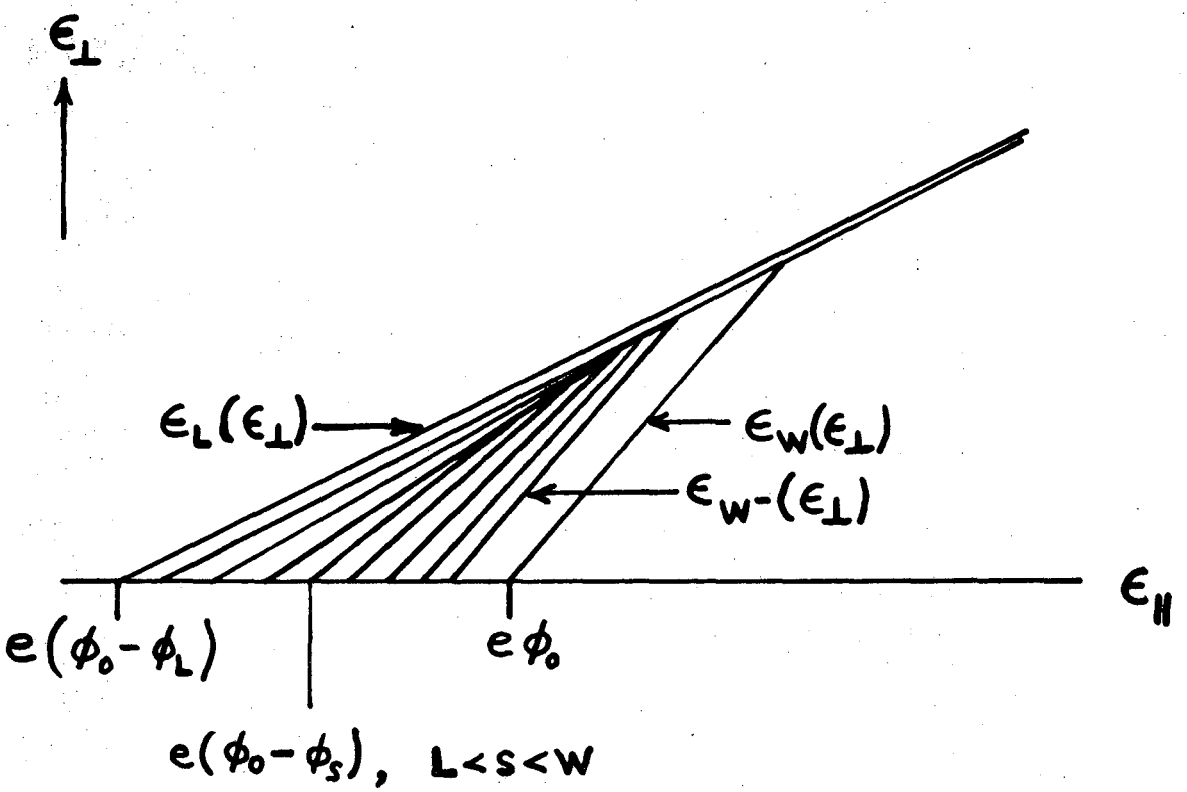

XBL 712-254

Fig. 2. The lines $\epsilon_\parallel = \epsilon_s(\epsilon_\perp)$ in midplane energy space, for various s, $L < s < W$. Electrons with $\epsilon_\parallel > \epsilon_s(\epsilon_\perp)$ have turning points beyond patial point s, if they can reach s. Electrons with midplane energies to the right of all these lines are lost from the device. Those with energies between $\epsilon_{W^-}(\epsilon_\perp)$ and $\epsilon_W(\epsilon_\perp)$ are reflected by sheath at the wall.

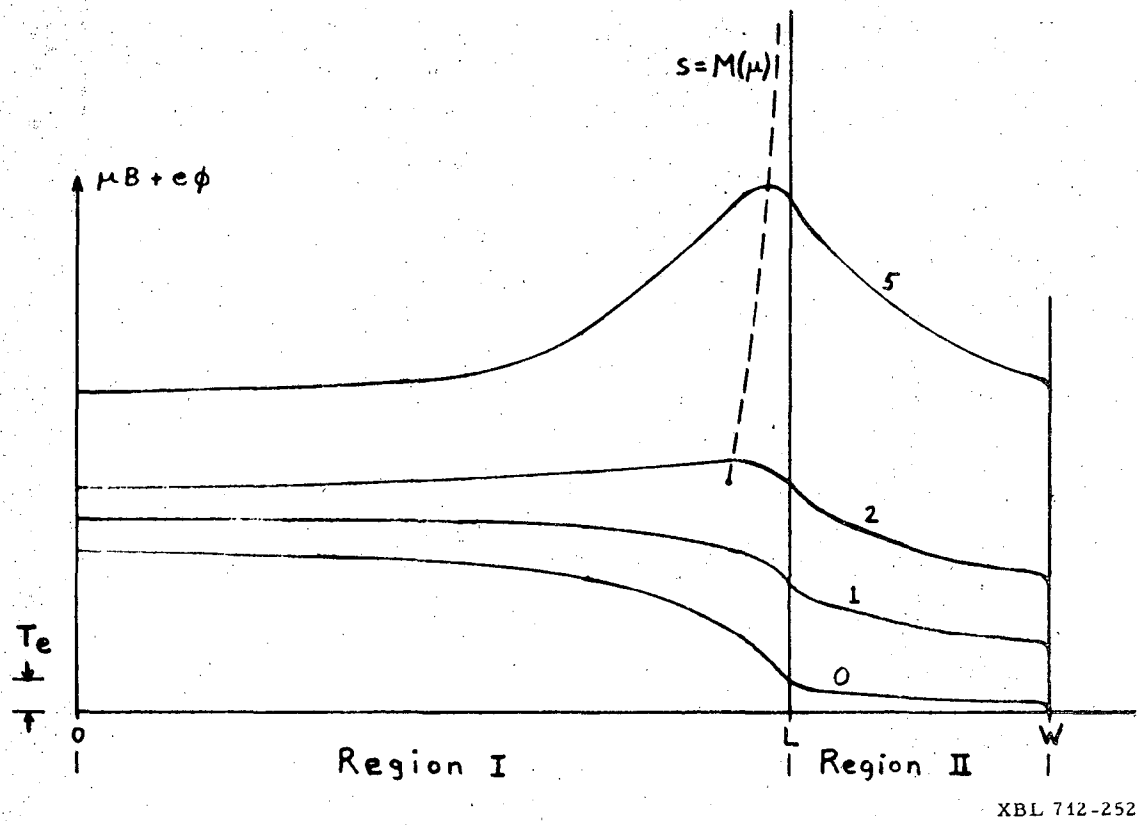

Fig. 3. Ion potential energy $\mu B(s) + e\phi(s)$ vs s, for $\mu B_0/T_e = 0, 1, 2, 5$.

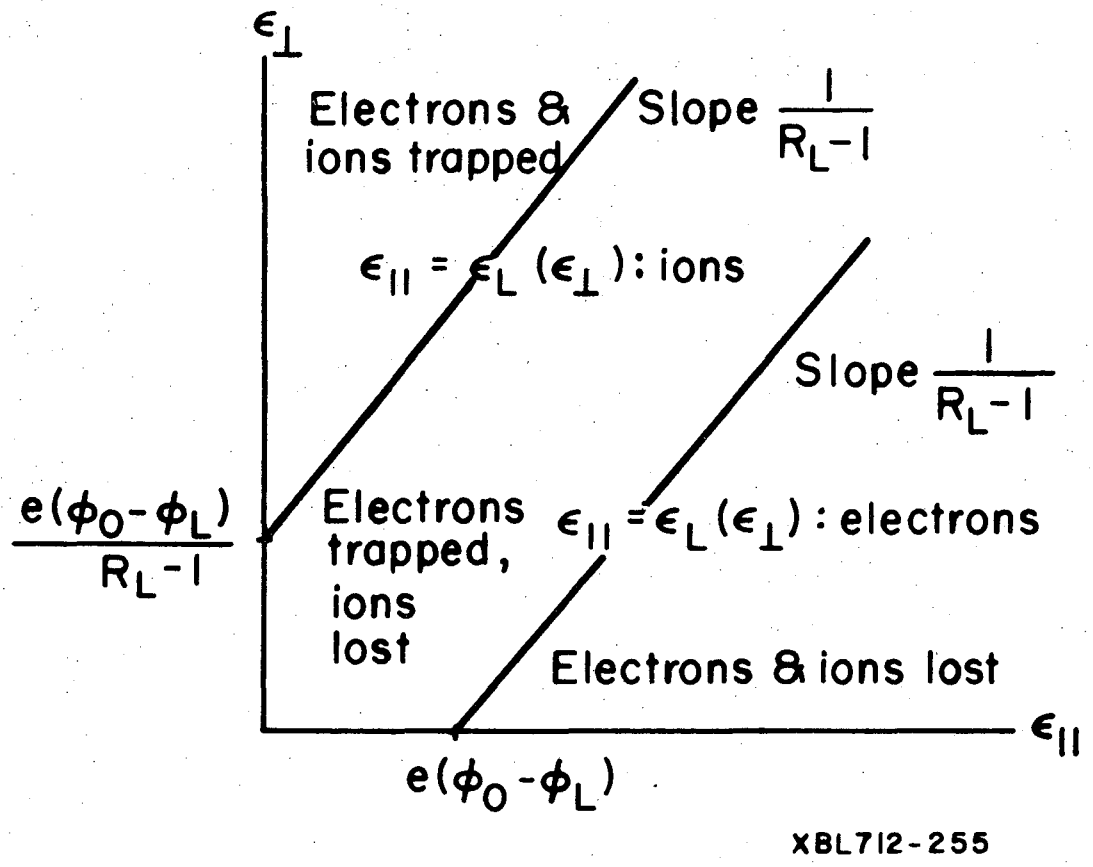

Fig. 4. Loss regions in midplane energy space for an isolated mirror-confined plasma.

at s = 0 (for the ions) or s = W (for electrons). The location or absence of $M(\mu)$ determines where and whether particles with this value of μ are trapped. If $|d\phi/ds|$ is reasonably small, $M \approx L$ for most trapped ions. If $\mu dB/ds < ed(-\phi)/ds$ for some s, μ where $s < M(\mu)$, some ions can be trapped locally, i.e., without passing through s = 0; but this case does not usually arise and we will ignore it. Particles with turning points beyond $s = M(\mu)$ are lost from the device. Hence the curve

$$\epsilon_{\|} = \epsilon_M(\epsilon_\perp) \equiv \left[R_M(\epsilon_\perp) - 1\right]\epsilon_\perp - q\left[\phi_0 - \phi_M(\epsilon_\perp)\right]$$

is called the (exact) loss boundary.

4. Density at s in Terms of Midplane Distribution

Now consider a collisionless plasma in the potential profile of Eq. (1). The total energy of a particle is conserved:

$$\frac{m}{2} v_{\|}^2 + \frac{m}{2} v_\perp^2 + q\phi_s = \text{const.} = \epsilon_{\|} + \epsilon_\perp + q\phi_0 \qquad (3)$$

($\epsilon_{\|}$ and $\epsilon_\perp$ will always refer to energies at the midplane); and μ is conserved:

$$\frac{m}{2} v_\perp^2 = \epsilon_\perp R_s. \qquad (4)$$

[Combining these and using the turning point criterion $v_{\|} = 0$ gives Eq. (2).] Let $f(s; v_{\|}, v_\perp)$ be the velocity distribution of one species at spatial point s (f is explicitly a function of $v_{\|}$ and $v_\perp$ only, but its parameters depend on s).

Assuming that all particles contributing to

$$n(s) = \int 2\pi v_\perp dv_\perp \int dv_\parallel f(s;v_\parallel,v_\perp)$$

include $s = 0$ in their orbits, we can use the Jacobian of the transformation in Eqs. (3) and (4) to transform the integration variables to midplane velocities

$$\frac{\partial(v_\parallel,v_\perp^2)_s}{\partial(v_\parallel,v_\perp^2)_0} = \frac{v_0 R_s}{\sqrt{v_{\parallel 0}^2 - x_s^2}},$$

where $x_s^2 = v_{\perp 0}^2(R_s - 1) - \frac{2q}{m}(\phi_0 - \phi_s) \equiv \frac{2}{m}\epsilon_s(\epsilon_\perp)$. We write the integration in terms of midplane velocities $x \equiv v_{\parallel 0}$ and $y \equiv v_{\perp 0}$:

$$n(s) = 2\pi R_s \int y dy \int \frac{x dx}{\sqrt{x^2 - x_s^2}} f(0;x,y), \tag{5}$$

where particles with turning points at $s' < s$ do not contribute and are excluded by restricting the region of integration to

$$|x| > \sup_{s'<s} x_{s'}(y).$$

C. Previous Analyses of Isolated Mirror-Confinement Systems With Evaluations of the Plasma Potential

1. Nature of the Plasma Potential

On the basis of single particle behavior, Eq. (1) with ϕ = constant[14] gives the familiar "loss cone" in midplane velocity space (or energy space). Since $d\phi/ds \equiv 0$, the maximum of $U(s,\mu)$ is at $s = L$ for all μ; particles with $\epsilon_\perp(R_L - 1) < \epsilon_\parallel$ have magnetic moment

too small to be confined, and they are lost in a transit time. The loss boundary, $\epsilon_{\|} = \epsilon_L(\epsilon_\perp) \equiv (R_L - 1)\epsilon_\perp$, is a cone in midplane velocity space.

But ordinarily we consider plasma densities, where quasi-neutrality must be ensured in the presence of scattering into the loss cone. The difference between electron and ion scattering rates leads to an ambipolar potential, ϕ, which balances electron and ion loss rates. Electrons scatter off electrons, ions, and neutrals, if any. Ions scatter off ions and neutrals, if any, and most ion-neutral encounters involve charge exchange. There is also some cooling of ions by electrons.[15] In the absence of neutrals, the scattering is assumed due to Coulomb encounters, and the ratio of electron scattering rate (for cumulative scattering through 90 deg) to the ion scattering rate is[16]

$$\left(\frac{m_i}{m_e}\right)^{1/2}\left(\frac{T_i}{T_e}\right)^{3/2}.$$

Hence unless $T_i/T_e < (m_e/m_i)^{1/3}$, the electron scattering rate is the larger one, and this leads to a positive ambipolar potential $\phi_0 - \phi_L$, which balances electron and ion loss rates by trapping low-μ electrons electrostatically.[17,18] The complications arising from collisions with neutrals are discussed elsewhere;[19] it suffices, for now, to say that for $T_i/T_e \gtrsim 1$, $\phi_0 - \phi_L$ is almost always positive. However, if almost all the ions are trapped for many transit times, one must have $e(\phi_0 - \phi_L) < (R_L - 1)T_\perp - T_{\|}/2$, where $T_{\|}$ and $T_\perp$ are the parallel and perpendicular ion temperatures in energy units. $T_{\|}/2$ is the mean parallel energy, $T_\perp$ is the mean perpendicular energy.

In this paper we use the term "isolated" to refer to a mirror-confined plasma whose density is zero outside the mirrors so that conditions there are irrelevant to the plasma contained inside. Usually this involves assuming that $U(s,\mu)$ has a maximum near $s = L$ for all μ representing trapped particles, and that all particles not trapped by this potential are lost from the system immediately. In the approximation that the maximum of U is <u>at</u> L, the loss boundaries for the system are just

$$\epsilon_{\parallel} = (R_L - 1)\epsilon_{\perp} + q(\phi_0 - \phi_L). \tag{6}$$

Thus the loss region in midplane velocity space is no longer a cone, but (in this approximation) a pair of hyperboloids,[11,13] one for electrons and one for ions, as shown in Fig. 5. This pair of boundaries is identical with the pair in Fig. 4, which is drawn in energy space.

2. <u>Survey of Fokker-Planck Calculations</u>

With the assumption of instant removal of untrapped particles (the limit of zero transit time), the steady-state distributions are zero in their respective loss regions. With these as boundary conditions, the distributions can be found, in principle, by solving simultaneous Fokker-Planck equations[20,21] for ions and electrons in $(s, v_{\parallel}, v_{\perp})$ phase space, with some appropriate source term for each species (or without, if a slow decay is allowed). If instability is also a scattering mechanism, the scattering terms are larger than for Coulomb interactions alone, but this makes no conceptual change in the process as long as the scattering rate remains very small compared to typical bounce frequencies.

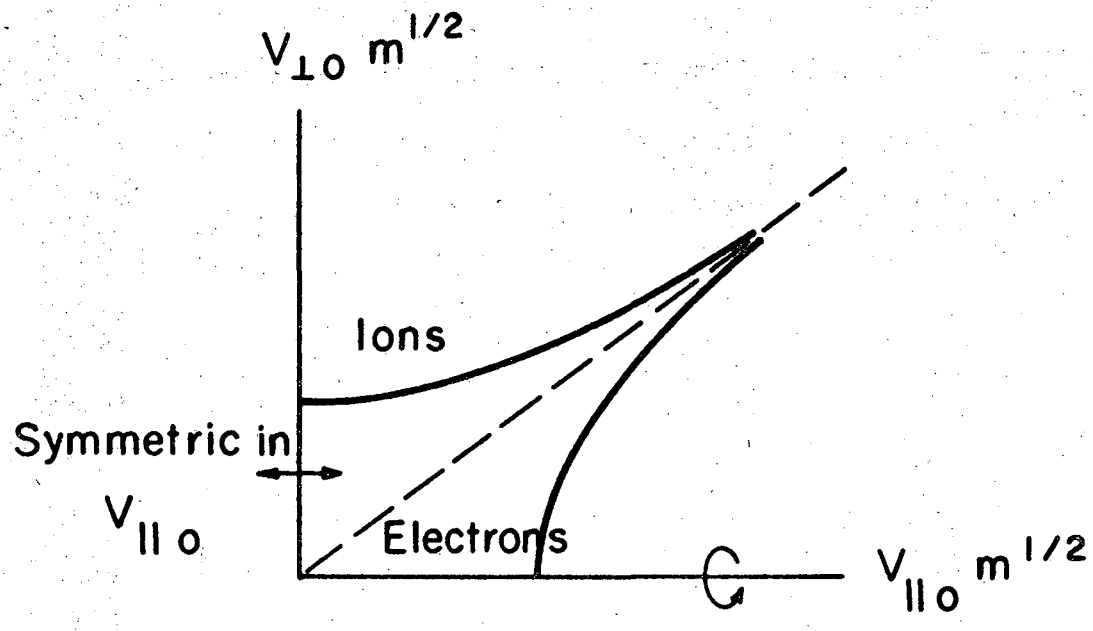

XBL697-3270

Fig. 5. Electron and ion loss boundaries in midplane velocity space when the plasma potential is nonzero.

Carrying out this calculation is difficult, and simplifying assumptions have always had to be made. (Note that the location of the boundaries depends on the solution of the problem.) We list some of these assumptions, roughly in order of increasing severity:

(a) In the calculation of ion scattering terms due to electrons, the electrons are assumed Maxwellian.

(b) In calculating $\phi_0 - \phi_L$, the loss region for the ions is taken to be a cone of altered slope

$$\epsilon_{\parallel} = (R_{eff} - 1)\epsilon_{\perp}$$

instead of Eq. (6). Here $R_{eff} \equiv R_L(1 + e\phi_0/T_i)^{-1}$, representing the loss cone angle for a particle with energy $\epsilon_{\parallel} + \epsilon_{\perp}$ just equal to T_i.[17] ϕ_L is taken identically zero, as the reference potential.

(c) The s-dependence of the problem is ignored because the decrease in scattering rate with $\underline{s}$ is more or less compensated by widening of the loss cone with $\underline{s}$. This is equivalent to assuming a square-well potential profile, hence constant density.

(d) The s-dependence can be calculated from the midplane velocity distribution using collisionless orbit theory.

(e) Given condition (c), the midplane ion distribution is separable in speed and pitch angle.

(f) Given condition (c), adequate information is obtained by solving a one-dimensional Fokker-Planck equation in energy alone. (The anisotropy in loss regions is translated into a loss factor in the scattering rate.)

(g) The ion-electron interaction is neglected.

(h) Ion and electron sources are assumed equal and processes involving neutrals are ignored.

(i) The plasma potential is ignored.

Several authors have used various of these assumptions in solving for loss rates, distribution functions, midplane potential, axial profiles, etc. We list those involving Fokker-Planck calculations, along with the assumptions contained in each (listed above). A "+" means the assumption is made; a "-" means it is not made. A "$\pm$" means both cases are treated, and a blank space means the assumption does not apply.

	a	b	c	d	e	f	g	h	i
Roberts et al.[22,23]			+		$\pm$	-	+	+	+
BenDaniel[1,24]	+	+	+	+	$\pm$	-	-	+	-
Fowler and Rankin[19,25]	+	+	+	+		+	-	-	-
Killeen and Futch[26]	+	+	+	+		+	-	-	-
Marx and Killeen[27,15]	+	-	$\pm$	-	-	-	-	+	-

In addition to the papers mentioned, Kaufman[17] and Persson[13] have done calculations of axial profiles of density and ϕ based on δ-fuction distributions in the collisionless limit, and Post,[28] Newcomb,[29] Grad,[30] Persson,[13] and others have discussed the nonlinear integral equations for $\phi(s)$ obtained from quasineutrality when assumption (d) holds. The Newcomb result is discussed in Appendix D.)

In the case where electron and ion sources (integrated over the trapping region) are assumed equal, $\phi_0 - \phi_L$ is found by equating approximate electron and ion loss rates.[17,1,26,13,15] Then in calcu-

lating the profile $\phi(s)$ from the quasineutrality condition one ignores the density of loss-component particles (on their way out) since they are assumed to exit "immediately" on being lost,[31] and also uses a better approximation to the true loss criterion. For example, BenDaniel calculates ϕ_0 using a single escape energy $e\phi_0$ for the electrons (purely electrostatic trapping) with the electron loss rate as calculated by Rosenbluth et al.[21] But in deriving ϕ_s, the electrons are assumed Maxwellian for $\epsilon_{\|} < \epsilon_{\perp}(R_L - 1) + e\phi_0$,[32] cut off abruptly at the loss boundary.

Only the Fowler and Rankin and Killeen and Futch papers treat more general sources, namely ionization events which create cold electrons (trapped) and cold ions (untrapped), as well as an energetic ion source.

3. The Zero of Density near the Mirrors

With the assumption of instant removal of untrapped particles (the limit of zero transit time), there are no particles outside the maxima of $U(s,\mu)$. Assuming that these are at $s = \pm L$, the density goes to zero there in a manner related to the behavior of the midplane velocity distributions near the loss boundary. With these assumptions and assumption (d), we have the following:

Theorem 1.

If the distribution in midplane velocities x,y goes to zero at the loss boundary $x = x_L(y^2)$ in such a way that

$$f(x,y) \propto (x_L^2 - x^2)^p, \quad \text{with integer } p > 0,$$

as $x \to x_L$ from below, then

$$n(s) \propto (L - s)^{2p+1} \qquad \text{as } s \to L \text{ from below,}$$

provided the maximum of $U(s,\mu)$ is a simple one:

$$U(L) - U(s) \propto (L - s)^2.$$

The proof is given in Appendix A. Typical steady-state Fokker-Planck calculations[17,1,26,13,15] give $p = 1$ (f has finite, nonzero slope at the loss boundary), so that $n(s) \propto (L - s)^3$.

SYNOPSIS OF CHAPTER II

The importance of several instability modes in mirror confinement depends on the axial profile of density, $n(s)$, near the ends of the plasma and particularly between the mirror and the end wall outside the mirror. We show in part A of this chapter that these end regions (collectively called region II) are usually plasma-like (i.e., have small enough Debye length) even if the coulomb scattering loss from the confinement region is the only source of the external particles. The density in region II can be estimated roughly in terms of the ion loss flux [see Eq. (10), p. 23], because the average ion streaming velocity is more or less a known function of position (from energy conservation). In this external region these ions, all of which are escaping, are neutralized by electrons, most of which cannot be escaping. This can only happen if the electrostatic potential decreases from the mirror to the wall.

The electron or ion density at a point in region II depends on the electron velocity distribution and the potential energy profile $U(s,\mu) = \mu B(s) + q\phi(s)$. If the "collision frequency" is small compared with the reciprocal transit time, the distribution in phase space can be generated approximately from $U(s,\mu)$ and the distribution in velocity at the midplane ($s = 0$), using collisionless orbit theory. [Recall Eq. (5) of Chapter I.] This is discussed in part B of this chapter; the discussion largely follows Persson.[13] These midplane velocity distributions are the solution of some complicated coupled Fokker-Planck equations and are non-Maxwellian over an important part of velocity space (the "loss region" or generalized loss cone), because of the rapid particle loss. For the purposes of this study, they can be modelled by analytic functions (which are not separable in energy and pitch angle). [See Eqs. (B16), p. 126, and (B8), p. 116, and Figs. B1, p. 114; and B3, p. 116, for ions; see Eq. (C1), p. 142, and Fig. 11, p. 47, for electrons.]

II. NONISOLATED MIRROR PLASMAS

A. Demonstration of External Plasma Conditions

1. Particle Loss Flux

In the study of instabilities in mirror plasmas, a topic of considerable interest is that of boundary conditions on the waves at the axial termination of the plasma. For the low frequency flute modes, one has the possibility of slowing or quenching the growth if the plasma is electrically connected along $\vec{B}$ to conducting walls.[33,34,3-5] For the Post-Rosenbluth loss-cone instability,[35] the reflection or damping of the axially convected waves depends on how n(s) falls off,[7,8] and hence on the behavior of the distribution functions near the loss boundaries.

For studies of this type, the "isolated" plasma approximation of section IC is inadequate; a further sophistication is necessary. In this section we show that in many cases of practical interest the streaming loss alone can give rise to a charged-particle density outside the mirrors that is generally large enough to require quasi-neutrality there. We also show that with equal ion and electron loss fluxes, the loss-component electrons alone cannot maintain the quasi-neutrality, and that the ambipolar $\phi(s)$ must continue to decrease out to the wall, with the result that some energetic electrons will have turning points well outside the mirrors and yet remain trapped. These electrons, which we denote by superscript ST (streaming outside the mirrors but still trapped) assist the loss-component electrons, denoted by superscript SF (streaming, free) in balancing the ion loss-component density. The region between mirrors (henceforth called

region I) is thus not isolated from the external region (region II: $s > L$).

We consider two qualitatively different types of loss mechanism in what follows. The first is a smooth diffusion in $\epsilon_\parallel$, $\epsilon_\perp$ due to many overlapping long-range encounters with charged particles (Coulomb scattering) or due to fluctuations and unstable waves. Guiding centers wander randomly but continuously in $\epsilon_\parallel$, $\epsilon_\perp$ (or equivalently, μ, H). Particles wander into the loss region only a small amount before their transit takes them out of the device, or at least out of the region where significant scattering occurs (particles with $\epsilon_\parallel$, $\epsilon_\perp$ very near the loss boundary $\epsilon_M(\epsilon_\perp)$ spend long times near their "turning points" at $s = M(\epsilon_\perp)$, but there is little chance for scattering while they are there.) The second loss mechanism is collisions with neutrals, which produces abrupt large changes in $\epsilon_\parallel$, $\epsilon_\perp$. We restrict our consideration here to loss by charge exchange, where a confined "hot" ion strikes a cold neutral and results in a fast neutral and a cold, untrapped ion. For statistical purposes, this process "moves" ions discontinuously in velocity space. Ions being lost by charge exchange do not spend long times near the mirrors since their $\mu \approx 0$, but they do spend rather long times in the interior of region I because their parallel velocities at birth are small. They are eventually accelerated out by $d\phi/ds$, but they may contribute an appreciable ion density n_0^{cx} at the midplane.

If diffusion takes place only in region I then the streaming ion flux is independent of s in region II except for the "area factor" $B(s)/B_L$:

$$F_i(s) = \int_0^L \frac{B(s)}{B(s_1)} \left(\frac{dn}{dt}\right)_{loss} (s_1)ds_1 \qquad \text{for } s > L. \tag{7}$$

If ν is the inverse loss time of a typical ion by the smooth diffusion mechanism,[36] then from Eq. (7)

$$F_i(s) \sim R_s L n_0^H \nu \qquad \text{for } s > L, \tag{8}$$

where n_0^H refers only to the hot (contained) ions. $n_0^H + n_0^{cx} = n_0$. (Since $F_i(W)$ is measurable, $F_i(W) = R_W L n_0^H \nu$ may be taken to define ν, or $F_i(W) = R_W \bar{L} n_0^H \nu$ may be taken to define an effective length $\bar{L}$. We adopt the first convention in all that follows.) We will occasionally denote as the "scattering parameter" the ratio

$$\frac{L\nu}{c_{i\|}} \equiv \frac{F_i(W)}{R_W n_0^H c_{i\|}}, \tag{9}$$

with $c_{i\|} \equiv (2T_\|/m_i)^{1/2}$ and $T_\|$ the parallel "temperature" of ions at the midplane. It is the ratio of a typical transit time $L/c_{i\|}$ to the loss time ν^{-1}. It is thus the smallness parameter for all of our analysis.

In the case of energy-preserving scattering, several authors[19,26] have expressed ν crudely as $\nu = \Pi\nu_0$, where ν_0 is the cumulative 90 deg scattering rate and Π is the probability of loss given 90 deg scattering, i.e., approximately the ratio of solid angle subtended by the loss region (at a given speed) to the total solid angle.

The formulation $\nu = \Pi\nu_0$ with $\Pi \leq 1$ is reasonable for large mirror ratios when particle sources are far from the loss boundary, but it is inadequate for small $R_L - 1$, where $\nu \to c_\|/L$ while ν_0 remains finite.

In this case an effective ν can be calculated only by solving the pitch-angle diffusion equation with the given sources. It is also true that ions with $\epsilon_\perp \approx e(\phi_0 - \phi_L)/(R_L - 1)$ will be lost significantly due to cooling by the electrons.[15] With sources neglected, and a simple random walk in pitch angle only, it can be shown that $(1 - \nu L/c_\parallel)^{-1}\nu/\nu_0 \sim (R_L - 1)^{-1}$ when $R_L - 1$ is small.

2. Minimum External Density and Maximum Debye Length

Consider the density, in region II, of ions lost by the smooth diffusion mechanism. B(s) decreases with s in region II and μB is the dominant force for these ions. (The potential $\phi(s)$ probably also decreases.) Ions are thus accelerated out from $s \approx L$, gaining parallel energy

$$\frac{1}{2} m_i v_\parallel^2 = \epsilon_\perp(R_L - R_W) + e(\phi_L - \phi_W)$$

by the time they reach $s = W^-$ (they creep over the barrier at $s \approx L$ with negligible $v_\parallel$). Let $T_\perp^{Loss}$ by a typical value for $\epsilon_\perp$ among these ions. Then

$$n_i(W) \approx \frac{F_i(W)}{v_\parallel} \approx \left[\frac{T_\perp^{Loss}(R_L - R_W) + e(\phi_L - \phi_W)}{T_\parallel}\right]^{+1/2} R_W \frac{L\nu}{c_{i\parallel}} n_0. \tag{10}$$

The value of T^{Loss} depends on the mirror ratio as well as $T_\parallel$ and $T_\perp$; for $R_L - 1 \ll 1$, $T_\perp^{Loss} \approx T_\perp \gg T_\parallel$; but for $R_L - 1 \gg 1$, $T_\perp^{Loss} \sim (R_L - 1)^{-1}\left[e(\phi_0 - \phi_L) + T_\parallel\right]$, as a look at Fig. 6 indicates (the ensemble over which $\epsilon_\perp$ is being averaged lies very nearly on the loss boundary).

If charge exchange is important and if it occurs with a rate ν_{cx}

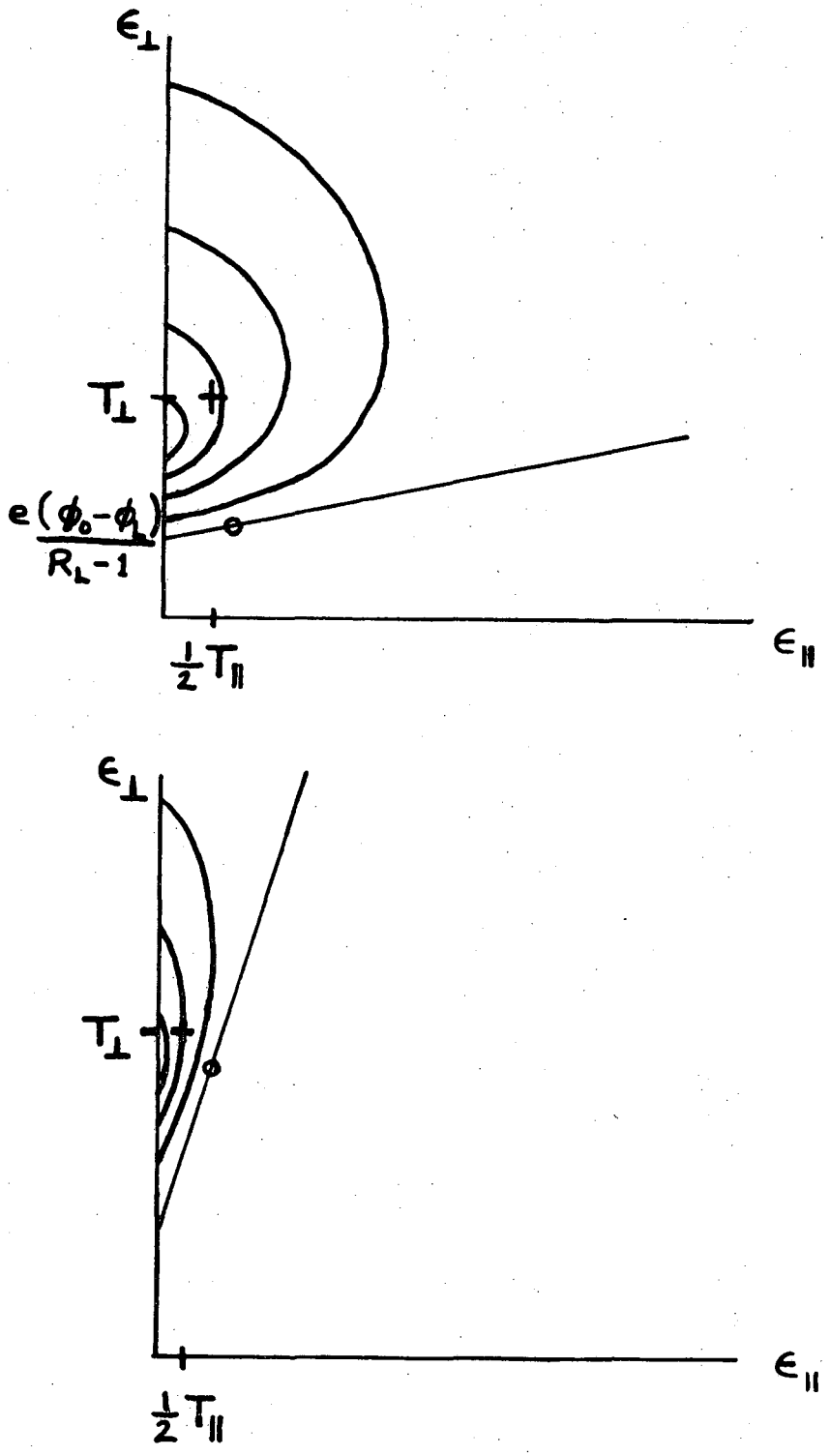

XBL 712-256

Fig. 6. Midplane energy space for ions. Contours of ion distribution for large mirror ratio (top) and small mirror ratio (bottom). Energy of typical loss-component ion (small circle) and typical trapped ion (cross).

and mostly in the central region where $\phi \approx \phi_0$, then the resulting cold ions are accelerated out of the plasma by $d\phi/ds$; they produce an additional density in region II, which comes to

$$n_i^{cx}(W) \approx \left[2e(\phi_0 - \phi_W)/m_i\right]^{-1/2} R_W L \nu_{cx} n_0^H \qquad (11)$$

at s = W. The quantity $R_W L \nu_{cx} n_0^H$ is just the charge exchange loss flux at s = W. (Both Eqs. (10) and (11) apply at other points s in region II if W is replaced by s everywhere in the equations and if s is not too near the mirror, where Eq. (10) is improper.)

When both loss mechanisms are important, the ion density in region II is just the sum of Eqs. (10) and (11). These ions, whose density cannot be matched by SF electrons, as we will show, cause a large positive potential and attract electrons (from region I if there are no others available) until quasineutrality is established, provided that the resulting Debye length is smaller than the size of the external region. We have

$$\underset{L<s<W}{\text{Max}} \; \lambda_D(s) = \text{Max} \left[\frac{T_e^{EXT}(s)}{4\pi e^2 n_i(s)}\right]^{1/2},$$

where we have assumed $n_e \sim n_i$ and written $T_e^{EXT}(s)$ for the local mean electron temperature at s. In the absence of any externally supplied electrons, we expect this temperature to be less than or at most equal to the midplane temperature T_e. Using this fact and Eqs. (10) and (11), we have

$$\max_{L<s<W} \lambda_D(s) < \left(\frac{T_e}{4\pi e^2 n_0}\right)^{1/2} Q^{-1/2} \left(\frac{R_W L \nu}{c_{i\|}}\right)^{-1/2} \tag{12}$$

with

$$Q \equiv \left\{ \left[\frac{T_\perp^{\text{Loss}}(R_L - R_W) + e(\phi_L - \phi_W)}{T_\|} \right]^{-1/2} + \frac{\nu_{cx}}{\nu} \left[\frac{e(\phi_0 - \phi_W)}{T_\|} \right]^{-1/2} \right\} \frac{n_0^H}{n_0} .$$

For $\nu_{cx}/\nu \ll 1$, we have $n_0^{cx} \ll n_0$ and

$$Q^{-1/2} \approx \left[\frac{T_\perp^{\text{Loss}}(R_L - R_W) + e(\phi_L - \phi_W)}{T_\|} \right]^{1/4}, \tag{13}$$

which is a maximum if we assume $T_\perp^{\text{Loss}} \sim T_\perp$. If $R_L - R_W \sim 1$ and the electron temperature $T_e \ll T_\perp$, we have

$$Q^{-1/2} < \left[\frac{T_\perp}{T_\|} (R_L - R_W) \right]^{1/4},$$

since $e(\phi_L - \phi_W)$ cannot be much greater than T_e. Now certainly $\nu \gtrsim 1/2\ \nu_{90\ \text{deg}}$ for $R_L - 1 \sim 1$ (the actual coefficient depends on R_L, going to 0 for $R_L \to \infty$ and to ∞ for $R_L \to 1$), where

$$\nu_{90\ \text{deg}}\ (\text{sec}^{-1}) \sim 0.7 \times 10^{-7} \frac{n_0 \ln \Lambda}{A^{1/2} T^{3/2}}\ (n \text{ in cm}^{-3},\ T \text{ in eV}) \tag{14}$$

is the usual cumulative 90-deg Coulomb scattering rate for particles of mass A (amu).[16] Though f_i is not Maxwellian we assume Eq. (14) holds within a factor of 2 or so, and use $T^{3/2} = (T_\| T_\perp^2)^{1/2}$. If instability is the dominant loss mechanism, then we expect ν to be much larger than this Coulomb estimate.

Using these Coulomb scattering losses alone, consider two examples, both with $R_L = 3$, $R_W = 2$, A = 1 amu, L = 100 cm, and $T_\perp \gg T_e$:

(1) for $n_0 = 10^{10}$ cm^{-3}, $T_e = 10$ eV, $T_\parallel = 10$ eV, $T_\perp = 100$ eV:

$$\left.\begin{aligned} \lambda_D(0) &= 0.02 \text{ cm} \\ Q^{-1/2} &< 1.8 \\ \frac{L\nu}{c_{i\parallel}} &= 3.3 \times 10^{-4} \end{aligned}\right\} \lambda_D(W) < 1.5 \text{ cm}$$

(2) for $n_0 = 10^{13}$ cm^{-3}, $T_e = 100$ eV, $T_\parallel = 1$ keV, $T_\perp = 10$ keV:

$$\left.\begin{aligned} \lambda_D(0) &= 2.3 \times 10^{-3} \text{ cm} \\ Q^{-1/2} &< 1.8 \\ \frac{L\nu}{c_{i\parallel}} &= 0.4 \times 10^{-4} \end{aligned}\right\} \lambda_D(W) < 0.5 \text{ cm}.$$

In general this upper bound on $\lambda_D(W)$ scales as

$$L^{-1/2} n_0^{-1} T_\parallel^{1/4} T_\perp^{3/4} T_e^{1/2} (\ln \Lambda)^{-1/2}$$

when the loss is dominated by ion-ion collisions (i.e., minimal loss).

When charge exchange losses are dominant,

$$Q^{-1/2} \left(\frac{R_W L\nu}{c_{i\parallel}}\right)^{-1/2} \approx \left[\frac{e(\phi_0 - \phi_L)}{T_\parallel}\right]^{1/4} \left(\frac{n_0^H R_W L \nu_{cx}}{n_0 c_{i\parallel}}\right)^{-1/2}.$$

Consider a low density, high temperature system, with $R_L = 3$, $R_W \sim 2$, and $L = 10^3$ cm:

(3) for $n_0 \sim n_0^H = 10^8$ cm^{-3}, $T_e = 100$ eV, $T_\parallel = 1$ keV, $T_\perp = 300$ keV, and $\nu_{cx} = 0.2$ sec^{-1}:

$$\left.\begin{aligned} \lambda_D(0) &= 0.74 \text{ cm} \\ \left[\frac{e(\phi_0 - \phi_L)}{T_\parallel}\right]^{1/4} &\lesssim 0.8 \\ \frac{L\nu_{c\ell}}{c_{i\parallel}} &= 4.5 \times 10^{-6} \end{aligned}\right\} \lambda_D(W) \lesssim 200 \text{ cm.}$$

In the absence of rapid instability losses, the loss-component particles in this example probably do not constitute a plasma in region II.

By these examples we have verified the intuitive scaling based on $n_W/n_0 \sim R_W(L\nu/c_{i\parallel})$; i.e.,

$$\lambda_D(W)/\lambda_D(0) \lesssim (R_W L\nu/c_{i\parallel})^{-1/2}, \tag{15}$$

where ν is the total ion loss rate. We have also shown that for relatively high densities and not-too-large temperatures, the scattering loss alone usually gives rise to an external plasma in region II.

3. Electrons in Class "ST"

Since electron and ion fluxes must be equal, however,[37] the density of streaming SF electrons at s = W is

$$n_e^{SF}(W) \sim \frac{F_i(W)}{v_{e\parallel}} \sim n_0 \left[\frac{T_e(R_L - R_W) - e(\phi_L - \phi_W)}{(m_e/m_i)T_\parallel}\right]^{-1/2} \left(\frac{R_W L\nu}{c_{i\parallel}}\right),$$

where ν, $T_\parallel$, and $c_{i\parallel}$ still refer to the ions. One sees from this that unless $e(\phi_L - \phi_W)/T_e \approx R_L - R_W$ the streaming electron density n_e^{SF} is insufficient for charge neutrality at s = W, and similarly at s not too near L. But if $e(\phi_L - \phi_W)/T_e \approx R_L - R_W \sim 1$, many of the electrons

at $s \geq L$ would be in class ST, not in SF as assumed.

4. Physical Significance of External Parallel Electric Field

Because of the small factor $(m_e/m_i)^{1/2}$ in the equation for $n_e^{SF}(W)$, we must either have $n_e^{ST}(W^-) \gg n_e^{SF}(W^-)$, or $e(\phi_L - \phi_W)/T_e \sim R_L - R_W$, or both. The latter alternative means an outward electric field of order $T_e|dR/ds|$, i.e.,

$$\frac{ed\phi}{dB} \sim \frac{T_e}{B_0}$$

in the outer portion of region II. (In Appendix D we shall derive the same result by other dimensional methods. Such an electric field is always present when magnetic (or other)[38] forces accelerate one species (say, with lower mass) more than the other. The magnitude of the electric field is such as to make the acceleration of a typical electron equal that (primarily magnetic acceleration) of a typical SF ion. This is done by increasing the number of electrostatically decelerated electrons. The same situation should occur in plasma rocket nozzles where the magnetic field expands, although we find no explicit mention of this in the literature.

B. Model for Estimating the External Density

1. Collisional and Collisionless Particle-Following

When there is no scattering, the density at any point s is related to the outer portion of the midplane velocity distribution by Eq. (5), assuming there are no sources with $\epsilon > \epsilon_s$ between 0 and s. This reflects the fact that the velocity distribution $f(s;v_\parallel,v_\perp)$ is the image of $f(0;x,y)$ under the mapping of Eqs. (2) and (3) and under the condi-

tion (on the normalization) that the spatial density of guiding centers in the image of $2\pi ydydx$ increases proportional to B as the field lines converge. This mapping we call V since the corresponding phase space density in canonical variables is governed by the Vlasov equation in s and $v_{\|}$. Consider, for example, the ion phase space cross section, at some fixed μ for which there is an x-type singular point $s = M(\mu)$ near $s = L$. The separatrix (see Fig. 7) is the phase-space loss boundary, and at $s = 0$ it is just $x = x_M(y)$, the midplane loss boundary. ($y^2 \propto \mu B_0$.) The orbits are deterministic, as the Vlasov equation is linear. Thus if $f(0;x,y) = 0$ for $|x| \geq x_L(y)$ then the density is zero beyond $s = L$. The same is true with L replaced by $M(\mu)$.

When the orbits are not collisionless, the problem of the density of particles escaping over a potential barrier is not trivial. The case with a velocity-independent barrier where the diffusion coefficient D is velocity- and space-independent, and where the dynamic friction is just $(Dm/T)v$, i.e.,

$$v \frac{\partial f}{\partial s} + \Omega^2(s - L) \frac{\partial f}{\partial v} = \frac{\partial}{\partial v}\left(\frac{Dm}{T} vf\right) + D \frac{\partial^2 f}{\partial v^2}$$

(with Ω^2 some constant and T the constant temperature) was treated by Chandrasekhar,[39] with the additional requirement that the reference or midplane distribution (i.e., the boundary condition, f at s_0) be Maxwellian (rather than truncated or damped by rapid transit time of the escaping particles). The difficulty of generalizing this situation analytically to the ion escape problem has let us to seek simpler

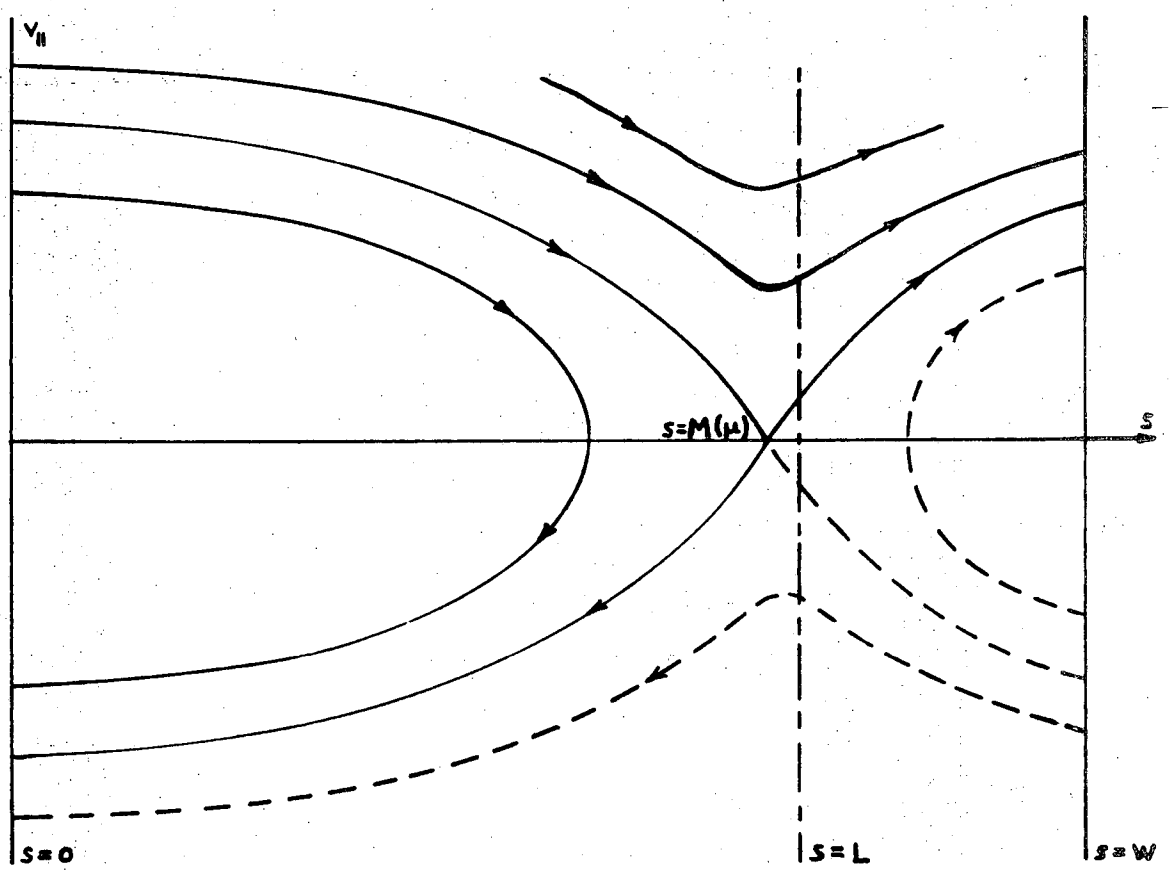

XBL 712-257

Fig. 7. Ion phase space for typical given μ. Unpopulated orbits shown dashed. Dot-dash line is where B is largest.

if more ad hoc techniques.

We look thus for a model by which we can estimate $n(s)$ for $s \geq L$ due to scattering (etc.), without really changing the Vlasov equations to the badly coupled pair of Fokker-Planck equations (parabolic, non-deterministic) including the detailed scattering mechanism. We need only a crude estimate of the density $n(s)$, not the detailed shape of f at $s > L$; so it is hoped that Fokker-Planck solutions can be circumvented.

To this end, notice that in the presence of slight scattering, $f(s;v_{\|},v_{\perp})$ is not mapped by V back onto part of $f(0;x,y)$ but onto some function $g(0;x,y|s)$ which differs noticeably from f near the escape boundary. Those particles which have scattered into the loss region during their transit from 0 to s, are mapped by V onto that part of midplane velocity space s,y outside the loss boundary. This definition of g is equivalent to defining x and y (for a particle at s) to be the values of $v_{\|}$ and $v_{\perp}$ that the particle would have if it returned (under time reversal) to $s = 0$ without undoing the scattering. The definitions of x,y in terms of μ and H are the same ($\frac{m}{2}x^2 = \epsilon_{\|} = H - \mu B_0 - q\phi_0$, $\frac{m}{2}y^2 = \epsilon_{\perp} = \mu B_0$, so that x,y is equivalent to H,μ except for asymmetries in x), but now μ,H are stochastic functions whose expectation value in general depends on s. But if scattering can be neglected in the low-density region II and at the singular points $M(\mu)$ (in region I but near $s = L$), the dependence of g on s there is negligible. For this case we abbreviate $g(0;x,y|s) = g(x,y)$.

How does $g(x,y)$ compare with the exact, observable $f(0;x,y)$? Consider a typical ion near the separatrix. Starting from $s \approx -L$,

where it must certainly be trapped in order to have $v_{\|} > 0$, it wanders typically outside the separatrix during its transit to s = 0, and continues to do so during transit to $s \approx +L$, where it is lost. If the ion loss boundary in phase space is treated as a source of these ions, the width of the diffusing tail in velocity varies roughly as the square root of time, starting with the particles near s = -L, where the diffuse tail is freshly "scraped off" by loss of ions that were previously outside the separatrix. Thus by symmetry, the spread of g(x,y) outside $x_L(y)$ is about $\sqrt{2}$ times the spread of f(0;x,y) outside $x_L(y)$. At the singular point, the loss-component particles are scraped off (see Fig. 7), i.e., not reflected; Since there are no returning particles for s > M, $g(x,y) \equiv 0$ for $x < -x_M(y)$. g is thus not symmetric in x, although f is.

Another consequence of this "scraping off" at $s = M(\mu)$ is that the density for this given μ abruptly decreases at $s = M(\mu)$. Integrating over μ to get the total density, we conclude that the ion density must fall off more rapidly than in the collisionless case for s just inside L, but it falls off to a nonzero value at s = L. To preserve quasineutrality, the electron density must fall of similarly. Since electrons have no singular point inside s = L, this requires a drop in potential just inboard of the mirrors. This phenomenon is not dependent on any model assumptions except that scattering be zero at the singular point. (Particles near the separatrix spend long times near the singular point, as in the case of the inverted pendulum.)

The diffusion just discussed could be stated as a diffusion in μ

and the action, $J = m\oint v_{\|} ds$, but the assumption of well-defined J in the canonical equations breaks down for the loss component particles, and $\partial/\partial J$ becomes somewhat undesirable at the separatrix, even when J is redefined so as to change continuously across it.

We use ordinary velocity space coordinates and velocity distributions because of their widespread usage and direct physical interpretation. (For example, the physical significance of $\partial f(\mu,J)/\partial\mu$ at constant J is not as obvious as that of $\partial f(v_{\|},v_{\perp})/\partial v_{\perp}$.) In addition, we deal with nonsymmetric distributions in $v_{\|}$ (e.g., SF particles in region II) so that $v_{\|}$ is more appropriate than $\epsilon_{\|}$ or H.

Since ordinarily one avoids having sources in the loss region of phase space, we ignore their contribution to the external density. If such sources are present between s = 0 and s = L, they may be taken to be at -s instead of s, so that they are counted in the fictitious midplane distribution g. Cold ions from charge exchange are in this class, but are treated separately in what follows.

2. Smallness of Spatial Diffusion Effects

Spatial diffusion due to radial density gradients makes only a small contribution to the effective ν and the amount, $\Delta(x^2)$ or $\Delta(y^2)$, which an ion diffuses in parallel or perpendicular energy in a transit time. Because the step size for cross-field spatial diffusion is of order a_i (the ion gyroradius), the spatial diffusion coefficient is of order $\nu_0 a_i^2$ while the velocity diffusion coefficient is $\nu_0 c_i^2$. The spatial contribution to the spread $\Delta(x^2)$ in velocity-squared near the loss boundary is then of order

$$\Delta(x^2) \sim \left(\frac{2L\nu_0}{c_{\|}^3}\right)^{1/2} \left[y^2 \frac{dR}{dr} + \frac{2e}{m_i} \frac{d(\phi_0 - \phi_L)}{dr} \right] a_i$$

[and similarly for $\Delta(y^2)$ with an additional factor of $(R_L - 1)^{-1}$]. We have simply used the equation for the approximate ion loss boundary in terms of R_L and $\phi_0 - \phi_L$, which vary with "radius" (i.e., flux surface). The factor involving $\nu_0^{1/2}$ is just the normal velocity spreading in a transit time (see, for example, part 3 of Appendix B), and these corrections are thus of order a_i/r_p, where r_p is the scale length over which R_L and ϕ change radially; typically r_p is of order of the plasma radius.

SYNOPSIS OF CHAPTER III

The principal results of this study of external plasma are given in this chapter, in the order: ions (A), electrons (B), and potential (C). We begin by showing that the conceptually simple model of having all the escaping ions come from the loss boundary in velocity space is inadequate because it gives infinite density near the mirror; instead, ions must populate a finite fringe of the loss region. On p. 38, theorem 2 relates the density $n(L)$ at $s = L$ to the loss flux $F(L)$ and the fringe width ("tail" width) $1/\kappa$ of the distribution function. Then $1/\kappa$ is estimated from the collision rate. From this one has estimates of the density at $s = L$ proportional to (loss rate/typical ion bounce frequency)$^{3/4}$ [see Eq. (18)]. Continuity and energy conservation then give the ion density at $s \gtrsim L$ [Eq. (20)] in terms of the local magnetic field ratio R_s and the potentials ϕ_s and ϕ_L. The additional density contributed by charge exchange is given in Eq. (21), p. 41.

The electron density at a point s in region II depends mainly on the potential energy $U(s,\mu)$ at s (locally), which involves R_s and ϕ_s. The density is given at $s = L$ by Eq. (23) (see Figs. 12 and 13) and at the sheath edge near $s = W$ by Eqs. (26) and (27).

Equating $n_i(s)$ (a function of R_s and ϕ_s, etc.) with $n_e(s)$ (a function of R_s and ϕ_s, etc.) would of course give ϕ_s as a function of R_s (etc.). This is computed in Appendix F (see Fig. F1, p. 177). The procedure gives fairly simple analytic estimates at $s = L$ [Eq. (31) if $R_L - R_W \sim 1$, or Eq. (32) if $R_L - R_W \ll 1$] and at $s = W^-$ [Eq. (36) or (37), p. 57]. This latter is the magnitude of the potential fall across the sheath. Typical values are given on p. 58, and their scaling with ν explicitly and through φ_0 is discussed on p. 60.

III. RESULTS OF MODEL CALCULATIONS OF EXTERNAL DENSITY AND POTENTIAL

A. Ion Density Outside the Mirrors

1. Ions Near the Loss Boundary

As discussed in the preceding section, we seek to describe $n_i^{SF}(s)$ for $s \geq L$ by following the collisionless dynamics of a set of particles placed just outside the midplane loss boundary, adjusting this set to reproduce a specified loss flux. Since real diffusing ions are removed as they wander past the loss boundary, the simplest model would seem to be to place all the escaping ions exactly on the escape boundary. This, however, would lead to $n_i^{SF}(s)$ having an infinity at $s \approx L$ (which would physically be rounded off by diffusion due to fluctuations there). We demonstrate this singularity as follows: Since at $s = M(\mu)$ the potential energy is a maximum, particles on the escape boundary will have $v_{\|} = 0$ at $s = M(\mu)$; and at some s a short distance away,

$$\frac{m}{2} v_{\|}^2 = - d^2U(s,\mu)/ds^2\big|_{M(\mu)} \times \frac{1}{2} \left[s - M(\mu)\right]^2,$$

for all μ for which $s = M(\mu)$ is a smooth local maximum, i.e.,

$$-\infty < d^2U/ds^2\big|_{M(\mu)} < 0.$$

Now if $g(x,y) = \delta(x - x_M^+)f_y(y)$, where x_M^+ is on or just outside the exact loss boundary $x_M(y)$, then

$$n(s) \propto R_s \int 2\pi y dy \int_{x_M(y)}^{\infty} dx \frac{\delta(x - x_M^+)f_y(y)}{\sqrt{x^2 - x_s^2(y)}} = R_s \int \frac{2\pi y dy f_y(y)}{\sqrt{x_M^2(y) - x_s^2(y)}} .$$

But $x_M^2(y) - x_s^2(y)$ is just $v_\parallel^2$ at s. So with

$$h(y) \quad \left[- \frac{d^2U\left[s,\mu(y)\right]}{ds^2}\bigg|_{M\left[\mu(y)\right]} \right]^{1/2}$$

where $\mu(y) \equiv my^2/2B_0$, we have

$$\int_{L-\Delta}^{L+\Delta} n(s)ds \propto \int \frac{2\pi y dy f_y(y)}{h(h)} \int_{L-\Delta}^{L+\Delta} \frac{ds}{|s - M\left[\mu(y)\right]|} .$$

The s integration on the right hand side diverges logarithmically. When $\Delta > |L - M(\mu)|$ for more than zero measure in $\mu(y)$ on which $f_y(y) \neq 0$, the double integral diverges as a consequence. Then since there are an infinite number of particles between $L \pm \Delta$ and $L + \Delta$, the density is infinite somewhere in this interval.

Yet if small-angle scattering predominates, with only slight scattering during a single bounce period, then (x,y) for an escaping ion cannot be too far from $x = x_L(y)$. Physically, then, a small loss rate can produce fairly large densities near $s = L$ as particles creep over the potential barrier, creating a "traffic jam" there.

Since the simplest model is inadequate, we take $g(x,y) = g_0(x,y) + g_1(x,y)$, where g_0 would be $f(0;x,y)$ in the limit of zero transit time; g_1 includes a "tail" for $x > 0$ and $y \sim y_L(x)$ sufficient to give the observed loss flux. Only the width of the tail of g_1 should be important, not the exact shape.

2. Relation Between Density and Loss Flux

In Appendix B we prove

Theorem 2: If $g(x,y)$ is zero outside the loss boundary $y_L(x)$ for $x < 0$ and decays outside the loss boundary for $x > 0$ with a decay width κ^{-1} in y^2, and if $\kappa^{-1} \ll y_L^2(x)$ for all x, then

$$n(L) \sim (R_L - 1)^{-1/2} F(L) \kappa^{1/2}. \tag{16}$$

(For mathematical convenience we have written the loss boundary as $y_L(x)$ instead of $x_L(y)$: "Outside the loss boundary" refers to $y > y_L(x)$.) In other words, in the dimensional equation $F(L) = n(L)\bar{v}$, the velocity $\bar{v}$ is proportional to the square root of the decay width of g in velocity-squared. We see then why the model decay width must be non-zero if the loss flux is nonzero. (The theorem is proved assuming κ independent of y, but it holds even if κ depends strongly on y.)

The height of g at the origin is crudely of order $n_0(c_\parallel c_\perp^2)^{-1}$. If the height of $g(x,y)$ at the loss boundary $y = y_L(x)$ is $C(x)$, with

$$\int_0^\infty d(x^2) C(x) \sim \frac{n_0}{c_\parallel c_\perp^2} \frac{1}{\kappa}$$

then $F(L) \propto 1/\kappa^2$ and $n(L)/n_0 \sim \left[F(L)/n_0 c_\parallel\right]^{3/4}$. This follows from the definitions of $F(L)$ and g.

3. Distribution Tail Width and Diffusivity

Appendix B continues with a very rough estimate of κ in terms of the velocity-space diffusivity, or, equivalently, the scattering rate. It is found that indeed $\kappa^{-1} \propto \nu^{1/2} \propto F(L)^{1/2}$; in fact

$$\kappa^{-1}/c_{\|}^{2} \sim 2^{3/2}(R_L - 1)^{-1/2}(L\bar{D}/c_{\|}^{3})^{1/2} \tag{17}$$

with $\bar{D}$ the bounce-averaged velocity diffusivity for ions near the loss boundary; $\bar{D} \sim (c_{\|}^{2} + c_{\perp}^{2})\nu_0$, where ν_0 is the effective scattering rate ($\nu_0 = \nu_{90}$ defined in Eq. (14) if Coulomb scattering is dominant.)

4. Ion Density at the Mirror and Beyond

Using this estimate of κ in theorem 2, one has

$$\frac{n_i(L)}{n_0} \sim R_L\, P\left(\frac{\nu}{\nu_\theta}\right)^{1/2}\left(\frac{L\nu}{c_{i\|}}\right)^{3/4} \tag{18}$$

where

$$P \equiv \frac{c_{\|}^{2}}{c_{\perp}^{2}(R_L - 1)} \qquad \text{and} \qquad c_{\|}^{2}/c_{\perp}^{2} \lesssim 1.$$

Those ions found near $x = L$ are highly anisotropic, with almost all of their energy in gyration. This may lead to instabilities which modulate $U(x,\mu)$, and especially near $s = L$ these modulations, say of order $e\delta\phi$ in amplitude, can affect κ if they are large enough. The ions found near $s = L$ spend long times there because they are near the loss boundary; consequently the loss boundary is effectively diffused to a width of order $e\delta\phi$ in parallel energy. (The same phenomenon makes the continuum limit of atomic physics indistinct.)[40] Since κ^{-1} refers to the spread in y^2 instead of x^2, we replace Eq. (17) by

$$\kappa^{-1}/c_{\|}^{2} \sim (R_L - 1)^{-1} e\delta\phi/T_{i\|}$$

if this larger than Eq. (17). Assuming this diffusion at $s \approx L$ is equivalent to diffusion of the fictitious distribution $g(x,y)$ at the

midplane, the density n(L) is reduced by a factor of order

$$(R_L - 1)^{1/4}(L\bar{D}/c_{\|})^{1/4}(e\delta\phi/T_{i\|})^{-1/2}$$

when cyclotron diffusion dominates κ. In fact, when both processes contribute, κ^{-1} should be just the sum of the two values given above.

Equation (18) was derived to corroborate an earlier estimate based on another model for g(x,y) which falls off exponentially with $y - y_L$ instead of $y^2 - y_L^2$. This model is also included in Appendix B. Writing $g(x,y) = g_0(x,y) + g_1(x,y)$, where g_0 would be f_0 in the absence of scattering, we choose $g_1(x,y)$ so that $g = g_0 + g_1$ has continuous slope and gives the same density as g_0. (This last requirement is a somewhat artificial one which helps give an estimate of the decay width.) For $g_0(x,y)$ we take a function Maxwellian at large velocities inside the trapping region, but going to zero at the loss boundary $y = y_L(x)$.

The decay width k^{-1} in $y - y_L$ is proportional to the typical decay width κ^{-1} in $y^2 - y_L^2$, and it is again found that approximately

$$k^{-1} \propto \left[F(L)\right]^{1/2}.$$

The result,

$$\frac{n_i(L)}{n_0} \sim R_L(P\sqrt{1+P})^{1/4}\left(\frac{L\nu}{c_{i\|}}\right)^{3/4} \tag{19}$$

compares rather well with Eq. (18) in which one needs a model for ν/ν_0 as a function of $T_{\|}/T_{\perp}$ amd R_L. (ν is the loss rate; ν_0 is the scattering rate. Their relation was discussed briefly in section IIA.

As one moves away from the mirror, this value of n_i/n_0 goes over to

$$\frac{n_i(s)}{n_0} \sim \left[\frac{T^{Loss}(R_L - R_s) + e(\phi_L - \phi_s)}{T_\parallel}\right]^{-1/2} R_s\left(\frac{L\nu}{c_{i\parallel}}\right) \qquad (20)$$

as in Eq. (10), assuming $v_\parallel = 0$ at $s = L$. Equation (20) is improper at $s = L$, but it reaches the magnitude (19) fairly close to $s = L$ (see Fig. 8). (When $T_\perp = 10T_\parallel$ and $L\nu/c_\parallel = 0.4 \times 10^{-3}$, equality occurs at $e(\phi_L - \phi_s)/T_\parallel \lesssim 0.02$.) The actual transition shape is calculated in the last part of Appendix B and is shown in Fig. 9 for typical parameters.

5. Effects of Charge Exchange

Charge exchange contributes an additional density of cold ions

$$\frac{n_i^{cx}(s)}{n_0^H} \sim \left[\frac{e(\phi_0 - \phi_s)}{T_\parallel}\right]^{-1/2} R_s\left(\frac{L\nu^{cx}}{c_{i\parallel}}\right). \qquad (21)$$

Because the charge-exchanged cold ions do not accumulate for long times near $s = L$ as do the SF ions from smooth diffusion, $n_i^{cx}(L)/n_i^{SF}(L)$ is small until

$$\frac{\nu_{cx}}{\nu_{diff}} \gtrsim \left[\frac{n_{diff}(L)}{n_0}\right]^{-1/4}\left[\frac{e(\phi_0 - \phi_L)}{T_\parallel}\right]^{1/2},$$

which is typically about 10. (Subscript "diff" refers to quantities in Eq. (19), i.e., smooth diffusion.)

The estimation of n_0^H/n_0 with a given source rate of cold (say charge-exchanged) ions is an interesting and apparently an unsolved problem. The density $n^{cx} \equiv n - n^H$, of course, comes from ions produced

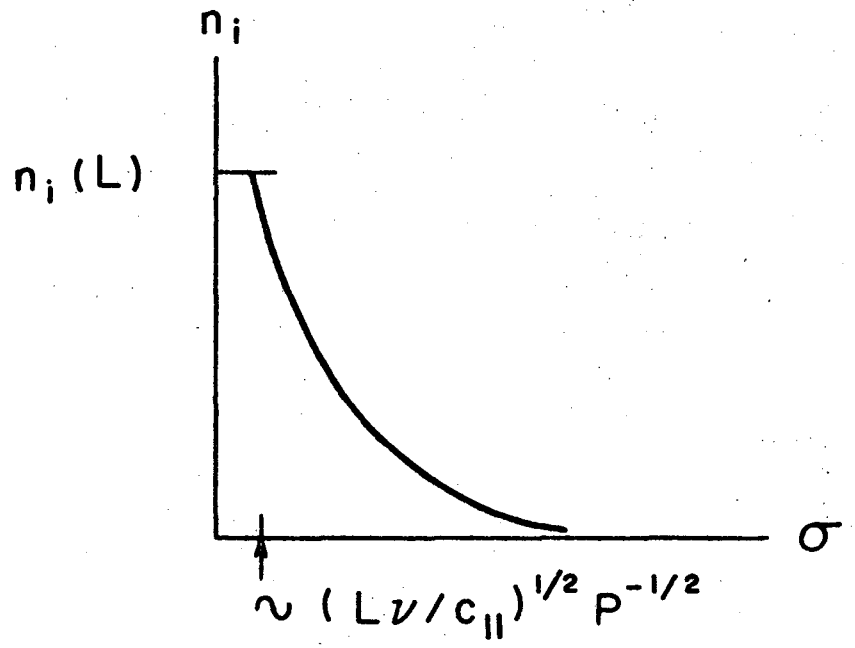

$$\sigma = \frac{T_{\perp}^{Loss} (R_L - R_s) + e(\phi_L - \phi_s)}{T_{\parallel}}$$

XBL697-3271

Fig. 8. Approximate density outside the main confinement region. ν = ion loss rate, P = anisotropy factor, $T_{\perp}^{Loss}$ = mean perpendicular energy of escaping ions.

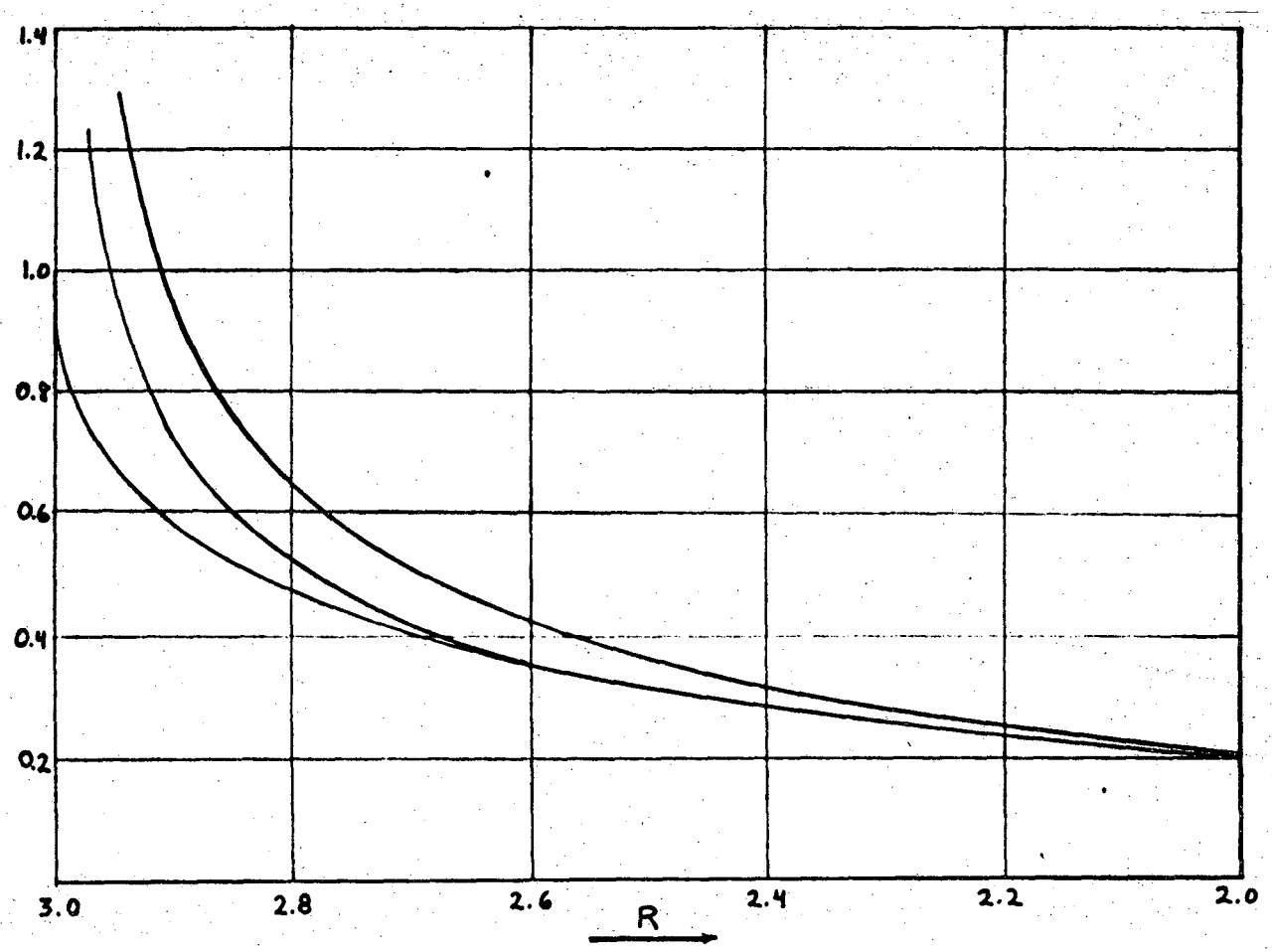

Fig. 9. Relative density vs R outside the mirror. Top curve: approximate formula [Eq. (20)] with φ neglected. Middle curve: approximate formula [Eq. (20)] with computer φ. Bottom curve: computer result.

almost-cold at and around the top of a potential-hill (the plasma potential); thus n_0^{cx} can be rather large. The separation-of-variables technique used by Chandrasekhar[39] for a Fokker-Planck equation near a potential maximum fails when a uniform source is present, and it is possible that a Boltzmann-type collision integral is more appropriate for the scattering term when the ions are cold and can scatter off neutrals of the same temperature as well as cold and hot ions. A crude dimensional estimate of n_0^{cx} may be made by equating the production rate $s = \nu^{cx} n_0^{H}$ with n_0^{cx}/τ_D, where τ_D is the time it takes a cold cx ion to scatter in energy an amount equal to its temperature T_c, or the time it takes a cold cx ion to drift out of the device without acceleration, whichever is less.

B. External Electron Density in Terms of the Potential

1. "Damped Maxwellian" Distribution

Since the electron loss bounary does not pass near the origin in x,y space, the electron "distribution" g(x,y) will be very nearly Maxwellian in most of the trapping region. It will then fall off near the loss boundary, to some small fraction ξ of its normal Maxwellian value at the boundary, and will decay fairly quickly to zero outside the loss boundary. We take g(x,y), for the electrons, to be a "damped Maxwellian":

$$g(x,y) = G(x,y)H(x,y),$$

where G(x,y) is Maxwellian with temperatures $T_{e\parallel}$ and $T_{e\perp}$, and H(x,y) is nearly unity well inside the containment region in x,y and zero well inside the loss region, with a smooth transition in between. A

model for H(x,y) is given by Eq. (C1), and g and H are pictured in Figs. 10 and 11.

2. Density at the Mirror

In Appendix C we perform the integration in Eq. (5) to obtain the mirror density $n_e(L)$ as a function of $\varphi_L \equiv e\phi_L/T_{e\|}$ (and of $\varphi_0 \equiv e\phi_0/T_{e\|}$, and other parameters). The result is found to be somewhat sensitive to the abruptness with which H(x,y) drops off, but some estimate of this is made in part 4 of Appendix C. The result is then extended for $s > L$ out to $s = W^-$, using an approximation for Sup $\epsilon_{s'}$, $(s' \leq s)$, i.e., for the integration region. We summarize here the results of these calculations for the case of isotropic electrons ($T_{e\|} = T_{e\perp} = T_e$).

Instead of $n_e(L)/n_0 = e^{-\varphi_0} e^{\varphi_L}$, which one would get with a Maxwellian g, we find

$$n_e(L) \approx n_e^{ST}(L) \tag{22}$$

for ξ small and $\varphi_L > 2\xi$ ($n_e^{SF}(L)/n_0 < \xi e^{-\varphi_0}$), and

$$n_e^{ST}(L)/n_0 = e^{-\varphi_0} EST(\varphi_L, a_L, b, \xi) \tag{23}$$

where the function $EST(\varphi,a,b,\xi)$ (replacing e^{φ_L}) is given by Eq. (C5), and where ξ is the height of H(x,y) at the (approximate) loss boundary, $x = x_1(y)$; $a_L \equiv R_W/(R_L - R_W)$ for isotropic electrons; and $b + 1 \equiv \kappa'$ measures the abruptness with which H drops off for $x < x_1(y)$. Reasonable values of b lie in the range $0 \leq b \lesssim 2$. When $b = 0$, the profile of H at constant y is a Maxwellian minus a constant, for $x \leq x_1(y)$. The function $EST(\varphi,a,b,\xi)$ is shown plotted against φ for several values of a,b in Figs. 12 and 13, which also show the pure Maxwellian result,

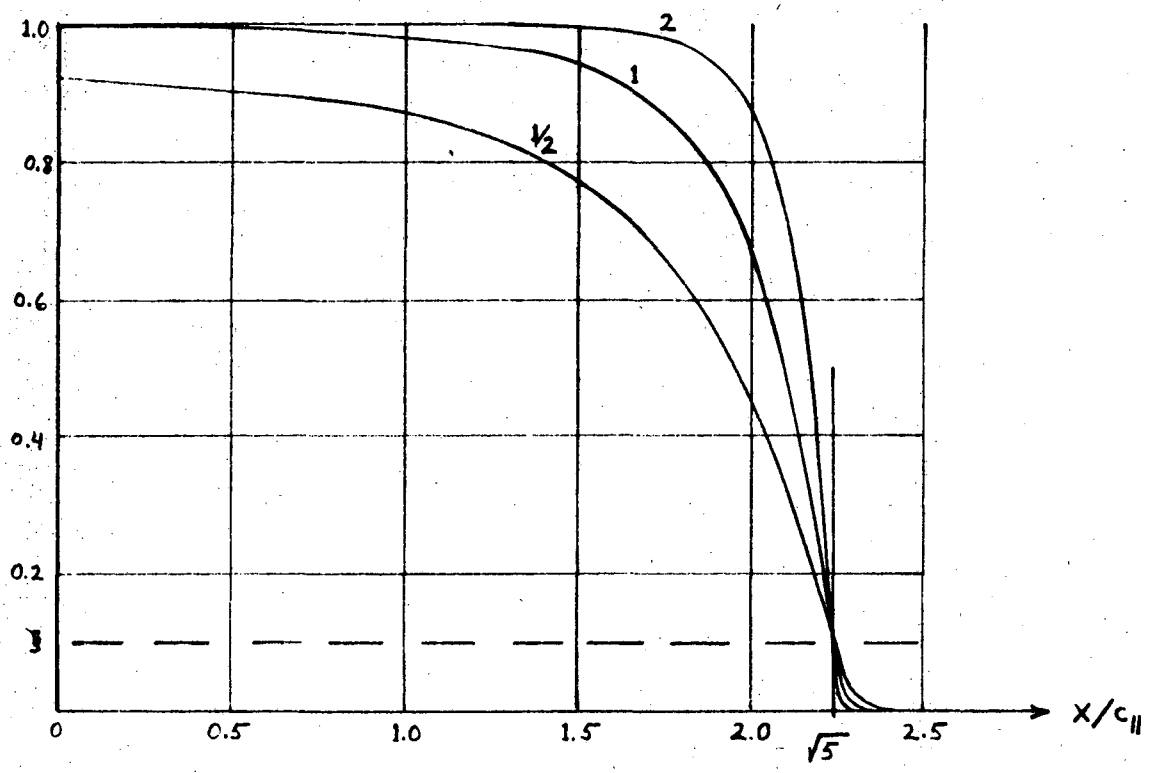

XBL 712-251

Fig. 10. "Damping function" H(x,y) [Eq. (C1) of Appendix C] for $y = 0$, $\xi = 0.1$, $\phi_0 = 5T_e$, and $\kappa' = 2, 1, 1/2$.

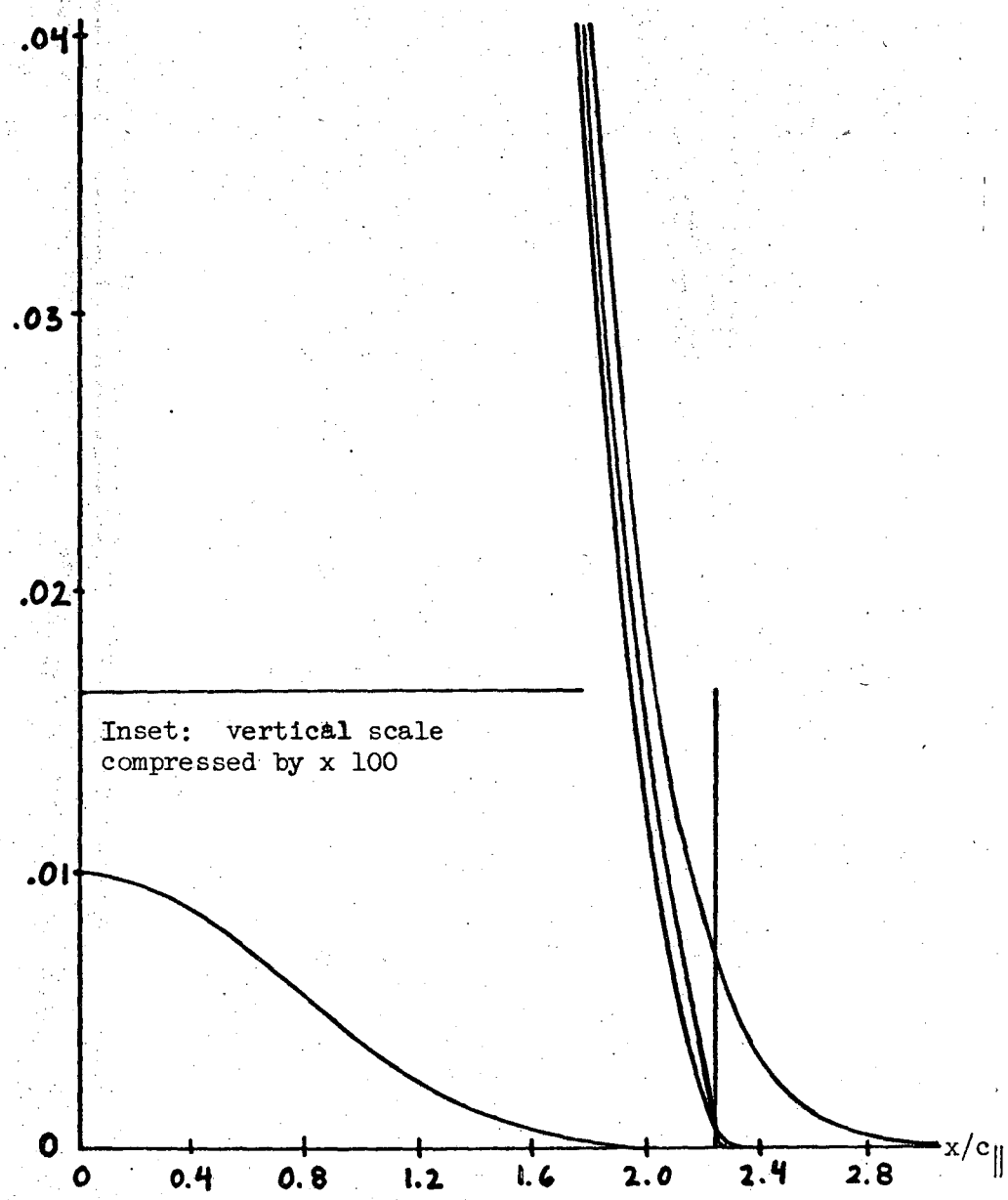

Fig. 11. Damped Maxwellian distribution function. Steep curves: ordinary Maxwellian f(x, 0) (top) and same distribution multiplied by damping function of Fig. 10 with $\kappa' = 1$ (bottom curve) and $\kappa' = 2$ (middle). Loss boundary is at $x/c_{||} = \sqrt{5}$. All 3 curves are almost indistinguishable at thermal velocities (inset).

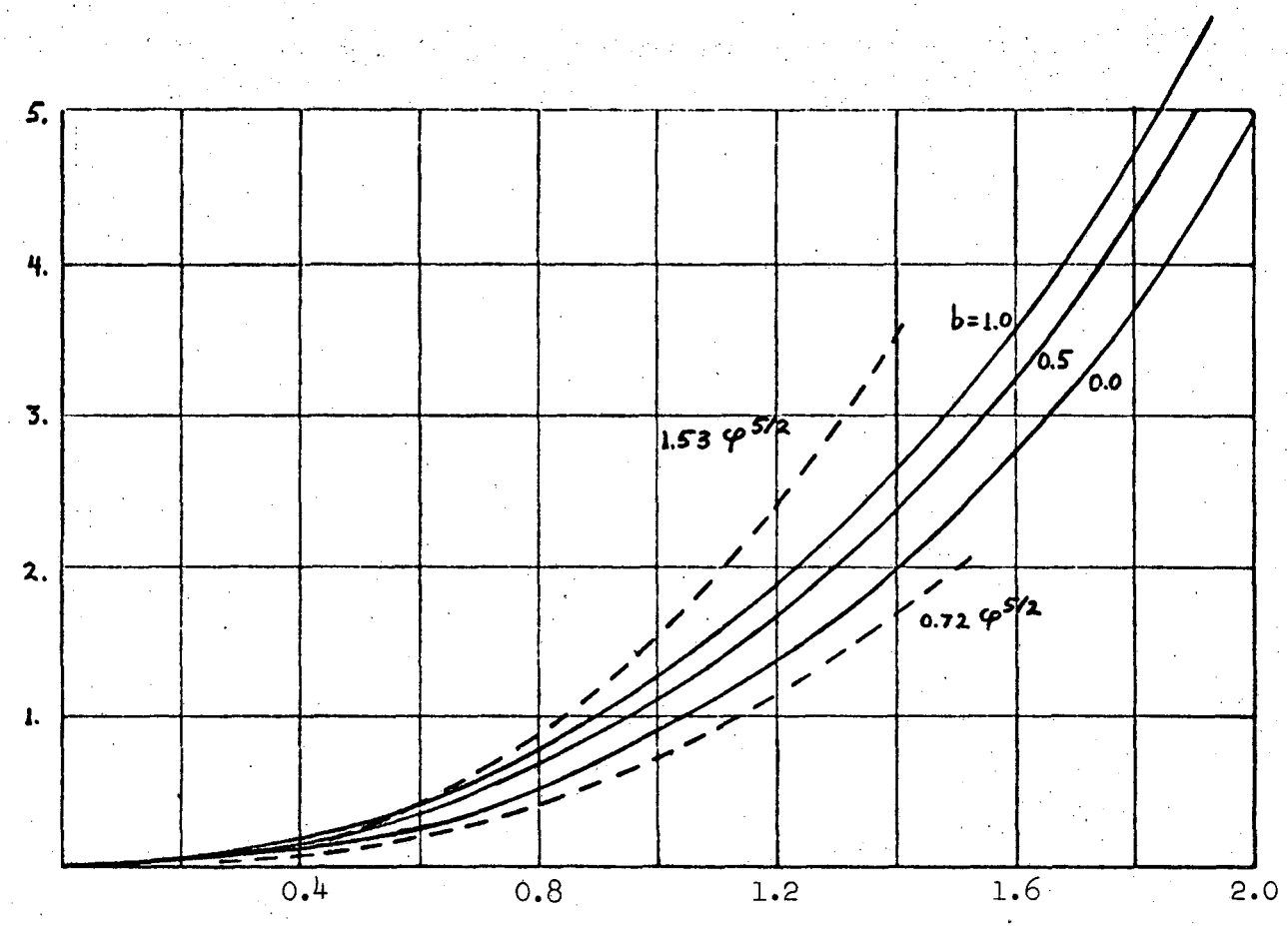

Fig. 12. EST(φ,a,b,ξ) defined in Eq. (C5), vs φ, for ξ = 0.1, a = 2, and b = 0, 0.5, 1.0 (solid curves). Dashed curves: Eq. (C7) (approximation to EST) for ξ = 0.1, a = 2, b = 0 (lower curve) and b = 1 (upper curve).

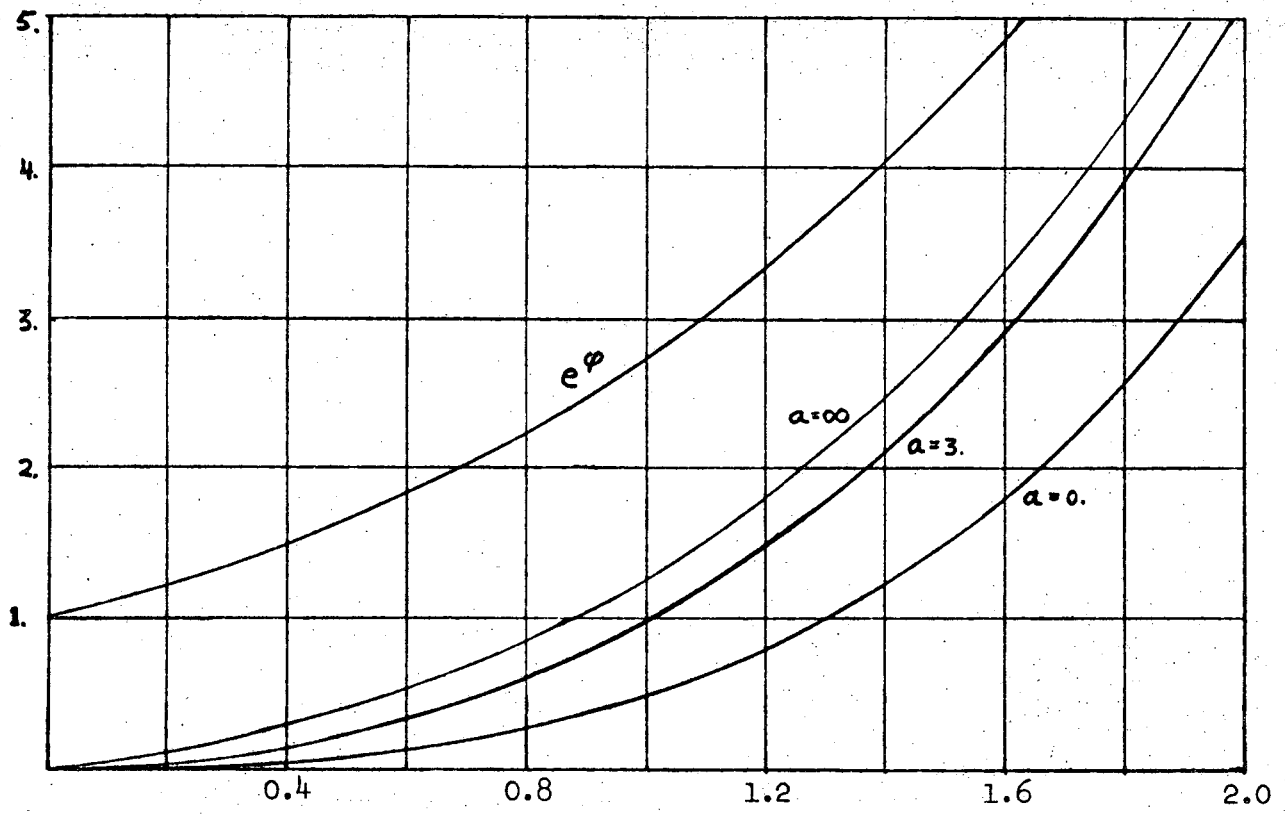

Fig. 13. EST(φ,a,b,ξ) defined in Eq. (C5), vs φ, for ξ = 0.1, b = 0, and a = 0, 3, ∞. Also shown: e^{φ} vs φ.

e^{φ}, and an approximation to EST,

$$EST(\varphi,a,b,\xi) \sim 0.3(a+1)\left[(b+1) - \xi(a+b)\right]\varphi^{5/2} \qquad (24)$$

good for $a\varphi \lesssim 3$, $b \lesssim 1$, and $2\xi < \varphi < 1$. For $e\phi_L$ or order T_e, then, $n_e(L)$ is roughly proportional to $R_L/(R_L - R_W) \equiv a_L + 1$, when this parameter is not too large; and $n_e(L)$ is an increasing function of ϕ_L, varying roughly as $\varphi_L^{5/2}$. These features are also reproduced by a simple dimensional model in part 6 of Appendix C.

3. Density Outside the Mirror

For $s > L$

$$\frac{n_e^{ST}(s)}{n_0} \approx e^{-\varphi_0}\left\{EST(\varphi_s,a_s,b,\xi) - \exp\left[-\frac{R_W}{R_L - R_s}(\varphi_L - \varphi_s)\right] EST\left[\varphi_s - (\varphi_L - \varphi_s)\frac{R_W}{R_L - R_s}, a_s, b, \xi\right]\right\} \qquad (25)$$

where the last term constributes only slightly, and only for s fairly far from L. At the sheath edge, $s = W^-$,

$$\frac{n_e^{ST}(W)}{n_0} \quad e^{-\varphi_0}\left[1 - e^{-a_L(\varphi_L - \varphi_W)}\right] EST(\varphi_W,\infty,b,\xi) \qquad (26)$$

and an expression for $EST(\varphi,\infty,b,\xi)$ is given in Eq. (C14) which is of order

$$\varphi^{3/2}\left[1 + 0.4(1-b)\varphi + \cdots\right]$$

when $\xi \ll \varphi \ll 1$, or of order $\xi\varphi^{1/2}$ when $\varphi \lesssim \xi$.

For the SF electrons, which may be relatively more important at the wall

$$\frac{n_e^{SF}(W)}{n_0} \sim \frac{1}{2}\,\xi k^{-1/2} e^{-\varphi_0}\left[1 - e^{-a_L\varphi_L}\right] e^{k\varphi_W}\ \mathrm{erfc}\ \sqrt{k\varphi_W}\ . \qquad (27)$$

Electrons produced at the wall or in region II are treated separately in Chapter IV.

C. Estimate of the External Potential

In this section we equate expressions for n_i and $n_e(\varphi)$ at $s = L$ and at $s = W^-$ to estimate φ_L and φ_W. The detailed shape of $\varphi(s)$ between L and W^- is not of great interest as long as $\varphi(s)$ is monotonically decreasing, and the complexity of the formulas leads us to avoid detailed calculation of $\varphi(s)$.

1. Potential at the Mirror

When charge exchange is unimportant, we can substitute Eq. (19) for $n_i(L)$ and Eq. (23) for $n_e^{ST}(L)$ into $n_i^{SF}(L) = n_e(L) \approx n_e^{ST}(L)$:

$$R_L(P\sqrt{1+P})^{1/4}(L\nu/c_{i\|})^{3/4} e^{\varphi_0} = EST(\varphi_L, a_L, b, \xi), \qquad (28)$$

where R_L is the mirror ratio,

$P = \dfrac{c_\|^2}{(R_L - 1)c_\perp^2}$ for the ion distribution,

$\dfrac{L\nu}{c_{i\|}}$ is the scattering parameter (transit time x loss rate), for ions, discussed in section IIA

$\varphi_0 = e\phi_0/T_e$ with ϕ_0 the midplane plasma potential,

$\varphi_L = e\phi_L/T_e$ with ϕ_L the potential at the mirrors,

$$a_L = \frac{R_w}{R_L - R_w} = \frac{B(W)}{B(L) - B(W)} ,$$

$b = \kappa' - 1$ is a constant < 1, describing how the electron distribution falls off near the loss boundary (see Appendix C),

$\xi < 1$ is the height of the delectron distribution g, at the loss boundary, divided by the height of a Maxwellian there. Typically $\xi \ll 1$.

From the graphs of EST in Figs. 12 and 13 we can get a solution for φ_L if

$$0.1 < R_L(P\sqrt{1+P})^{1/4}(L\nu/c_{i\|})^{3/4}e^{\varphi_0} < 5. \qquad (29)$$

The solution lies in the range $0.2 < \varphi_L \lesssim 2$. Typically $\varphi_0 \sim 5$ ($e^{\varphi_0} \sim 10^2$), $L\nu/c_{i\|} \gtrsim 10^{-4}$ (from section IIA), $R_L \sim 3$, and $10^{-2} < P < 10^2$; so that inequality (29) is satisfied (at least for $L\nu/c_{i\|} \lesssim 2 \times 10^{-3}$. If $L\nu/c_{i\|} \gtrsim 2 \times 10^{-3}$, the value of φ_L may be larger than 2 and thuss off the scale of Figs. 12 and 13, but the Eq. (28) is still valid).

Since EST is a monotonically increasing function of φ, it follows that φ_L is increased by increasing L, ν, φ_0, R_L, or $c_{i\|}/c_{i\perp}$ independently; however, one should note that ν is actually a decreasing function of R_L, as is P, and φ_0 is an increasing function of R_L. The case $R_L - 1 \ll 1$ is treated in Appendix E. The dependence of φ_0 on ν is discussed later.

In the range $0 < a_L\varphi_L < 3$, $0 \leq b \equiv \kappa' - 1 \leq 1$, and $2\xi < \varphi_L \lesssim 2$, where one has the approximation

$$EST \sim 0.3 \frac{R_L}{R_L - R_W} \kappa'^{5/2} \tag{30}$$

ignoring the ξ term in Eq. (24), one can express Eq. (28) as

$$\varphi_L \approx 1.6 \; e^{\varphi_0 \frac{(R_L - R_W)}{\kappa'}}{}^{0.4} (P\sqrt{1+P})^{0.1} \left(\frac{L\nu}{c_{i\|}}\right)^{0.3}. \tag{31}$$

Because $\kappa' \sim 1$ and because of the weak dependence on P, one may use as a rule of thumb, for reasonable mirror ratios ($10^{-2} < P < 10^2$),

$$\varphi_L \sim \left[e^{\varphi_0}(R_L - R_W)\right]^{0.4} (L\nu/c_{i\|})^{0.3}$$

when $R_L - R_W \gtrsim R_W\varphi_L$, $L\nu/c_{i\|} \ll 1$, and $\nu_{cx} < \nu$. For large $\underline{a}$, the function $EST(\varphi,a,b,\xi)$ becomes independent of $\underline{a}$; so for $a_L \gg 1$ and for $b \leq 1$, $\xi \ll 1$ and φ_L in the range $a_L^{-1} \ll \varphi_L \leq 2$, one has from Eq. (C13)

$$EST(\varphi_L, a_L, b, \xi) \sim \varphi_L^{3/2}, \qquad \text{for } \varphi_L > \xi.$$

Using this in Eq. (28) gives

$$\varphi_L \sim (e^{\varphi_0} R_L)^{2/3} (L\nu/c_{i\|})^{0.5}, \tag{32}$$

where again the $P\sqrt{1+P}$ term has been dropped. This result applies when $R_W \approx R_L$.

When charge exchange is the dominant loss mechanism ($\nu_{cx} \gtrsim 10^2\nu$), we substitute Eq. (21) for $n_i^{cx}(L)$ and Eq. (23) for $n_e^{ST}(L)$ into

$$n_i^{cx}(L) \approx n_e(L) \approx n_e^{ST}(L)$$

$$(T_{i\|}/T_e)^{1/2} e^{\varphi_0} (n_0^H/n_0)(L\nu_{cx}/c_{i\|}) = (\varphi_0 - \varphi_L)^{1/2} EST(\varphi_L, a_L, b, \xi)$$

to get φ_L. When $L\nu/c_{i\|} \ll L\nu_{cx}/c_{i\|} < \xi^2 e^{-\varphi_0}$, this equation may give $\varphi_L < \xi$, in which case the approximation $n_e^{SF}(L) \ll n_e^{ST}(L)$ fails, and one must add the contribution of SF electrons (see Appendix C). A careful estimate of the decay width κ for electrons in Eq. (C1) must then be made, as φ_L can depend fairly sensitively on it. This difficulty will arise again in estimating φ_W, which is typically $\ll \varphi_L$. When $(L\nu_{cx}/c_{i\|})e^{\varphi_0}$ is in the range between ξ^2 and 3, the approximation (30) is useful and gives

$$\varphi_L \sim \left[\frac{R_L - R_W}{0.3R_L} \frac{n_0^H}{n_0}\right]^{0.4} \left[\frac{T_{i\|}}{e\phi_0}\right]^{0.2} \left[\frac{L\nu}{c_{i\|}} e^{\varphi_0}\right]^{0.4} \tag{33}$$

2. Potential Drop at the Sheath

To estimate the sheath potential drop, ϕ_W, we again start with the case where charge exchange contributes negligibly to n_i and we substitute Eq. (10) for $n_i(W^-)$, and Eqs. (26) and (27) for $n_e^{ST}(W^-)$ and $n_e^{SF}(W^-)$ into

$$n_i^{SF}(W^{-1}) = n_e^{ST}(W^-) + n_e^{SF}(W^-):$$

$$(T_{i\|}/T_e)^{1/2}\left[(R_L - R_W)T^{loss}/T_e + (\varphi_L - \varphi_W)\right]^{-1/2} R_W(L\nu/c_{i\|})e^{\varphi_0}$$

$$\approx \left[1 - \exp\left(-R_W \frac{\varphi_L - \varphi_W}{R_L - R_W}\right)\right] EST(\varphi_W, \infty, b, \xi)$$

$$+ \left[1 - \exp\left(-R_W \frac{\varphi_L}{R_L - R_W}\right)\right] \frac{1}{2}\xi k^{-1/2} e^{k\varphi_W} \operatorname{erfc}\sqrt{k\varphi_W}\,, \tag{34}$$

where $k^{-1}T_e$ is the parallel temperature of the SF electrons striking the wall, and ξ is the height of the electron distribution $g_e(x,y)$ at the loss boundary, divided by the height of a Maxwellian there. Except for a factor of $e^{-\varphi_0}$, the first term on the right hand side of this equation is $n_e^{ST}(W^-)$ and the second term is $n_e^{SF}(W^-)$. $EST(\varphi,\infty,b,\xi)$ is given by Eq. (C13) in Appendix C; for $\xi \ll \varphi_W < 1$,

$$EST(\varphi_W,\infty,b,\xi) \sim \varphi_W^{3/2}$$

but for $\varphi_W \ll \xi \ll 1$,

$$EST(\varphi_W,\infty,b,\xi) \approx \frac{2}{\sqrt{\pi}}\,\xi\varphi_W^{1/2}.$$

Of course, $EST(0,\infty,b,\xi) = 0$. By contrast, $n_e^{SF}(\varphi_W,\infty,k,\xi)$ (where $k^{-1}c_e^2$ is the decay width of the electron distribution $g(x,y)$ outside the loss boundary) is <u>not</u> zero at $\varphi_W = 0$, and in fact decreases with φ_W:

$$e^{k\varphi_W}\operatorname{erfc}\sqrt{k\varphi_W} \approx 1 - \frac{2}{\sqrt{\pi}}(k\varphi_W)^{1/2}, \qquad \text{for } (k\varphi_W)^{1/2} \ll 1.$$

But this decrease is more than offset by the increase in EST ($\propto \xi\varphi_W^{1/2}$ for $\varphi_W \ll \xi$). For such small φ_W, we neglect the φ_W in the first "exp" factor of Eq. (33), since φ_L is not usually so small; then the right hand side of Eq. (33) becomes

$$\left[1 - \exp\left(-\frac{R_W\varphi_L}{R_L - R_W}\right)\right]\left\{\frac{1}{2}\,\xi k^{-1/2}\left[1 + \frac{2}{\sqrt{\pi}}\,(k\varphi_W)^{1/2}\right] + O(\varphi_W^{3/2})\right\}$$

when $k\varphi_W \ll 1$, and the $O(\varphi_W^{3/2})$ term is negligible when $\varphi_W \ll \xi$.

We digress to mention that ξ/k is proportional to $(L\nu/c_{i\|})e^{\varphi_0}$, because the electron loss flux, proportional to $(\xi/k)e^{-\varphi_0}$, must equal the ion loss flux, proportional to $L\nu/c_{i\|}$. Equation (C10) of Appendix C gives the constant of proportionality. Using (C10) for $/k$ in the above we find that for $\varphi_W \ll \xi, k^{-1}$, $R_W(L\nu/c_{i\|})e^{\varphi_0}$ cancels out of Eq. (34), leaving φ_W determined by

$$1 + \frac{2}{\sqrt{\pi}}\,(k\varphi_W)^{1/2}\left[1 + O(\varphi_W/\xi)\right]$$

$$\sim \left\{\pi k(m_e/m_i)\left[(R_L - R_W)(T^{Loss}/T_e) + (\varphi_L - \varphi_W)\right]\right\}^{-1/2}. \qquad (35)$$

Here we have used $a_L \equiv R_W(R_L - R_W)$ and the fact that the ratio $(1 - e^{-a_L\varphi_L})\left[1 - (a_L + 1)^{-1}e^{-a_L\varphi_L}\right]^{-1}$ is always nearly unity, both when $a_L\varphi_L \gtrsim 2$ (as in the usual mirror end region), and in the case of magnetic expansion for direct conversion of ion loss energy,[41] where $R_W \approx 0$ and thus $a_L \approx 0$. The φ_W dependence of the right hand side of Eq. (35) is almost always negligible; the φ_W dependence on the left hand side is obvious. Thus when the right hand side of Eq. (35) is of order unity, the value of φ_W depends on the electron scattering (through k) and not explicitly on the ion loss rate ν. (We shall see shortly that φ_W depends on k and not ν even when $\varphi_W \gtrsim \xi$, because $e^{\varphi_0} \propto \nu^{-1}$.)

However, the right hand side of Eq. (35) is usually much larger than unity because of the small mass ratio m_e/m_i. Returning to Eq. (34) and keeping only the EST term on the right, approximating EST by $\varphi_W^{3/2}$, we get

$$\varphi_W \sim \left[\frac{T_{i\parallel}}{T_\perp^{Loss}} \frac{R_W^2}{R_L - R_W}\right]^{1/3} \left[\left(\frac{L\nu}{c_{i\parallel}}\right) e^{\varphi_0}\right]^{2/3} \tag{36}$$

for $a_L\varphi_L \gtrsim 2$, or

$$\varphi_W \sim \left[\frac{T_{i\parallel}}{T_\perp^{Loss}} \frac{R_L}{\varphi_L^2}\right]^{1/3} \left[\left(\frac{L\nu}{c_{i\parallel}}\right) e^{\varphi_0}\right]^{2/3} \tag{37}$$

for the $R_W \approx 0$ case. (We have neglected $\varphi_L - \varphi_W$ compared with $(R_L - R_W)(T_\perp^{Loss}/T_e)$ on the left side of Eq. (34) and made the appropriate expansion of $1 - e^{-a_L\varphi_L}$.) In each of Eqs. (36) and (37) the 1/3-power coefficient is of order unity, and thus as a "rule-of-thumb",

$$\varphi_W \sim \left[(L\nu/c_{i\parallel}) e^{\varphi_0}\right]^{2/3},$$

if this is much larger than ξ.

Typically, however, $\varphi_W \sim \xi \sim k^{-1}$ (i.e. neither approximation is valid), and we have only an upper bound and an order of magnitude estimate of φ_W, unless k and ξ are known well enough for a graphical solution of Eq. (34).

When charge exchange in region I is the dominant source of ions in region II, we substitute Eq. (21) for $n_i^{cx}(W^-)$ in place of the left hand side of Eq. (34). Proceeding as before, we have

$$1 + \frac{2}{\sqrt{\pi}} (k\varphi_W)^{1/2} \sim \left[\pi k \frac{m_e}{m_i} \varphi_0 \right]^{-1/2}$$

when $\varphi_W \ll k^{-1}$, ξ, and

$$\varphi_W \sim \left(\frac{T_{i\|}}{e\phi_0} \right)^{1/3} \left[R_W \left(\frac{L\nu}{c_{i\|}} \right)^{cx} e^{\varphi_0} \right]^{2/3}$$

when $\varphi_W \gg \xi$, with the R_W replaced by R_L/φ_L when $R_W \ll 1$. (we have used $\varphi_W \ll \varphi_L$, φ_0, and $R_W \ll R_L$ in this case.)

3. Typical Values

To illustrate the calculations of this section, we present the following numerical estimates: For $R_L = 3$, $R_W = 2$, $\varphi_0 \equiv e\phi_0/T_e = 5$,[1] we show φ_L and φ_W for the two cases (1) and (2) discussed in section IIA:

(1) $n_0 = 10^{10}$ cm^{-3}, $T_e = 10$ eV, $T_{i\|} = 100$ eV, $T_i = 100$ eV, which gives $L\nu/c_{i\|} = 3.3 \times 10^{-4}$ from Coulomb scattering, and

(2) $n_0 = 10^{13}$ cm^{-3}, $T_e = 100$ eV, $T_{i\|} = 1$ keV, $T_i = 10$ keV, which gives $L\nu/c_{i\|} = 0.4 \times 10^{-4}$ from Coulomb scattering.

$\frac{L\nu}{c_{i\|}}$	(1) 0.3×10^{-3}	(2) 0.4×10^{-4}
$\frac{e\phi_L}{T_e}$	0.8	0.4
$\frac{e\phi_W}{T_e}$	$\sim 0.16^{(-)}$	≤ 0.06

The sign "(-)" means that the figure is an upper bound and a good estimate to within about a factor of 2. In both cases (1) and (2) we have estimated $T_\perp^{Loss}$ from

$$T_\perp^{Loss} \sim (R_L - 1)^{-1}\left[e(\phi_0 - \phi_L) + T_\parallel\right].$$

We have included the anisotropy factor $(P\sqrt{1+P})^{0.1}$ in Eq. (31); it reduced the results by 25%. We have taken $\kappa' = 1$ in Eq. (31).

When $R_W \approx R_L$ (i.e., no magnetic field expansion in region II), ϕ_W is increased to $\phi_L \approx \phi_W$, and ϕ_L given by Eq. (32) is not significantly different from the value in the table, i.e., the value for $R_L - R_W \sim 1$. When $R_W \approx 0$ (complete magnetic field expansion, as in direct conversion[41]), the calculated values of ϕ_L and ϕ_W for the parameters illustrated are not significantly different from the values in the table, although the calculations are not very good for this case (see Appendix C). In the table, ϕ_L is overestimated and ϕ_W is probably underestimated.

Charge exchange gives smaller values of ϕ_L for given loss rate because, as pointed out in section IIA, the low-magnetic-moment ions created by charge exchange do not spend long times near the mirror as do ions of high magnetic moment, lost by gradual velocity-wandering. Because $n_i^{cx}(L) \propto L\nu^{cx}/c_{i\parallel}$ while $n_i^{SF}(L) \propto (L\nu/c_{i\parallel})^{3/4}$, the dependence of φ_L on the appropriate small scattering parameter is slightly stronger in the case of charge-exchange loss. This makes φ_L smaller by about a factor of 3 when charge exchange provides $L\nu^{cx}/c_{i\parallel} \sim 10^{-4}$ instead of Coulomb scattering with $L\nu/c_{i\parallel} \sim 10^{-4}$. The estimate for φ_W is unchanged when ν is replaced by ν^{cx}.

4. Discussion of Results

The value of ϕ_W scales more or less with k^{-1}, i.e., with the SF electron parallel temperature $k^{-1}T_e$, instead of with T_e, the midplane temperature. This is true both when $\varphi_W < \xi, k^{-1}$ (where $\varphi_W \propto (k^{-1})^p$ with p between 1/2 and 1) and when $\varphi_W > \xi$ (where $\varphi_W^{3/2} \propto (L\nu/c_{i\parallel})e^{\varphi_0} \propto \xi k^{-1}$).

The values of $L\nu/c_{i\parallel}$ due to Coulomb scattering are, of course, underestimates; but it is well to remember that e^{φ_0} varies roughly as ν_{0e}/ν_{0i} for constant mirror ratio,[17] where ν_{0i} and ν_{0e} are the cumulative 90-degree scattering rates for ions and electrons respectively. (A more refined calculation[1] gives $\varphi_0^{3/2}e^{\varphi_0} \propto \nu_{0e}/\nu_{0i}$.) Thus the quantity $(L\nu/c_{i\parallel})e^{\varphi_0}$ appearing in the equations of this section is really sensitive only to changes in the <u>electron</u> scattering rate. If the <u>electrons</u> diffuse anomalously fast in velocity space because of turbulent fields, then the estimates for φ_W will be <u>larger</u> (instead of smaller as one might guess) because φ_0 will be larger. On the other hand, if the <u>ions</u> are lost anomalously fast, φ_0 decreases but φ_W does not. The picture is less clear with φ_L, but from Eq. (31) and this argument,

$$\varphi_L \propto \nu_e^{0.4}\nu_i^{-0.1},$$

so that φ_L decreases when ions (only) are lost more rapidly (again, opposite to what one might guess) because φ_0 decreases. φ_L and φ_W do not change proportionally to φ_0.

We have noted that the sheath potential ϕ_W scales more or less with the temperature of electrons near the wall, rather like the ordinary sheath problem. But care must be exercised in estimating the

resistance of this sheath. In the usual problem of plasma in a box without internal magnetic forces, the dc sheath resistance is calculated as $d(F_i - F_e)/d\phi_0$ holding the distribution functions constant. It is assumed that the Maxwell tail of the electron distribution is always replenished. But in problems where unbound particles are quickly lost, the distribution function changes (on both collisional and transit time scales) when ϕ_0 changes, because the loss boundary depends on ϕ_0. (This vaguely resembles the problem of a probe which has absorbed nearly all the ions in the flux tube it intercepts.)

Changes in ϕ_0 on a time scale slower than collision times cause changes in loss flux because the tail parameters depend on the location of the loss boundary. (This is just the problem of determining ϕ_0.) Such changes are inconsistent with equal steady-state loss fluxes. Changes in ϕ_0 on a time scale faster than collisions but slower than bounce times are rectifying: when the loss boundary eats into the distribution, the loss flux temporarily increases, more than it decreases if the loss boundary recedes to higher velocities. Such changes in ϕ_0 also produce changes in F_e proportional to $d\phi_0/dt$ rather than ϕ_0 itself, whenever ϕ_0 is decreasing to a new low.

A fast, purely oscillatory perturbation on ϕ_0 simply moves the steady effective loss boundary for electrons inward to where it would be if ϕ_0 were replaced by $\phi_0 - \delta\phi$ (with $\delta\phi$ the perturbation amplitude), and then causes ϕ_0 to readjust upward on a collisional time scale. Localized oscillations in ϕ with wavelength $\lambda_\parallel$ along B cannot take place slower than the transit time $\lambda_\parallel/v_{e\parallel}$ of the fastest electrons (i.e., parallel phase velocities cannot be less than either the local

electron thermal speed or the local electron excape velocity) because such disturbances would create significant local space charge. Thus one cannot discuss low frequency ($I\omega/2\pi c_{e\|} < 1$) local changes in ϕ_w and assume ϕ_0 constant. Damping of low-frequency electrostatic waves with $k_\| \neq 0$ always involves particle loss to the end walls.

The calculations in this section clearly show that the steady-state φ ordinarily continues to decrease with s in region II, in contradiction to the common statement that $d\phi/dB$ is proportional to the local difference in anisotropies of ions and electrons (see Appendix D). The reason for the discrepancy lies in the vacancy of part of phase space (the dashed orbits in Fig. 7), which, because of subtleties discussed in Appendix D, complicates the usual relation between $d\phi/ds$ and dB/ds.

SYNOPSIS OF CHAPTER IV

Up to this point the discussion has been of ions and electrons born inside the plasma and appearing out past the mirrors. In this chapter we discuss the influence of electrons which may be born in region II; between the mirror and end wall, or at the wall (either wall cathode or secondary emission). Ions born here cannot penetrate the plasma potential and are returned to the wall, but electrons are accelerated into the confinement region. (How many of these electrons become trapped in region I is a delicate matter involving their energy loss, as discussed in part 7 of Section IVA.) Their contribution to unbalancing the source input fluxes of electrons and ions, together with the change in energy loss fluxes of each species, causes the plasma potential to change [see Eq. (54), p. 73]. If almost all externaly born electrons ("x"-electrons) are trapped, the change $\Delta\phi_0$ is of order T_e times the ratio of external-source flux F_x to internal-source flux F. These matters are discussed in Section IVA.

The possibility of two-stream instability caused by the x-electrons is discussed in Section IVB. After pointing out that the stability criteria are not the same as in the ordinary case (because parallel velocities are swept out of resonance by the magnetic forces), we discuss what the nonlinear-steady-state distribution $f_e(x,y)$ might look like with the x-electrons somewhat diffused in energy by wave-particle interactions (Fig. 16, p. 91; Fig. 17, p. 95). It is assumed that the waves are primarily space-charge waves carried with the "beam" of x-electrons. (This beam is injected "cold" but is quickly flattened to a "quasi-plateau" on the electron distribution.) An important fact is that the source is not cut off and the distribution function is not allowed to relax. The quasi-plateau in midplane velocity space results only because the interactions are strong.

IV. EFFECTS OF EXTERNAL SOURCES

In this chapter we consider the small change in the steady state of an imperfectly confined plasma when "additional" plasma is slowly introduced into the equilibrated system by an external source (such as emission of secondaries from end walls of the chamber, or a weak electron beam running through the plasma along magnetic field lines).

A. Effect of External Sources on Confinement: Stable Case

1. Definition of the Problem

The first question facing such an analysis is whether the streaming of the externally supplied electrons (which are supplied near one edge of a potential well) causes additional instability (loss-cone modes may already be present). An intense beam or even a cold source at the end walls would produce a bump in the tail of the electron distribution and would excite two-stream modes. The analysis of this unstable, inhomogeneous system would be difficult; a qualitative discussion is presented in the next section. Here we consider only the case in which the total energy in waves due to such interactions is small compared with $n^{SF}e\phi_W$--i.e., the case of a very weak beam--and we take two equal counterstreaming components for symmetry. We also assume that the spectrum of any preexisting instability is not changed by the new electron stream, and that the ion distribution is not altered by the new waves.

For simplicity, let us assume that the primary (internal) source that sustains the plasma is unaffected by the new weak electron input from the ends. (There is no input of ions at the ends; they are all repelled by the plasma potential.) We will neglect any changes in the

energy loss by radiation, and any changes in the particle loss by diffusion across the magnetic field.

2. Particle and Energy Balance

We specialize for now (until part 8 of this section) to the case where the additional electron input is from the end walls. The input flux of electrons supplied externally from the ends is just $|F_x|$, the emission rate at the wall, in electrons/cm^2 sec. (The absolute value is used here only because outgoing flux is usually taken as positive. We will consider F_x as a positive quantity in what follows.) Since there is already an effective input flux F of electrons which just equals the loss flux, this additional input flux $|F_x|$ must give rise to an additional loss flux, $\Delta F = |F_x|$, in order that a new steady state results.

And what is true of particle fluxes is also true of energy fluxes, if both ions and electrons are taken into account: in the resulting new steady state energy cannot be accumulating or draining, so the net energy loss flux must be unchanged.

$$\Delta \mathcal{F}_i + \Delta \mathcal{F}_e \approx |F_x| T_W, \tag{38}$$

where the energy flux

$$\mathcal{F} \approx \pi R_W m \int_{SF} x\,dx\; y\,dy\; g(x,y)(x^2 + y^2) \tag{39}$$

for each species, and where T_W is the input temperature of the wall-born electrons from the external source ("x" electrons). Here Δ indicates the change due to addition of the "x" electrons, and if their

input temperature is negligible, as we will assume, the right hand side of Eq. (38) is zero. The original energy loss rate comes from ions leaving with energy $\epsilon + e\phi_0$ at the wall (ϵ at the midplane), and electrons leaving in equal numbers (if the sources are pairs), with energy $\epsilon - e\phi_0$ at the wall. The ϵ's refer to midplane kinetic energy ($\| + \perp$). If we use a bar and superscript SF to indicate an average over only the loss region appropriate to the given species, so that $\bar{\epsilon}^{SF}$ is the average midplane energy of a particle that is leaving the system, we may write

$$\mathcal{F}_i \sim F_i(\bar{\epsilon}_i^{SF} + e\phi_0), \qquad \mathcal{F}_e \sim F_e(\bar{\epsilon}_i^{SF} - e\phi_0)$$

where F_i and F_e are the ion and electron loss fluxes measured at the wall. Equation (38) thus becomes

$$\Delta\left[F_i(\bar{\epsilon}_i^{SF} + e\phi_0) + F_e(\bar{\epsilon}_e^{SF} - e\phi_0)\right] \approx 0, \tag{40}$$

where we have neglected $F_x T_W$ as second order in Δ. Since the externally supplied electrons are assumed not to affect the internal source of ions balancing F_i we must have $\Delta F_i = 0$. We also assume $\Delta\chi \ll \chi$ for all quantities $\chi = e\phi_0$, $\bar{\epsilon}^{SF}$, F, appearing in Eq. (40), i.e., we assume F_x is sufficiently small that the macroscopic properties of the new steady state are not greatly different from those in the absence of F_x.

Two more-or-less compensating errors in the earlier discussion of this problem[42] should now be pointed out. Equation (40) may be expanded so that it has the form

$$(\bar{\epsilon}_e^{SF} - e\phi_0)\Delta F_e + F(\Delta\bar{\epsilon}_e^{SF} + \Delta\bar{\epsilon}_i^{SF}) \approx 0.$$

First, the $e\phi_0$ term was missing (cf Eq. (11) of that report). Second it was stated that $\bar{\epsilon}_e^{SF} \approx e\phi_0$, i.e., the midplane energy of the escaping electrons was taken to be just the electrostatic barrier height. This is not generally true, because the electrons carry out their perpendicular energy (unless they have none when they are lost). Using the model electron distribution given by Eq. (C1) in Appendix C, we now show that for an isotropic damped Maxwellain, $\bar{\epsilon}_e^{SF} - e\phi_0 \sim T_e$.

3. Evaluation of Mean Electron Loss Energy

The height of the distribution $g(x,y)$ at the loss boundary $x = x_l(y)$ is

$$g\left[x_l(y),y\right] \equiv C(y) = \xi e^{-y^2/c_e^2} e^{-x_l^2(y)/c_e^2}$$

$$\approx \xi e^{-(R_W y^2 + 2e\phi_0/m)/c_e^2}$$

where $x_l(y)$. Eq. (C1) of Appendix C has been approximated by $x_l^2 = (R_W - 1)y^2 + 2e\phi_0/m$ for all y, not just $y < y_0$. (The difference occurs in a lightly populated part of velocity space.) Since the SF distribution comes mostly from a narrow strip of constant width in x^2 just outside x_l^2, the properties of the SF distribution are those of $C(y)$. The quantity $\bar{\epsilon}_e^{SF} - e\phi_0$ is then

$$\frac{\frac{m}{2}\int C(y)\left[y^2 + x_l^2(y) - 2e\phi_0/m\right] 2\pi y dy}{\int C(y) 2\pi y dy},$$

so

$$\bar{\epsilon}_e^{SF} - e\phi_0 \approx \frac{mc_e^2}{2} \frac{\int_0^\infty e^{-u} u du}{\int_0^\infty e^{-u} du} = \frac{mc_e^2}{2},$$

where $u \equiv R_w y^2/c_e^2$. Thus

$$\bar{\epsilon}_e^{SF} - e\phi_0 \approx \Psi_e. \tag{41}$$

4. Separation into Beam and Plasma Electrons

We proceed on the basis of several new assumptions:

(a) Electrons born at the wall have a distribution f_x in the midplane velocity space, and are treated as distinguishable from electrons from the primary internal plasma source. The latter have a distribution f_p. Exchange of electrons between f_p and f_x is not allowed, but energy exchange does occur. The total electron distribution is $f_e = f_p + f_x$, with density $n_e = n_p + n_x$. Likewise for the altered distribution g_e defined in Section IIB: $g_e = g_p + g_x$. Densities will refer to midplane values.

(b) Since the external source flux F_x is small compared with the internal electron source flux F_p, it is physically reasonable to assume that the plasma still contains mainly p-electrons in the new steady state, i.e., $n_x \ll n_p$. Since n_p cannot increase with time in the new steady state, this forces us to assume n_p is constant. In the new steady state, the loss rate ν_p of a p-electron is time-invariant, and the loss flux $F_p = n_p L \nu_p$ is still equal to the internal p-electron input flux (which is equal to the ion input flux). This means $\Delta F_p = 0$, where Δ indicates the change from the old steady state (with $F_x = 0$) to the new steady state (with $F_x > 0$). Since $n = n_p + n_x$ is time-invariant, so is n_x, and thus all the x-electrons going into f_x are coming out. So the loss flux F_x is equal to the input flux $|F_x|$ from the

wall: $\Delta F_x = F_x$. F_x is first order in Δ.

(c) Ions and electrons of p-source origin are born with average midplane kinetic energies $\bar{\epsilon}_i$, $\bar{\epsilon}_e$ which are independent of ϕ_0 (as in the case of Lorentz ionization). We have already tacitly assumed this by not including changes in the energy source rates in Eq. (38).

(d) The result $\bar{\epsilon}_e^{SF} - e\phi_0 \approx T_e$ just derived applies to the essentially isotropic p-distribution: $\bar{\epsilon}_p^{SF} - e\phi_0 \approx T_p$. Thus the mean energy carried out upon loss of a p-electron is T_p, and $\mathcal{F}_p = F_p T_p$. Similarly we will define T^* as the mean energy carried out upon loss of an x-electron: $\mathcal{F}_x = F_x T^*$. In general $T^* < T_{x\perp}$ because the loss process is biased toward losing newly-injected cold x-electrons rather than thermalized x-electrons.

(e) Because the x-electrons are injected near the phase-space loss boundary, their typical loss rate ν_x (including transit time) will not be less than ν_p, and in general $\nu_x \geq \nu_p$. If pitch-angle scattering predominates, the x-electrons will be scattered <u>into</u> the trapping region (because of its shape and the fact that x-electrons are injected with the minimum escape energy, i.e., $\epsilon_\parallel = e\phi_0$). In this case $\nu_x \sim \nu_p$. But if energy spreading can increase the energy of any significant fraction of x-electrons at a rate comparable to that for angle-scattering, then $\nu_x \gg \nu_p$.

(f) The x-electrons are injected cold; so when ν_x is of the order of the reciprocal transit time, T^* is some rather small value ($T^* \ll T_p$), and $T_{x\parallel}$ is of order $e\phi_0$. Then f_x is sharply peaked at $\epsilon_\parallel = e\phi_0$, $\epsilon_\perp \approx 0$. However, f_x may still have a hump of thermalized electrons centered at $x = 0$, $y = 0$. This hump should have an effective temperature $\sim T_p$,

reflecting the fact that these electrons were thermalized before they were lost, and thus their loss time is of order $\nu_p \ll \nu_x$.

(g) The p-electron loss rate ν_p is a function of n, ϕ_0, and T_p. The distribution f_p remains essentially isotropic, so

$$\Delta\nu_p = \frac{\partial\nu}{\partial\phi_0}\Delta\phi_0 + \frac{\partial\nu}{\partial n}\Delta n + \frac{\partial\nu}{\partial T_p}\Delta T_p.$$

(h) The ion loss rate ν_i is essentially independent of the electron distribution, and depends only very weakly on ϕ_0. Since $\Delta F_i = 0$ (F_i equals the unaltered ion source flux), $F_i = Ln_i\nu_i$ then implies n is constant: $\Delta n \approx 0$. Also note that $n_i = n = n_p + n_x$ and $n_x = F_x/L\nu_x$ together imply

$$\Delta n_p = \Delta n - \frac{n\nu_p}{\nu_x}\frac{F_x}{F} \approx -\frac{n\nu_p}{\nu_x}\frac{F_x}{F}.$$

(Waiving of this assumption is discussed below.)

(i) The energy carried out by ions is $\mathcal{F}_i = F_i(\bar{\epsilon}_i^{SF} + e\phi_0)$, where $\bar{\epsilon}_i^{SF}$ depends very weakly on ϕ_0 through $\phi_0 - \phi_L$ (discussed below), and is also essentially independent of the electron distribution. This allows us to set $\Delta\bar{\epsilon}_i^{SF} \approx 0$.

To see the physical significance of condition (i), observe first that $\bar{\epsilon}_i^{SF}$ depends on ϕ_0 only through $\phi_0 - \phi_L$, since only $\phi_0 - \phi_L$ occurs in the expression for the ion loss boundary. If, for example, all the potential change $\Delta\phi$ occurs in region II, i.e., if the potential shape between s = L and s = -L is not changed, then condition (i) is satisfied. It is also satisfied to a good approximation if the ion loss comes almost entirely from pitch-angle scattering: ions wander

out along the lines $\epsilon_{\parallel} + \epsilon_{\perp}$ = constant, and each element of density on the old loss boundary transforms to one with the same total energy on the altered loss boundary, except for the very small region near the minimum ion trapping energy.

5. Results

We summarize assumptions (a) through (i) as follows:

$$\Delta F_p = \Delta F_i = 0 \qquad \Delta F_x = F_x$$

$$F_i = L\nu_i n_i = L\nu_i n \qquad \nu_i \text{ independent of } \phi_0,\ T_e \therefore \Delta n \approx 0$$

$$F_p = L\nu_p n_p$$

$$F_x = L\nu_x n_x$$

$$n_p + n_x = n$$

$$\mathcal{F}_i = F_i(\bar{\epsilon}_i^{SF} + e\phi_0) \qquad \bar{\epsilon}_i^{SF} \text{ depends only on } T_i \therefore \Delta\bar{\epsilon}_i^{SF} \approx 0.$$

$$\mathcal{F}_p = F_p T_p$$

$$\mathcal{F}_x = F_x T^*$$

$$\nu_p = \nu_p(n, \phi_0, T_p)$$

These assumptions allow a solution for $\Delta\phi_0$ and ΔT_p. To express $\Delta T_{e\perp}$ and ΔT_e in terms of ΔT_p, we proceed from the definitions

$$T_{p\perp} \equiv \frac{\int \epsilon_\perp f_p d^3v}{n_p} \qquad T_{x\perp} \equiv \frac{\int \epsilon_\perp f_x d^3v}{n_x}$$

$$T_{e\perp} \equiv \frac{\int \epsilon_\perp f_p d^3v + \int \epsilon_\perp f_x d^3v}{n_p + n_x}$$

$$= T_p\left(1 - \frac{n_x}{n}\right) + T_{x\perp}\frac{n_x}{n} \qquad \text{to first order in } n_x/n$$

$$\text{because } T_{p\perp} \approx T_{p\parallel} \approx T_p$$

so $$\Delta T_{e\perp} = \Delta T_p + \frac{n_x}{n} (T_{x\perp} - T_e) \tag{42}$$

since $T_e = T_p$ to zero order. Likewise,

$$\Delta T_{e\parallel} = \Delta T_p + \frac{n_x}{n} (T_{x\parallel} - T_e). \tag{43}$$

With assumptions (a) through (i), the equations for conservation of particle flux and energy flux

$$n_p \Delta v_p + v_p \Delta n_p = \Delta F_p = 0$$

and $$\Delta \mathcal{F}_i + \Delta \mathcal{F}_p + \Delta \mathcal{F}_x = 0,$$

becomes $$n_p \left(\frac{\partial v_p}{\partial \phi_0} \right)_{n,T_p} \Delta \phi_0 + n_p \left(\frac{\partial v_p}{\partial T_p} \right)_{n,\phi_0} \Delta T_p + v_p \Delta n_p \approx 0 \tag{44}$$

and $$e\Delta\phi_0 + \Delta T_p + T^* F_x / F \approx 0. \tag{45}$$

Then, from $n_p + n_x = n$ and $\Delta n \approx 0$,

$$\Delta n_p \approx - n \frac{v_p}{v_x} \frac{F_x}{F}. \tag{46}$$

These equations give

$$\frac{\Delta e\phi_0}{T_e} \approx - \Gamma \frac{F_x}{F} \left[\frac{v_p}{v_x} + \frac{T^*}{T_e} \left(\frac{T_e}{v_p} \frac{\partial v_p}{\partial T_p} \right) \right] \tag{47}$$

and $$\frac{\Delta T_p}{T_e} \approx \Gamma \frac{F_x}{F} \left[\frac{v_p}{v_x} + \frac{T^*}{T_e} \left(\frac{T_e}{v_p} \frac{\partial v_p}{\partial e\phi_0} \right) \right], \tag{48}$$

where $$\Gamma = \left[- \frac{T_e}{\nu_p} \frac{\partial \nu_p}{\partial e\phi_0} + \frac{T_e}{\nu_p} \frac{\partial \nu_p}{\partial T_p} \right]^{-1} . \tag{49}$$

The square brackets in Eqs. (47) and (49) are positive since ν_p increases with T_p and decreases with ϕ_0. Using Eqs. (42) and (43) then one has

$$\frac{\Delta T_{e\perp}}{T_e} \sim - \frac{F_x}{F} \left[\Gamma \frac{T^*}{T_e} \left(- \frac{T_e}{\nu_p} \frac{\partial \nu_p}{e\phi_0} \right) - \frac{\nu_p}{\nu_x} \left(1 - \Gamma - \frac{T_{x\perp}}{T_e} \right) \right] \tag{50}$$

and

$$\frac{\Delta T_{e\parallel}}{T_e} \sim - \frac{F_x}{F} \left[\Gamma \frac{T^*}{T_e} \left(- \frac{T_e}{\nu_p} \frac{\partial \nu_p}{\partial e\phi_0} \right) - \frac{\nu_p}{\nu_x} \left(\frac{T_{x\parallel}}{T_e} - 1 - \Gamma \right) \right] . \tag{51}$$

At this point let us introduce a model for $\nu_p(\phi, n, T_p)$:

$$\nu_p \propto n\phi_0^{-\gamma} e^{-e\phi_0/T_p} \tag{52}$$

where γ is a dimensionless constant of order unity. When $\gamma = 3/2$, this is just the model used by BenDaniel.[1] In the model of Appendix C,

$$\gamma = - \frac{\partial \ln (\xi/k)}{\partial \ln \varphi_0} \qquad (\varphi_0 \equiv e\phi_0/T_e)$$

so that γ measures the sensitivity of the electron distribution tail shape to changes in the escape energy $e\phi_0$. (Features of the velocity distribution near the loss boundary cutoff are discussed by deBoer[43] for hard sphere collisions; the Coulomb case is mentioned.)

With the model (52) for ν_p, Eqs. (47) through (51) become

$$\frac{\Delta e\phi_0}{T_e} \approx - \Gamma \frac{F_x}{F} \left[\frac{\nu_p}{\nu_x} + \varphi_0 \frac{T^*}{T_e} \right] \tag{53}$$

$$\frac{\Delta T_p}{T_e} \approx \Gamma \frac{F_x}{F}\left[\frac{\nu_p}{\nu_x} - \left(1 + \frac{\gamma}{\varphi_0}\right)\frac{T^*}{T_e}\right] \tag{54}$$

$$\Gamma = (\varphi_0 + 1 + \gamma/\varphi_0)^{-1} \qquad (\Gamma < 1) \tag{55}$$

$$\frac{\Delta T_{e\perp}}{T_e} \approx -\frac{F_x}{F}\left[\left(1 - \Gamma - \frac{T_{x\perp}}{T_e}\right)\frac{\nu_p}{\nu_x} + \left(1 + \frac{\gamma}{\varphi_0}\right)\frac{T^*}{T_e}\right] \tag{56}$$

$$\frac{\Delta T_{e\parallel}}{T_e} \approx -\frac{F_x}{F}\left[-\left(\frac{T_{x\parallel}}{T_e} - 1 + \Gamma\right)\frac{\nu_p}{\nu_x} + \Gamma\left(1 + \frac{\gamma}{\varphi_0}\right)\frac{T^*}{T_e}\right]. \tag{57}$$

It is obvious that when the x-electrons are not assimilated, i.e., when $\nu_x \gg \nu_p$ and $T^* \ll T_e$, all the quantities $\Delta e\phi_0/T_e$, $\Delta T/T_e$ are much smaller than F_x/F. In the opposite limit, when the x-electrons are isotropized and assimilated into the ordinary p-electron distribution shape, $\nu_x \approx \nu_p$; and since the energy loss flux comes from a thermalized bump of density n_1 ($n_1 \ll n_x$) with loss rate ν_p and not from the nonthermalized spike of essentially zero perpendicular energy, one has

$$\frac{T^*}{T_e} \sim \frac{n_1}{n_x}\frac{\nu_p}{\nu_x}$$

where $n_1 \approx n_x$ in the limit of good thermalization. (We have used $F_x = n_x\nu_x$.) In this case then

$$\frac{e\Delta\phi_0}{T_e} \sim -\frac{F_x}{F}$$

$$-\frac{\Delta T_p}{T_p} \sim \frac{\gamma\Gamma}{\varphi_0}\frac{F_x}{F} \ll \frac{F_x}{F}$$

$$-\frac{\Delta T_{e\perp}}{T_e} \sim \frac{\gamma\Gamma}{\varphi_0}\frac{F_x}{F} \ll \frac{F_x}{F}$$

$$\frac{\Delta T_{e\parallel}}{T_e} \sim \left[\left(\frac{T_{x\parallel}}{T_e} - 1\right) - \frac{\gamma\Gamma}{\varphi_0}\right]\frac{F_x}{F} \ll \frac{F_x}{F}.$$

Thus the temperature changes are small in either case, but the plasma potential changes noticeably if the electrons from the wall are randomized in velocity, i.e., well trapped by the plasma.

6. Discussion

Let $\nu_p/\nu_x \equiv \alpha$. When $\alpha \ll 1$, the quantities $|e\Delta\phi_0/T_e|$ and $|e\Delta T_j/T_e|$ for $j = p, e_\perp, e_\parallel$ are small, of order α, compared with F_x/F. Most of the electrons from the walls return to the walls within a few transit times and their distribution has a sharp peak at $x^2 = 2e\phi_0/m$, $y \approx 0$. Because this is at the loss boundary, the distribution of SF electrons (those escaping) has the same sharply peaked shape in y, superimposed on a broader gaussian in $\dot{y}$ representing the p-electrons and those x-electrons which have been trapped. The SF electrons in the sharp peak do not carry appreciable energy out of the plasma. They entered with none, and leave with none. The plasma potential ϕ_0 need not decrease much to bring the total electron loss flux up to $F + F_x$, the new total input flux, because this is done by the change in the shape of the distribution $f_p + f_x$.

In the opposite limit, $\alpha \approx 1$, electrons from the wall have a dis-

tribution with more or less the same shape as the ordinary plasma electrons, because they are effectively thermalized and trapped. There may be a small peak in their distribution as described above, but this is swamped by the larger, nearly isotropic, nearly Maxwellian hump. These electrons entered with no $\epsilon_\perp$. They gain energy from the plasma through scattering and enhance the perpendicular energy loss when they are lost; this means the ions must carry out less energy, and ϕ_0 must drop ($\Delta\phi < 0$) to accomplish this.

In either of these cases, Eqs. (38) and (40) give

$$\Delta\bar{\epsilon}_i^{SF} + \Delta\bar{\epsilon}_e^{SF} = - T_e F_x/F. \tag{58}$$

In general, escaping electrons and ions have exchanged energy via collisions and via the plasma potential. When $F_i = F_e$, the sum $\bar{\epsilon}_e^{SF} + \bar{\epsilon}_i^{SF}$ must equal the sum of the source energies. But when the wall emits electrons as an additional source, in excess of the ions source strength, the loss rates are correspondingly unequal, so that Eq. (58) holds (assuming electrons born cold at the wall). This decoupling of the ion and electron throughput rates is similar to that discussed in Ref. 19.

When assumption (h) fails, i.e., when the ion loss rate ν_i changes (due to either the change in the ion loss boundary with $\phi_0 - \phi_L$, or the change in the electron distribution) one has

$$\frac{\Delta n_p}{n} = \frac{\Delta n}{n} - \frac{\nu_p}{\nu_x}\frac{F_x}{F};$$

Eqs. (47) and (53) then have on their right-hand sides the additional term $+\Gamma\Delta n/n$, and one can write

$$-\Delta n/n = \Delta\nu_i/\nu_i.$$

Also, if $\Delta\bar{\epsilon}_i^{SF}$ is not neglected, the right-hand sides of Eqs. (47)

and (53) have yet another extra term:

$$-\Gamma\varphi_0\Delta\bar{\epsilon}_i^{SF}/T_e,$$

and the equations for $\Delta T_{e\|}/T_e$ and $\Delta T_{e\perp}/T_e$ have an extra term $-\Delta\bar{\epsilon}_i^{SF}/T_e$ on the right-hand sides.

In all the results of this section, the values of ν_x and T^* have been left as arbitrary parameters, discussed only in limiting cases. The actual values depend on the details of the scattering mechanism. Even once a mechanism is assumed (say Coulomb scattering without non-thermal waves or neutrals) the values must be found by computer solution of the appropriate Fokker-Plance equation (although it appears that the linearized F-P equation for f_x may be used instead of the full F-P equation for $f_p + f_x$). Such a computation has not been done as part of this study, but represents an interesting, well-defined area for further exploration. The resultant electron distribution f_x should look qualitatively as in Fig. 14.

7. Fraction of x-Electrons Trapped for Longer than One Transit

A lower bound on the fraction of "x" electrons trapped for more than one transit comes from the energy and angle diffusion of test electrons in a thermal plasma. (This gives a lower bound because if the electron distribution decays rapidly outside the loss boundary, scattering of a test electron upward in energy is less probable than for a thermal distribution of background electrons.) For $e\phi_0 \sim 4T_e$ and $c_e \sim 10c_i$ the ions contribute negligibly, and the expectation value of the energy loss of an electron with kinetic energy $\epsilon_{\|}$ after passing a distance L though a thermal plasma of density n and Debye length λ_D

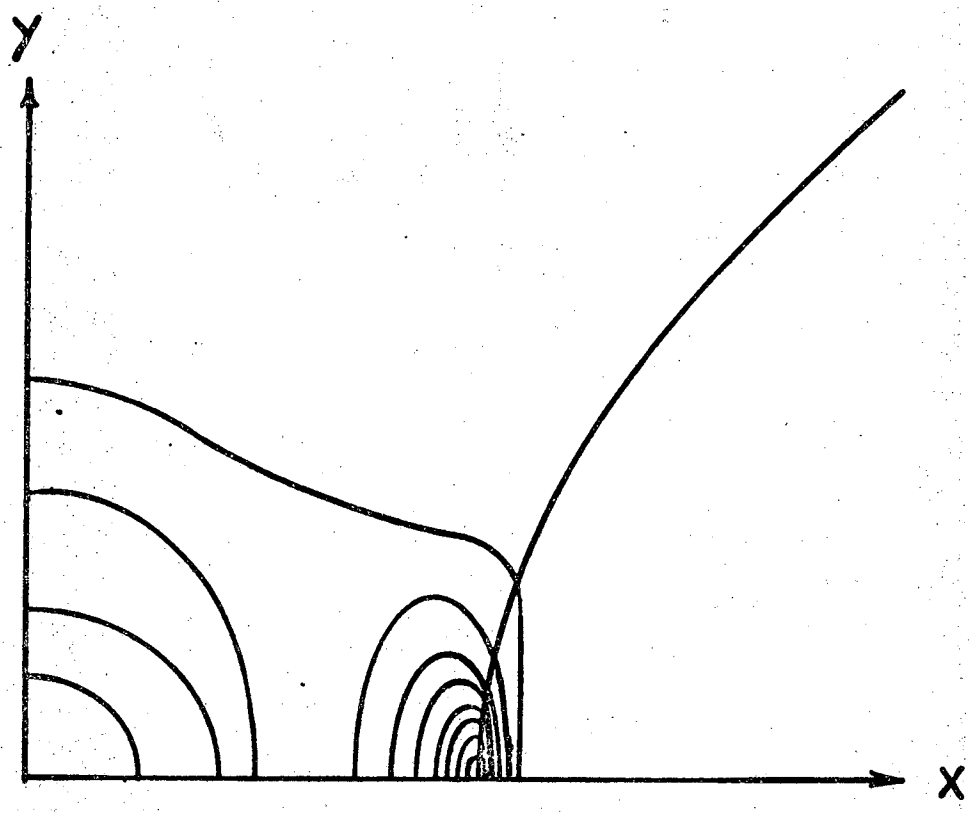

Fig. 14. Contours of hypothetical midplane velocity distribution, f_x, of electrons born cold at the end-walls. Also shown: electron loss boundary.

is[44]

$$-\frac{\overline{\delta\epsilon}}{T_e} \sim \frac{1}{2}\left(\frac{T_e}{\epsilon_\parallel}\right)^{1/2}\frac{L}{\lambda_D}\Lambda^{-1}(1+\tfrac{1}{2}\ln 3.5\Lambda), \tag{59}$$

where $\Lambda = 4\pi n\lambda_D^3$. When this is small, the increase in the parallel energy spread of f_x is

$$\frac{\delta\epsilon_\parallel}{T_e} \sim \left(\frac{\overline{\delta\epsilon}}{T_e}\right)^{1/2} \tag{60}$$

[see Eqs. (5-15) and (5-16) of Ref. 16. Limitations of the estimate are discussed there.] Thus the spreading due to diffusion is much larger than the slowing due to dynamic friction when these are related in the usual collisional way. (With nonthermal waves present the relation may change, and diffusion may be strongly velocity-dependent near the velocity-space boundary of the wave spectrum.) The mean square angle deflection is 45.

$$(\delta\theta)^2 \sim \left(\frac{T_e}{\epsilon_\parallel}\right)^2 \frac{L}{\lambda_D}\Lambda^{-1}\ln\Lambda. \tag{61}$$

For $\epsilon_\parallel = e\phi_0 = 4T_e$,

$$(\delta\theta)^2 \approx \frac{1}{2}\left(\frac{\delta\epsilon_\parallel}{T_e}\right)^2 \approx \frac{1}{2}\frac{\delta\epsilon}{T_e}.$$

For $n \sim n_0 = 10^{10}$ cm^{-3} and $T_e = 10$ eV, or for $n_0 = 10^{13}$ cm^{-3} and $T_e = 100$ eV, one has $n\lambda_D^3 \approx 1.2 \times 10^5$ so that

$$-\overline{\delta\epsilon}/T_e \sim 0.6 \times 10^{-6}\, L/\lambda_D.$$

For a one-meter traversal, $-\overline{\delta\epsilon}/T_e \sim 3 \times 10^{-3}$ in $n = 10^{10}$ at 10 eV, and $-\overline{\delta\epsilon}/T_e \sim 0.03$ in $n = 10^{13}$ at 100 eV. In the latter case,

$$(\delta\theta)_{rms} \sim 7 \text{ deg.}$$

But the sensitive dependence on T_e ($\overline{\delta\epsilon}/\epsilon_{\|} \propto T_e^{-2}$) means that for $n = 10^{13}$ and $T_e = 10$ eV, $\delta\epsilon/T_e \sim 3$ and $(\delta\theta)_{rms} \sim \pi/2$, so that the minimum (collisional) scattering is not always small.

If dynamic friction is small, diffusive spreading causes somewhat less than half of the flux F_x to be scattered into the loss region (see Fig. 14) in a transit time. Thus the trapping fraction is larger than 1/2. The actual value can be determined only from computer calculation with a model for the scattering process. Finite temperature T_W of the x-electron source reduces this trapping fraction (by creating more electrons above the escape energy), and larger $R_W - 1$ increases the trapping fraction (by magnetically trapping electrons that have diffused in pitch angle).

8. Distributed External Source

The effective temperature of the x-electrons (and thus their stability) can be greatly increased if they are produced in region II by, for example, photoionization, instead of at the wall. Then they populate the segment between $e(\phi_0 - \phi_L)$ and $e(\phi_0 - \phi_W)$ in midplane energy space along the $\epsilon_{\|}$ axis. Their $T_{\perp}$ is still small, but spreading of their parallel energy at any spatial point implies a much smaller peak height. For this case, also, all the x-electrons are trapped, since the external source is in the trapping region rather than just outside the loss boundary. The only practical difference in flux

balance conditions is that cold ions are also produced by the "x" source, and are accelerated out by the electric field. Thus the measured ion flux at the wall is once again equal to the electron flux (assuming equal internal sources). Thus there is a ΔF_i and

$$\Delta\left[F_i(\bar{\epsilon}_i^{SF} + e\phi_0)\right] \sim \langle e\phi\rangle_{II}|F_x(L)|\,\frac{R_W}{R_L} + F\Delta e\phi_0 + F\Delta\bar{\epsilon}_i^{SF}$$

where F_x now must be measured inboard of the x-source, say at $s = L$, and where $\langle e\phi\rangle_{II}$ is a source-weighted average over region II. (The new cold ions from the "x" source are not included when calculating $\bar{\epsilon}_i^{SF}$, since they do not pass through the midplane.) To maintain steady state without a change in the primary internal source, one must have

$$\Delta F_e(L) = F_x(L),$$

or

$$\Delta F_e(W) = (R_W/R_L)F_x(L).$$

The flux of x-ions coming out at $s = W$ is the same, except for the flux-tube area factor R_W/R_L, as the flux of new x-electrons going into region I at $s = L$. Writing $F_x \equiv (R_W/R_L)F_x(L)$ and $\Delta F_e \equiv \Delta F_e(W)$ as before, Eq. (45) is modified to read

$$\Delta e\phi_0 + \Delta T_p + (T^* + \langle e\phi\rangle_{II})F_x/F \approx 0 \qquad (62)$$

(again neglecting $\Delta\bar{\epsilon}_i^{SF}$). This is the same as Eq. (45), but with T^* replaced by $T^* + \langle e\phi\rangle_{II}$. Thus the equations for $\Delta e\phi_0$, ΔT_p, $\Delta T_{e\perp}$, $\Delta T_{e\parallel}$ are the same as Eqs. (47) through (51) [or (53) through (57)] with the exception that T^* is replaced by $T^* + \langle e\phi\rangle_{II}$. The physical significance of the $\langle e\phi\rangle_{II}$ contribution is that not only do the x-electrons gain energy from the plasma by scattering and then lose it to the walls, but

also x-ions born in region II transfer energy to the walls immediately when they are accelerated out. Thus the external source heats the end-walls at the expense of reducing ϕ_0, and this occurs even more when electron-ion pairs are born at nonzero $\phi(s)$ in region II than when they are born at the wall, where $\phi = 0$.

Incidentally, we note that this analysis is also true for a cold source placed in region I also, since the location of the source with respect to the mirror was not essential to the argument given. For a localized cold source $\langle e\phi \rangle_{II}$ is replaced by $e\phi$ at the source, wherever it is situated. The case of emission from the wall is now seen to be a special case of this more general result, as long as the stability is not altered.

B. Two-Stream Instability Resulting from External Electron Source

1. Nature of the Problem

In this section we consider qualitatively the results of unstable interaction between electrons emitted by the walls and the plasma in regions I and II. Analyses of an electron beam entering a uniform, bounded plasma[46,47] have predicted instability most violent rather near the plasma boundary, and this is in agreement with observations.[48,49] The same situation is expected when electrons produced at the end-walls of a mirror device interact with the tenuous ST electron component in region II.

Of course, the full problem of steady-state wave amplitudes in this inhomogeneous plasma-beam system (with particle source and loss) has not been solved. To do so would require taking into account:

(a) emission and absorption of waves at different points,

(b) regenerative effects[50] (where $\omega = N\omega_{bounce}$ for some large integer N) which can alter the usual Landau damping,

(c) finite-length effects on the wavenumber spectrum,

(d) nonlinear mode-coupling, e.g., between plasma waves and cyclotron waves[51] or low frequency beam waves,[52]

(e) the nonresonant part of the diffusion tensor (which allegedly heats the main distribution of electrons),[53]

(f) depletion of the distribution by the loss process,

(g) boundary conditions on waves at the sheath,

(h) failure of the WKB approximation at the turning points of particles resonant with a given wave, and

(i) beam bunching and coherence effects[47] due to trapping in finite amplitude waves.

Recent work by Kaufman and Nakayama[54] includes several of these effects (a, b, c), and gives the formal equations for a one-dimensional problem, although applying them to a case like the present one is quite difficult. Portions of topics (a) and (d) are treated by Kopecky and Preinhaelter,[51] but their results do not apply where $\omega_{pe} \ll \omega_{ce}$ everywhere in the system. In this case there is no coupling to electron cyclotron oscillations.[55] Since $\omega_{pe}^2 \equiv 3 \times 10^9$ n (c.g.s.), while a typical ω_{ce}^2 (B = 10 kG) would be 3.4×10^{22}, it follows that $\omega_{pe}^2/\omega_{ce}^2$ is small everywhere in the device unless $n/B^2 > 10^5$ cm^{-3} G^{-2}, e.g. $n > 10^{13}$ cm^{-3} and/or B < 10 kG. Since densities in region II are expected to be much smaller than the central density n_0, certainly the end region can be regarded as "highly magnetized," so that diffusion

characteristics in the resonant region of local velocity space will be lines of constant $v_\perp$.[55] In other words, μ is approximately conserved by the instability. Even if electrostatic waves propagate at an angle to $\vec{B}$ there is no significant quasilinear diffusion in $v_\perp$ except due to gyroresonance at uninterestingly large velocities.

2. The Unstable Waves

A representative dispersion relation $k(\omega)$ for a (homogeneous plasma with a weak bump in the tail of f_e is given in Fig. 15.[56,49] This weak-beam situation probably describes fairly well the quasi-plateau state a moderate distance away from the introduction of a nearly mono-energetic beam. We will assume that, at low densities as here, the cyclotron wave interactions are weak compared with the interaction (circled in Fig. 15) between plasma waves

$$\mathrm{Re}\ \omega_k^{(p)} \approx \omega_p \left[1 + \frac{3}{2}(k\lambda_D)^2 + \cdots\right] \quad \text{for } k\lambda_D \ll 1 \tag{63}$$

and beam space-charge waves (doppler shifted)[52]

$$\mathrm{Re}\ \omega_k^{(b)} \approx kv_0 \pm (n^x/n^{ST})^{1/2}\mathrm{Re}\left[|k^2 v_0^2/\omega_p^2 - 1|^{-1/2}\right] \tag{64}$$

where n^x is the density of beam electrons. If the wavelengths of interest are short compared with other spatial gradient lengths, a wave excited at $s = s_1$ will propagate to s_2 with ω constant, and k given by the local (WKB) dispersion relation, (63), or (64), with $\omega_p \to \omega_p(s)$ and $v_0 = v_0(s)$,

$$v_0(s) = \left[2e\phi(s)/m_e\right]^{1/2}.$$

The beam waves have $\omega/k \approx v_0$ and thus their wavelength increases as they

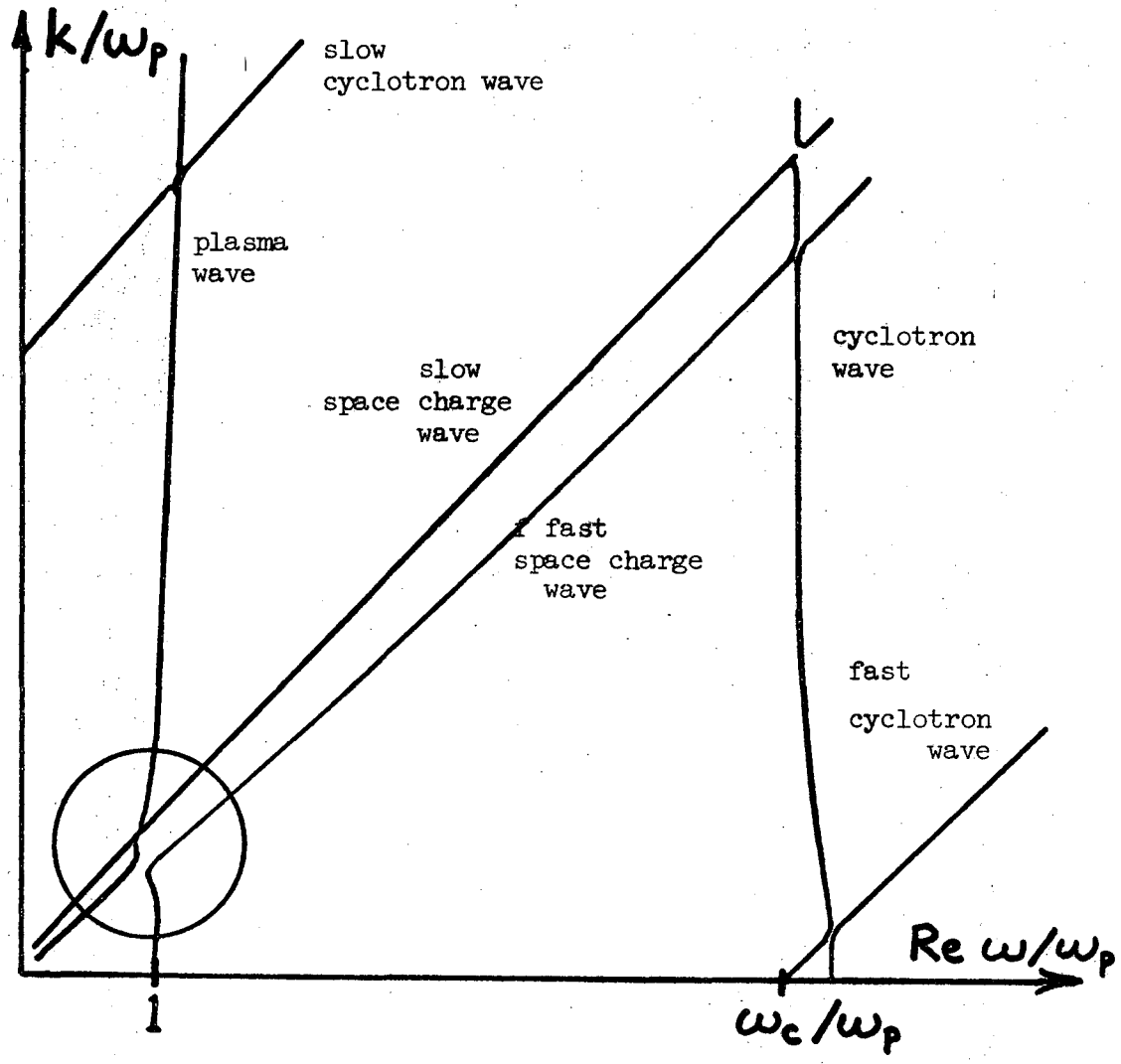

Fig. 15. Dispersion relation for plasma and weak beam ($\Delta v/v_0 \approx 0.6\sqrt{n^x/n}$).

Modes shown as intersecting inside circle have differing Im ω.

$\omega \approx \omega_p$ plasma wave

$\omega \approx \omega_c$ cyclotron wave

$\omega \approx kv_{0+}$ fast space charge wave on beam

$\omega \approx kv_{0-}$ slow space charge wave on beam

$\omega \approx \omega_c + kv_0$ fast cyclotron wave on beam

$\omega \approx -\omega_c + kv_0$ slow cyclotron wave on beam

propagate into region I. The plasma wave cannot go far toward s = 0 because the local plasma frequency increases with decreasing s, and the wave is soon attenuated by $\omega_p(s) > \omega$, or converted into a beam wave[52] in a distance of order $2\pi(n^{ST}/n^{x})^{1/2}\lambda_D$. (This description somewhat oversimplifies the dispersion relation in the circle region, where the wave is really neither of the above simple modes.)

Fainberg and Shapiro,[46] in theoretically analyzing a beam in a bounded but otherwise homogeneous plasma, conclude that after the wave saturation time the oscillations are strongest in a layer which in our problem is

$$\lambda_D(n_e^{ST}/n_e^{x})^{1/3} < W - s < (n_e^{ST}/n_e^{x})\lambda_D$$

(which may include all of region II and some of I). Energy carried into this region by the beam is carried out by oscillations. They estimate the energy density in this region; for our problem the estimate is

$$\mathcal{E}_{waves} \sim \left[e\phi(s)/4T_e(s)\right]^{1/2} n_e^{x} e\phi(s) ,$$

which is the same order as the beam kinetic energy $n_e^{x}e\phi(s)$, because the beam velocity is not much greater than thermal, i.e., the group velocity is not much smaller than the beam velocity. (If it were, the wave energy could be much larger than the beam energy.) This study, however, includes no reflection of waves from the opposite end of the device; the wave energy estimate may thus be too low.

Bernstein and Engelmann[57] estimate the wave energy for a homogeneous one-dimensional quasilinear problem. For our problem, where the plateau width at s in region II can be as large as the beam velocity

$v_0(s)$, their estimate becomes

$$\mathcal{E}_{wave} \lesssim \frac{\gamma_{max}}{\omega_p(s)} n_e(s) T_e(s) \ .$$

The linear growth rate[58] is of order $\omega_p(n_e^x/n_e)^{1/3}$, which is probably largest near the sheath, where $n_e^x/n_e \lesssim 1$. Thus

$$\mathcal{E}_{wave} \lesssim n_e(W^-) e\phi_W \ . \tag{65}$$

3. Model Assumptions

We proceed to illustrate a simple model based on the following ad-hoc assumptions:

(a) Electrons born at the wall are almost cold and are accelerated across the sheath potential $\phi_W > 0$ to form a beam. Any ions born at the wall return immediately to the wall without completely penetrating the sheath.

(b) The injected beam is strong enough not to be a "gentle" bump at $s = W^-$, but is not strong enough to violate $n_e^x < n_e^{ST} + n_e^{SF}$. The beam is emission limited, not space-charge limited.

(c) Wave-particle interactions near $s = W^-$ in region II are sufficiently strong that they scatter particles in $v_\parallel$ into a quasilinear or nonlinear final state in a time less than the transit time across region II. [The ratio of plasma period to transit time is of order $\lambda_D/(W - L)$.] Energy change in a transit time is thus not small, violating the assumption of Ref. 54.

(d) Particle trapping by waves may occur in the region of strongest interactions, and a quasi-plateau in f results, at least in the

midplane distribution.

(e) The waves travel into region I as space-charge waves on the beam, i.e., with $\omega \approx kv_b$, $v_b \approx \sqrt{2e\phi(s)/m_e}$. While the dispersion relation may be of "beam type" at $s = \bar{W}$, it is of "Landau type" farther inside the plasma because the sharp bump flattens to a plateau.[56]

(f) The waves cause rapid diffusion of plasma electrons in $v_\parallel$ over the resonance region, thus making $\partial f/\partial v_\parallel \approx 0$ in this region

4. Wave-Particle Resonance Localization in Mirror Systems

In the problem of a plasma in an electrostatic potential well, particles that resonate with a wave of phase velocity $v_0(s)$ at one point do so at all points, if the wave is "carried" on a beam moving with $v_0(s)$. Hence the stability criterion for such a wave is just

$$\frac{\partial}{\partial v_\parallel} \int dv_\perp^2 f(v_\parallel, v_\perp) \Big|_{v_\parallel = v_0} < 0 \ .$$

When magnetic mirror forces are present, this simple criterion breaks down, because only those particles with $v_\parallel = v_0$ and $\mu = 0$ resonate with the wave at all s. Those with $v_\parallel > v_0$ and $\mu \neq 0$ resonate only at some point on their orbit. The decrease in the number of resonantly absorbing particles at $v_\parallel = v_0$ is partly compensated for by the fact that all particles with $v_\parallel > v_0$ absorb small amounts of energy at some resonance points along their orbits.

This discussion leads to the conclusion that a system with bounce times dependent on μ should be less stable to two-stream turbulence onset than a system where the bounce time is independent of μ. A fairly sharp decrease in the maximum stable beam density should occur as a

slight magnetic field inhomogeneity is introduced. When the bounce time is independent of μ, all particles in the main distribution with $v_{\|} = \omega/k$ resonate with the beam space-charge wave and help damp it; but when only particles with $\mu \approx 0$ resonate for long path lengths, the same number of $\mu = 0$ beam electrons put energy into the wave, but fewer main-distribution electrons can effectively absorb the wave energy.

5. Electron Velocity Distribution with a Noninteracting "Beam of Externally Supplied Electrons

Consider the behavior of the electron distribution when a small flux $|F_x|$ of electrons is emitted by the walls. As a beginning stage, we imagine the case where the emitted x-electrons do not interact with each other or the rest of the electrons (and hence are not trapped). This give a spike in the tail of the electron distribution. Next, we turn on the two-stream interactions, assumed to produce scattering only in $v_{\|}$, not $v_{\perp}$. This gives the initial plateau on the electron distribution. Finally, we consider qualitatively the collisional steady state where the electrons, thrown into the plateau by plasma oscillations, diffuse in pitch angle as well as energy. A balance between the input rate to the plateau and diffusion out of the plateau (and eventually out of the system) determines the new steady state.

The wall, at zero potential, emits some distribution $f_x(W; v_{\|}, v_{\perp})$ of electrons. Each of these falls through the sheath, gaining kinetic energy $e\phi_W$ (ϕ_W is the potential at the sheath "edge" $s = W^-$, a Debye length or so away from the wall). Thus at $s = W^-$, no electron in class x has parallel energy less than $e\phi_W$. Compare this with the class of ST electrons, which has a rather ordinary, symmetric distribu-

tion function at $s = W^-$ (because they are being reflected by the sheath potential) with a temperature $T_e(W^-)$ certainly no greater than the mid-plane temperature T_e. The obvious conclusion is that, for any $s < W^-$, the $\underline{x}$ electrons form a spike, or bump, at

$$|v_\parallel| \geq \left(\frac{2e}{m_e}\phi_s\right)^{1/2}, \qquad (v_\parallel < 0),$$

just beyond the cutoff (for $\mu = 0$) of the symmetric ST distribution,

$$v_{esc} = v_0 \equiv \left(\frac{2e}{m_e}\phi_s\right)^{1/2}.$$

If the $\underline{x}$-electrons are born at the wall with a temperature $T_W \ll T_e(W^-)$, then at $s = W^-$ the bump corresponds to a density

$$n_e^{\,x} \sim \frac{|F_x|}{\sqrt{(2e/m_e)\phi_W}},$$

distributed over a velocity spread ($\delta\epsilon_\parallel \sim T_W$)

$$\delta v_\parallel = \frac{1}{2}\left(\frac{2}{m_e}T_W\right)\left(\frac{2}{m_e}e\phi_W\right)^{-1/2}, \qquad \delta(v_\perp^{\,2}) \sim \frac{2}{m_e}T_W, \tag{66}$$

even if none of these electrons are subsequently trapped in the system. This is to be compared with the density $n_e^{\,ST}(W^-)$, distributed over a velocity spread of order

$$v_\parallel \sim \left(\frac{2}{m_e}e\phi_W\right)^{1/2}, \qquad v_\perp^{\,2} \sim \frac{2}{m_e}(R_L - R_W)^{-1}e\phi_L, \tag{67}$$

provided $e\phi_L(R_L - R_W)^{-1} \leq T_e$. (This is just the maximum $\epsilon_\perp$ of the ST electrons; see Appendix C, section 1.) The flattening of the bump by waves leads to a profile at $v_\perp \approx 0$ qualitatively like the one in Fig. 16.

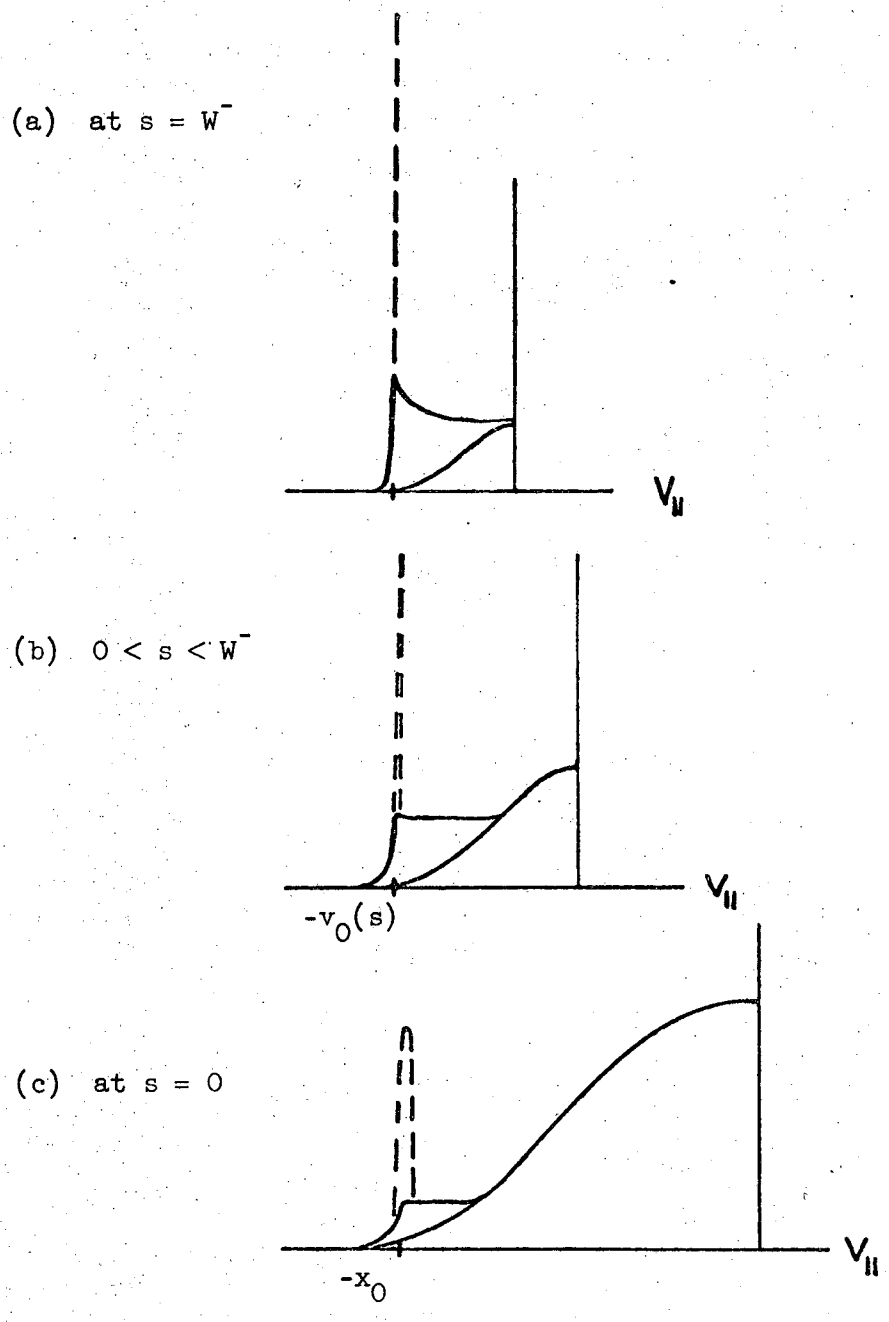

Fig. 16. Electron distribution function profile $f_e(s;v_{\|},0)$, for $v_{\|} < 0$, at various points s, Flattened "beam" is shown superimposed on the ST distribution. Unflattened "beam", in the absence of wave interactions, is shown dashed.

6. Velocity Distribution with a Diffusing "Beam" of Externally Supplied Electrons

We now discuss the collisional steady state problem when some of the flux $|F_x|$ is trapped for many transits. If one chooses to solve a Fokker-Planck-type equation[59] in velocity space alone at some spatial point s, there will be effectively a source at $v_{\|} = v_0(s)^+$, $v_\perp = 0$ (and one at $v_{\|} = -v_0(s)^+$, $v_\perp = 0$, if both walls emit). The loss condition may be represented approximately[60] by the boundary condition

$$f(s, v_{\|}, v_\perp) = 0$$

$$\text{at} \qquad v_{\|} = v_{esc}(s, v_\perp) + \Delta v(s, v_\perp)$$

$$\text{and} \qquad -v_{\|} = v_{esc}(s, v_\perp) + \Delta v(2L - s, v_\perp) \tag{68}$$

$$\text{where} \qquad \Delta v(s, v_\perp) \sim \int^s D_{\|} \frac{ds'}{v_{esc}} + (R_s - 1) \int^s D_\perp \frac{ds'}{v_{esc}}$$

corresponding to the decay width κ^{-1} in Appendix B. (Here $D_{\|}$ and $D_\perp$ are the elements of the velocity diffusivity tensor, assumed diagonal, at the escape boundary.) The integrated x-source strength at s is

$$\dot{n} = \frac{R_s}{R_w} \frac{|F_x|}{v_0(s)} \frac{\beta}{\tau} \tag{69}$$

where β is the fraction of the beam "absorbed", i.e., not lost to the walls in one transit (or sooner if there is beam reflection), and τ is the beam transit time. If s is near the emitting wall (but in the plasma and not the sheath), the velocity-space dimensions of the source are (as before)

$$\delta v_{\|} \sim (2v_0/c_w)^{-1} c_w , \qquad \delta v_{\perp} \sim c_w \equiv (2T_w/m_e)^{1/2}. \tag{70}$$

If s is not near the emitter, the sharply peaked "source" will have diffused to a width

$$\delta v_{\|} \sim \left[\int^{s} D_{\|} \frac{ds}{v_0}\right]^{1/2}, \qquad \delta v_{\perp} \sim \left[\int^{s} D_{\perp} \frac{ds}{v_0}\right]^{1/2} \tag{71}$$

by the time it reaches s to act as a source there.

But in addition to the spread $\delta v_{\|}$ in $v_{\|}$ due to ordinary diffusion, there will be a much larger spread, $v_0 - v_1$, caused by the waves. The "source strength" will be distributed from $v_1(s)$ (determined by marginal stability) up to $v_0(s)$ in such a way that $\partial f/\partial v_{\|} = 0$ over the source region; i.e., the source density will vary roughly as $f_p(v_1,0) - f_p(v_{\|},0)$, where f_p represents the distribution without waves or x-source. Though linear superposition does not really apply here, we may crudely consider f as the sum of f_p, maintained by the internal sources, and f_x due to the x sources alone. f_p satisfies a Fokker-Planck equation and is taken as given. To estimate f_x, one might ignore dynamic friction and the v-dependence of D;for v not too far from the source, f_x is approximately a solution of Poisson's equation

$$D_{\|} \frac{\partial^2 f_x}{\partial v_{\|}^2} + D_{\perp} \frac{1}{v_{\perp}} \frac{\partial}{\partial v_{\perp}}\left(v_{\perp} \frac{\partial f_x}{\partial v_{\perp}}\right) = S(v_{\|},v_{\perp}) + S(-v_{\|},v_{\perp}) \tag{72}$$

with the source S as just described, and boundary conditions (68). The peak height of f_x is then crudely of order

$$\frac{\dot{n} \ln \left[(v_0 - v_1)/\delta v_\perp\right]}{D_\perp (v_0 - v_1)}$$

where $\dot{n}$ is the integrated input rate, Eq. (69). This expression is derived as the maximum potential on the surface of a long prolate spheroid of uniform source density.[61] From this peak, f_x decays (e.g. in $v_\perp$) with a dependence somewhere between $1/v_\perp^2$ and $\ln 1/v_\perp$, for $v_\perp \lesssim c_e$. (Consider the weak dipole potential formed by a charged rod and its image in a grounded plane normal to it near one end.) For large $v_\perp$, or for $v_1 - v_\parallel \gtrsim c_e$, Eq. (72) breaks down (e.g., it gives infinite density), partly from neglect of dynamic friction, which moves particles toward the origin, and partly from the assumption of constant $D_\parallel$ and $D_\perp$ (a particle diffuses more or less along constant energy contours). The form of f_x for $v_\perp \gtrsim c_e$ should be Maxwellian in $v_\perp$.

A qualitative display of $v_\perp$ dependence of f at $v_\parallel \approx v_0$ is shown in Fig. 17, and the $v_\parallel$ dependence of f at $v_\perp = 0$ is shown in Fig. 16.

It is qualitatively obvious that if flattening of f by waves is ignored for $v_\perp \gg (2T_w/m_e)^{1/2}$, the external electron density $n_e(s)$ for a given value of $\phi(s)$ is increased by this trapping of $\underline{x}$ electrons. Quasineutrality thus requires a reduction of ϕ in region II. The magnitude of this reduction of ϕ depends on the final width in $v_\perp$ of the plateau. If this width is small, the change in $n_e(s)$ for given $\phi(s)$ will be small, but there is no reason to expect that this is the case. Some of the "density increase" from x-electron input is compensated by rapid diffusion of ST electrons with $\mu \approx$ zero across the resonance region and out of the system. The actual magnitude of the x-input flux

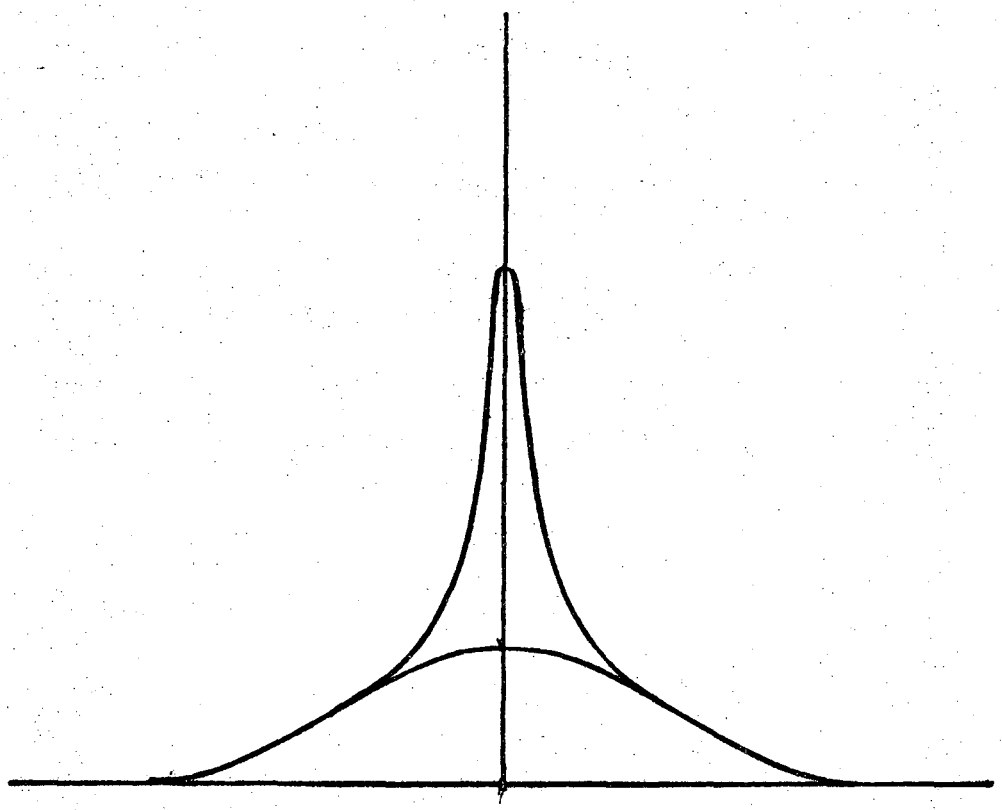

Fig. 17. Electron distribution profile $f(s;v_0(s)^{\bar{}},v_\perp)$, showing the unperturbed distribution f_p (lower curve) and the total $f = f_p + f_x$ (upper curve). Abscissa is any component of $v_\perp$.

is thus not easily distinguishable from the net input flux of particles with $T_e \sim T_W$; but this ambiguity is common to all two-stream analyses.

The "nearly collisionless" behavior of $f(s, v_\parallel, v_\perp)$ breaks down in the resonance part of phase space, including most or all of region II at low μ, because of the rapid diffusion in $v_\parallel$. See Fig. 18.

It is important whether wave amplitudes at the wall are small (as usually observed in experiments, e.g. Ref. 49). If they are not, there may be strong reflection of the beam on entry (in which case the "absorption coefficient" β is much reduced); in addition, the loss of resonant main-distribution electrons is enhanced. An estimate of β (or the "transmission coefficient" $1 - \beta$) from a purely diffusional model is not very reliable because dynamic friction slows beam electrons and increases the trapping. But in the unstable case, where the beam is spread downward over $\Delta v_\parallel \approx v_0 - v_1 \gg \delta v_\parallel$, essentially all beam electrons are trapped ($\beta = 1$) and lost much later by ordinary non-resonant diffusion processes.

7. Anisotropy Instability Near the Mirror

Finally, there is another streaming instability question to be looked at in connection with region II: ions are accelerated out (starting from a distribution, at $s = L$, with $T_\perp \gg T_\parallel$ locally) while the electron distribution is nearly symmetric in $v_\parallel$. In the frame of reference with the mean ion velocity (a non-inertial one) the electrons have a drift velocity that is maintained by the reflection of the ST electrons. Ordinarily this condition is sufficient for an ion cyclotron-wave streaming instability[62] if the difference between the mean velocities of ions and electrons is greater than a few times the ion velocity

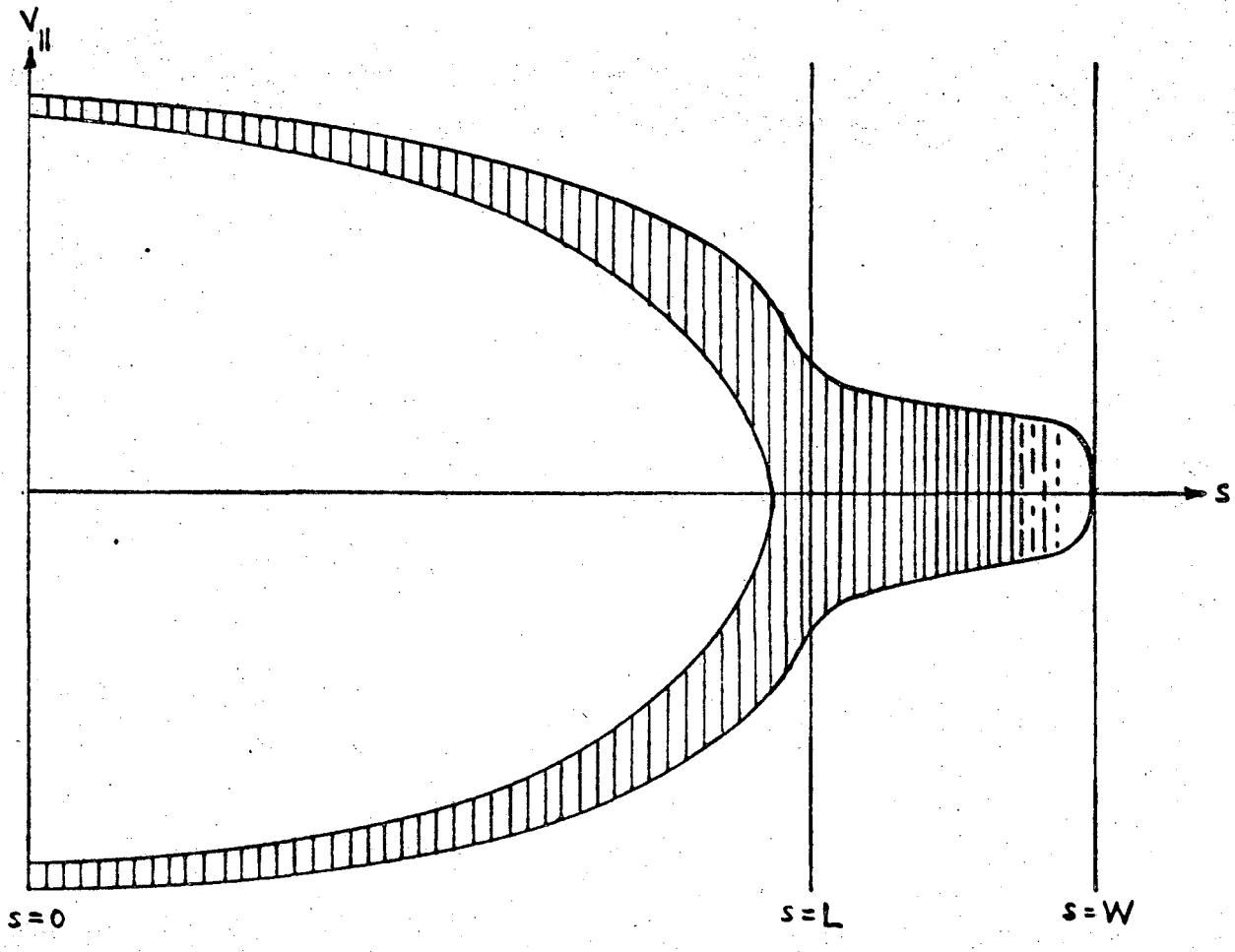

Fig. 18. Electron phase space for $\mu \approx 0$. Phase space density is flat in the shaded region.

spread about its mean. In the present case we expect that, although the spread in ion $v_{|||}$ is small near the mirror, the large spread in ion $v_{\perp}$ damps the cyclotron waves and the instability cannot grow. (And if the ion perpendicular energy is converted to parallel energy by magnetic expansion, the density becomes so low that the instability is probably unimportant even if it does exist far from the mirror.)

Perhaps more importantly, the large anisotropy of the ion distribution very near the mirror makes it susceptible to the anisotropy instability,[63,64] although the requirement of long parallel wavelength is probably not satisfied because of inhomogeneity. The behavior of these instabilities is not studied here but is suggested as a relevant research problem. Resonance between electron bounce and ion cyclotron motion probably does not need to be considered, as typically $\tau_e \omega_{ci} \gg 1$.

SYNOPSIS OF CHAPTER V

In this chapter we show that even with an external source of electrons, the steady-state density cannot <u>increase</u> with s in region II without being unstable to two-stream instability. This is because $\phi(s)$ and $B(s)$ both decrease in region II. (An exceptional s is the sheath at the wall, but stability conditions in terms of dn_e/ds at $s = W$ are well known.) This means that attempts to increase the external density to values exceeding the density at the mirror must result in instability (which slightly enhances the loss of confined electrons and also alters the conductivity of the external region). This appears to be true whether or not the orbits are nearly collisionless.

V. A COMMENT ON "DENSE EXTERNAL PLASMA"

Experimental and theoretical studies of plasma stabilization by "line tying"[3-5,65-67] both indicate that stabilization is usually improved as $n(s)$ in region II is made larger. In some experiments the density of cold plasma may be high throughout the device so that the plasma potential is reduced and the density $n(s)$ in region II is of the same order as n_0. However, in this section we show that in the absence of gradients due to recombination or directed sources in $L < s < W^-$, the values of $n(s)$ in region II in a <u>steady</u> state cannot be much <u>larger</u> than $n(L)$ without causing two-stream instability; the plasma purges most of the external density upon formation, sweeping electrons into region I as the plasma potential grows, and sweeping ions out to the walls.

We begin by defining a "normal" velocity distribution $f(s;v_\parallel,v_\perp)$ as one whose only maximum with respect to $v_\parallel$ is at $v_\parallel = 0$. We prove the following theorem:

Theorem 3: If $f(s;v_\parallel,v_\perp)$ is normal, and

If $\partial U_e(s,\mu)/\partial s > 0$ at s for all μ at which $f(s;v_\parallel,\sqrt{\frac{2}{m_e}\mu B}) \neq 0$,

Then $\frac{d}{ds}\frac{n(s)}{B(s)} < 0$

(and hence, if $dB/ds \leq 0$, certainly $dn(s)/ds < 0$).

Proof of theorem:

(a) <u>Collisionless Case</u>

In steady state, the Vlasov equation for guiding-center motion along s (with flux coordinates α,β normal to s) can be written

$$\frac{1}{m}\left[H,\rho\right] = v_{\|}\frac{\partial\rho}{\partial s} - \frac{1}{m}\frac{\partial U(s,\mu)}{\partial s}\frac{\partial\rho}{\partial v_{\|}} = 0 \qquad (73)$$

where $\rho = \rho(\alpha,\beta,s;v_{\|},v_{\perp})$ is $dN/d\alpha d\beta ds d^3v$ ($d^3v \equiv 2\pi v_{\perp}dv_{\perp}dv_{\|}$), and the density $dN/d^3r = n$ is $B\int d^3v\rho$, since $d\alpha d\beta ds = Bd^3r$. Hence $\int d^3v\rho = n/B$. Dividing Eq. (73) by $v_{\|}$ and integrating d^3v,

$$\frac{\partial(n/B)}{\partial s} = \frac{1}{m}\int d^3v\,\frac{1}{v_{\|}}\frac{\partial\rho}{\partial v_{\|}}\frac{\partial U}{\partial s}$$

$$= \frac{1}{m}\int 2\pi v_{\perp}dv_{\perp}\,\frac{\partial U(s,mv_{\perp}^2/2B)}{\partial s}\int dv_{\|}\,\frac{1}{v_{\|}}\frac{\partial\rho}{\partial v_{\|}} .$$

Now ρ is related to the usual velocity distribution $f(s;v_{\|},v_{\perp})$ at s;

$$d^3v f(s;v_{\|},\mathbf{v}_{\perp}) = n = B\int d^3v\rho(\alpha,\beta,s;v_{\|},v_{\perp}),$$

i.e., $\rho = f/B$. Using $B\frac{\partial}{\partial s}\left(\frac{n}{B}\right) = \frac{\partial n}{\partial s} - \frac{n}{B}\frac{\partial B}{\partial s}$ we have

$$\frac{\partial n}{\partial s} - \frac{n}{B}\frac{\partial B}{\partial s} = \frac{1}{m}\int 2\pi v_{\perp}dv_{\perp}\,\frac{\partial U}{\partial s}\int dv_{\|}\,\frac{1}{v_{\|}}\frac{\partial f}{\partial v_{\|}} . \qquad (74)$$

If f is "normal", $(1/v_{\|})(\partial f/\partial v_{\|})$ is always negative. Hence when $\partial U/\partial s > 0$ for all $v_{\perp}$,

$$\frac{\partial n}{\partial s} - \frac{n}{B}\frac{\partial B}{\partial s} < 0 .$$

(b) Collision-Dominated Case

For collision-dominated electrons $f \propto \exp\left[-(mv^2/2 + U)/T_e\right]$ and $n \propto Be^{-U/T_e}$, so

$$\frac{\partial n}{\partial s} - \frac{n}{B}\frac{\partial B}{\partial s} = \frac{n}{T_e}\frac{\partial U(s,0)}{\partial s} ,$$

the same as Eq. (74). (We neglect higher μ just for simplicity since

only cold electrons are collision-dominated.) This result should not be surprising, since if a collision term $\nu\rho$ is added to the Vlasov equation (73), the contribution after performing

$$\int_{-\infty}^{\infty} \frac{dv_{\|}}{v_{\|}} \nu\rho$$

is nearly zero, assuming ρ is almost even in $v_{\|}$.

For the same reason, a source $S(x,v_{\|},v_{\perp})$, even in $v_{\|}$, gives no contribution. This completes the proof.

Returning to Eq. (74), one may notice that for completely Maxwellian f and $d\phi/ds = 0$, the right side of (74) is just $-(n/B)dB/ds$, i.e. n(s) is constant. But when $\phi(s)$ decreases with s and dominates dU/ds, then n(s) decreases at least as fast as B(s), unless f is not "normal." From Fig. 2 one can show that when $\phi(s)$ decreases in region II, essentially all electrons there have

$$\mu < \frac{e(\phi_L - \phi_W)}{(B_L - B_W)} = \left\langle \frac{ed\phi}{ds} \right\rangle_{II} \left\langle \frac{dB}{ds} \right\rangle_{II}^{-1},$$

assuming that no electrons of greater μ are supplied externally. ($\langle\ \rangle_{II}$ indicates an average over s in region II.) Certainly at those s for which

$$\frac{ed\phi}{ds}\left(\frac{dB}{ds}\right)^{-1} > \left\langle \frac{ed\phi}{ds} \right\rangle_{II} \left\langle \frac{dB}{ds} \right\rangle_{II}^{-1}, \tag{75}$$

the $d\phi/ds$ term is larger in magnitude than the $\mu dB/ds$ term, so that n(s) decreases faster than B(s) at these s. When inequality (75) is

reversed but $d\phi/ds$ is still negative, $n(s)$ decreases more slowly than $B(s)$ but still does not increase, because the right-hand side of Eq. (74) cannot be as large in magnitude as $(n/B)|dB/ds|$.

From this theorem it follows that if, on the average in region II, $\partial U(s,\mu)/\partial s > 0$ for <u>almost</u> all the electrons at s; <u>and</u> if $n_e(s)$ is significantly larger than $n_e(L)$ somewhere in region II, then either f_e is not normal where dn/ds is large, or else the steady state assumption is violated, or there are directed sources or recombination gradients in $L < s < W$.

Barring very high neutral densities ($n_N^{-1} \lesssim W\sigma_{eN}$ with σ_{eN} the cross section for electron neutral collisions) this means that the steady-state case of dense external plasma, $n > n(L)$, is unstable unless $\partial\phi/\partial s$ is large and positive somewhere in region II (because for most electrons, $U(s,\mu) \approx - e\phi(s)$ and μ is small enough that the $\mu B(s)$ term does not dominate.

But $\phi(s)$ cannot decrease as usual in region I and then <u>increase</u> in region II, because <u>ions</u> produced by occasional ionization events (or scattered from elsewhere in velocity space) could then be trapped in the resulting potential depression. Since these ions would mostly be very cold, they could be trapped in the depression for very long times and thus contribute very high density--higher than could be neutralized by slight changes in ϕ bringing in more electrons. The density of these cold ions, n^c, would be at least of order

$$n^c \sim n_e \nu^*/\nu_{esc}$$

where n_e is the density of electrons doing the ionization, ν^* is the

frequency of ionizing collisions, and ν_{esc} is the escape rate of the cold ions from the depression. Ion-neutral collisions are probably the dominant mechanism for cold ion escape, and ν_{esc}/ν_{in} becomes exceedingly small when the depression depth ($\sim e\Delta\phi$) is more than about $5T_c$ (ν_{in} is the ion neutral collision frequency, T_c is the cold ion temperature).[43] We conclude, then, that for $n^c \ll n_e$, the depth of any such potential depression $e\Delta\phi$ can be of order T_c but <u>not</u> of order T_e. Large positive $d\phi/ds$ in region II is thus excluded.

VI. SUMMARY AND CONCLUSIONS

The importance of several instability modes in mirror confinement depends on the axial profile of density, n(s), near the ends of the plasma and particularly between the confinement region $-L < s < L$ ("region I") and the end wall ($s = \pm w$, $w > L$) outside the mirror. We have shown that these "end zone" regions $L < |s| < w$ (collectively called region II) are usually plasma-like (i.e., have small enough Debye length). The density there can be estimated roughly in terms of the ion loss flux, because the average ion streaming velocity is more or less a known function of position (from energy conversion). In this external region these ions, all of which are escaping, are neutralized by electrons, most of which are not escaping. This can only happen if the electrostatic potential decreases from the mirror to the wall.

The electron or ion density at a point in region II depends on the electron velocity distribution and the potential energy profile $U(s,\mu) = \mu B(s) + q\phi(s)$. If the "collision frequency" (for momentum transfer) is small compared with the reciprocal transit time, the distribution in phase space can be generated approximately from $U(s,\mu)$ and the distribution in velocity at the midplane ($s = 0$), using collisionless orbit theory.[13,26] This is discussed in Sections IB (and IIB); the discussion largely follows Persson.[13] This midplane velocity distribution is the solution of complicated coupled Fokker-Planck equations (whose Fokker-Planck coefficients are not always the ordinary ones due to Coulomb encounters). The distribution is non-Maxwellian over an important part of velocity space (the "loss region" or generalized loss cone), because of the rapid particle loss.

With infinitely rapid loss, there are no particles in the loss region. The Fokker-Planck solutions of several authors, discussed in Section IC (and another, for hot-electron plasma, in Appendix E), are of this type. These solutions, which we might call $f_0(x,y)$ (x, y the parallel and perpendicular velocities at the midplane) can be roughly modelled by analytic functions (which are not usually separable in energy and pitch angle). But the density n(s) of both species as calculated from either the computer codes or the analytic model f_0 goes to zero at the mirror, like the cube of the distance from the maximum of B (proved in Appendix A), and the density outside the confinement region is zero by assumption.

When transit times are finite, however, one must get a distribution f which is like f_0 well inside the trapping region, but has a small "tail" or fringe of particles diffused into the loss region. From the height and decay width of this fringe one calculates the density and flux in region II. (A theorem relating these is given in part 2 of Appendix B.) But both the flux and decay width are known from the macroscopically averaged (and measurable) loss rate and collision rate (see part 3 of Appendix B), so the density in region II can be calculated in terms of the $U(s,\mu)$ profile. For the electrons, $n_e(s)$ at a point s in region II depends mainly on $U(s,\mu)$ at s (locally) and not on $U(s',\mu)$ at other s'. For the ions, $n_i(s)$ depends mainly on the magnetic field at s and weakly on $\phi(s)$ and $\phi(L)$. Expressions for $n_i(s)$ and $n_e(s)$ are derived from the analytic model distributions in Appendices B and C, respectively, and are reported in Sections IIIA and IIIB of the main text. (Cold ions produced from

charge exchange are included.) Equating these densities gives the external potential $\phi(s)$, as reported in Section IIIC. Of interest is the magnitude of the abrupt potential drop at the end wall, $s = W$, and also the value and behavior of ϕ at the mirror, since this determines the relative number of electrons which can pass beyond the mirrors (to neutralize escaping ions) but still remain confined in the device ($-W < s \leq W$). Electrons of this class (called ST: streaming beyond mirrors but still trapped) are relatively isotropic in the end regions, while free streaming (SF) untrapped ions or electrons alone are far from isotropy. Another interesting feature of $\phi(s)$ is that the ratio $E_{\|}/\nabla_{\|}$ ln B changes sign near the mirror, but continues to scale with electron temperature. A comparison with an equation for $E_{\|}/\nabla_{\|}$ ln B is given in Appendix D.

Up to this point of our summary, the discussion has been of ions and electrons born inside the plasma and appearing out past the mirrors. In Chapter IV we discuss the influence of electrons which may be born in region II; between the mirror and end wall, or at the wall (either wall cathode or secondary emission). Ions born here cannot penetrate the plasma potential and are returned to the wall, but electrons are accelerated into the confinement region. How many electrons are trapped there is a delicate matter involving their energy loss, as discussed in Section IVA. Their contribution to unbalancing the source input fluxes of electrons and ions, together with the change in energy loss fluxes of each species, causes the plasma potential to change. If almost all externally born electrons ("x"-electrons) are trapped, the change $\Delta\phi_0$ is of order T_e times the ratio of external-source flux

to internal-source flux. These matters are discussed in Section IVA.

The possibility of two-stream instability caused by the x-electrons is discussed in Section IVB. After pointing out that the stability criteria are not the same as in the ordinary case (because parallel velocities are swept out of resonance by the magnetic forces), we discuss what the nonlinear-steady-state distribution $f_e(x,y)$ might look like with the x-electrons somewhat diffused in energy by wave-particle interactions. (Of course, information on the final wave spectrum is not available from any simple analytic methods.) It is assumed that the waves are primarily space-charge waves carried with the "beam" of x-electrons. (This beam is injected "cold" but is quickly flattened to a "quasi-plateau" on the electron distribution.) An important fact is that the source is not cut off and the distribution function is not allowed to relax. The quasi-plateau in midplane velocity space results only because the interactions are strong.

In Section V we show that even with an external source of electrons, the steady state density cannot increase with s in region II without being unstable to two-stream instability. This is because $\phi(s)$ and B(s) both decrease in region II. (An exceptional s is the sheath at the wall but stability conditions in terms of dn_e/ds at s = W are well known.[68] This means that attempts to increase the external density to values exceeding the density at the mirror must result in instability (which slightly enhances the loss of confined electrons and also alters the conductivity of the external region). This appears to be true whether or not the orbits are nearly collisionless.

Appendix E includes brief discussions of some interesting cases

not treated in the main analysis. The magnetosphere and other mirror configurations without an "external" region are mentioned in part 1 of Appendix E. The hot electron plasma, with $\phi(s)$ scaling with ion temperature and differing in topology from the usual case, is discussed in part 2. Part 3 treats weak mirrors, where all the ions are essentially untrapped even though their collision time may be long.

ACKNOWLEDGMENTS

It is a pleasure to acknowledge the encouragement and assistance of Professor Wulf B. Kunkel, who has guided the trend of this work with much physical insight and much patience. Special thanks go also to Margaret R. Thomas for the rather involved typing and for valuable suggestions on format, and to Professors Allan N. Kaufman and C. K. Birdsall for suggestions on improving the clarity and accuracy of several passages.

The work was supported by the United States Atomic Energy Commission under contract No. W-7405 eng-48.

APPENDICES

A. Density Near the Mirrors in the Limit of Zero Bounce Time

If the potential for parallel motion, $U(s,\mu)$, has a simple maximum at $s = L$ for all μ, and if all particles include $s = 0$ in their orbits, then we have the following,

Theorem 1

For a Vlasov guiding-center plasma with midplane distribution $f(x,y)$ such that $f = 0$ for $x \geq x_L(y^2)$ and $f(x,y) \propto \left[x_L^2(y^2) - x^2\right]^p$ with integer p, in the limit as $x \to x_L$ from below

$$n(s) \propto (L - s)^{2p+1} \qquad \text{as } s \to L \text{ from below.}$$

Proof:

$$n(s) = R_s \int_0^\infty 2\pi y\,dy \int_{x_s^2}^{x_L^2} \frac{d(x^2)}{\sqrt{x^2 - x_s^2}}\, f(x,y).$$

The x^2 integration is taken only out to x_L^2, since $f = 0$ for $x^2 > x_L^2$. x_s is the midplane parallel velocity for which particles just reach s, and it depends on y. x_L is the midplane parallel velocity for which particles just reach L, i.e. the escape velocity. Expanding $f(x,y)$

$$f(x,y) = \left.\frac{\partial^p f(x,y)}{\partial (x^2)^p}\right|_{x_L^2(y^2)} \left[x_L^2(y^2) - x^2\right]^p + \cdots$$

we have, for $s \to L$ from $s < L$,

$$n(s) \to R_s \int_0^\infty 2\pi y\,dy\, S(y) \int_{x_s^2}^{x_L^2} \frac{\left[x_L^2 - x^2\right]^p d(x^2)}{\sqrt{x^2 - x_s^2}}$$

where S(y) is the derivative just quoted.

Let $t = \sqrt{x^2 - x_s^2}$ so that $\dfrac{d(x^2)}{\sqrt{x^2 - x_s^2}} = 2\,dt.$

Let $x_s^2 = x_L^2 - \delta^2$ (δ^2 may depend on y), so that $x^2 = x_s^2$ maps onto $t = 0$ and $x^2 = x_L^2$ maps onto $t = \delta$. We have then

$$n(s) \to 4\pi R_L \int_0^\infty ydy \;\; (y) \int_0^\delta dt(\delta^2 - t^2)^p,$$

since $R_s \to R_L \neq 0$. For integer p, the t integration gives $a_p \delta^{2p+1}$, where a_p is a numerical constant ($a_0 = 2$, $a_1 = 4/3$, $a_2 = 16/15$).

Now, by hypothesis, $U(L,\mu) - U(s,\mu) \propto (L - s)^2$ as $s \to L$; and $x_L^2 - x_s^2 \propto U(L,\mu) - U(s,\mu)$, so $\delta^2 \propto (L - s)^2$; let us say $\delta^2(y) = D(y)(L - s)^2$. Then

$$n(s) \to (L - s)^{2p+1} I, \qquad \text{where}$$

$$I = 4\pi R_L a_p \int_0^\infty ydy\, S(y)\left[D(y)\right]^{p+1/2}.$$

In the preceding it was assumed that $U(s,\mu)$ has a maximum at $s = L$, independent of μ. Suppose the maximum of $U(s,\mu)$ is at $s = M(\mu)$ corresponding to escape velocity $x = x_M(y)$. If $M(\mu) \geq W$ for some μ, say $\mu < \mu_W$, then, assuming $f(x,y) \neq 0$ for $x < x_M(y)$ when $y = (2B\mu_W/m)^{1/2}$, there will be particles all the way out to $s = W$. These will be the particles with μ so small that $U(s,\mu)$ has no maximum inside the device. Such a case occurs for electrons when

$d\phi/ds < 0$ for $L \leq s < W$; electrons with small μ are trapped only by $U \approx - e\phi$, which ordinarily increases for all $s > 0$.

B. Model Calculations of External Ion Density Due to Scattering Loss

(A list of symbols and definitions peculiar to this appendix is given at the end of the appendix.)

1. Introduction

Because the ion loss region in midplane velocity space includes the origin, the ion midplane distribution is quite unlike a Maxwellian. We write the "distribution function" $g(x,y)$ (see section 4) as $g_0(x,y) + g_1(x,y)$, where g_1 is a small correction, but g_0 is nearly identical with the actual distribution function f for x,y well inside the trapping region, and g_0 goes to zero at the loss boundary. An analytic function with the general features of g_0 is shown in Fig. B-1. Computer calculations by Marx[27] have yielded typical ion midplane distributions g_0. These involved solving a two-dimensional Fokker-Planck equation for ions coupled to Maxwellian electrons. One result for g_0 is pictured in Fig. B-2. The analytic model function (Fig. B-1) rises more steeply with y but otherwise reproduces the qualitative features of Fig. B-2.

The correction $g_1(x,y)$ is small but nonzero at the loss boundary and decreases rapidly away from it. Such a correction is necessary to give nonzero loss flux. The loss flux (and the accompanying density of ions in region II) depend on the height and decay width of the "tail" g_1 in the loss region $\left[x > x_L(y) \text{ or } y < y_L(x)\right]$, but should be insensitive to the detailed shape of g_1. The general features of g_0, g_1, and $g = g_0 + g_1$ near the loss boundary are shown in Fig. B-3.

2. Density at "Mirrors", s = L

We now present a simple theorem relating the density at the mirror

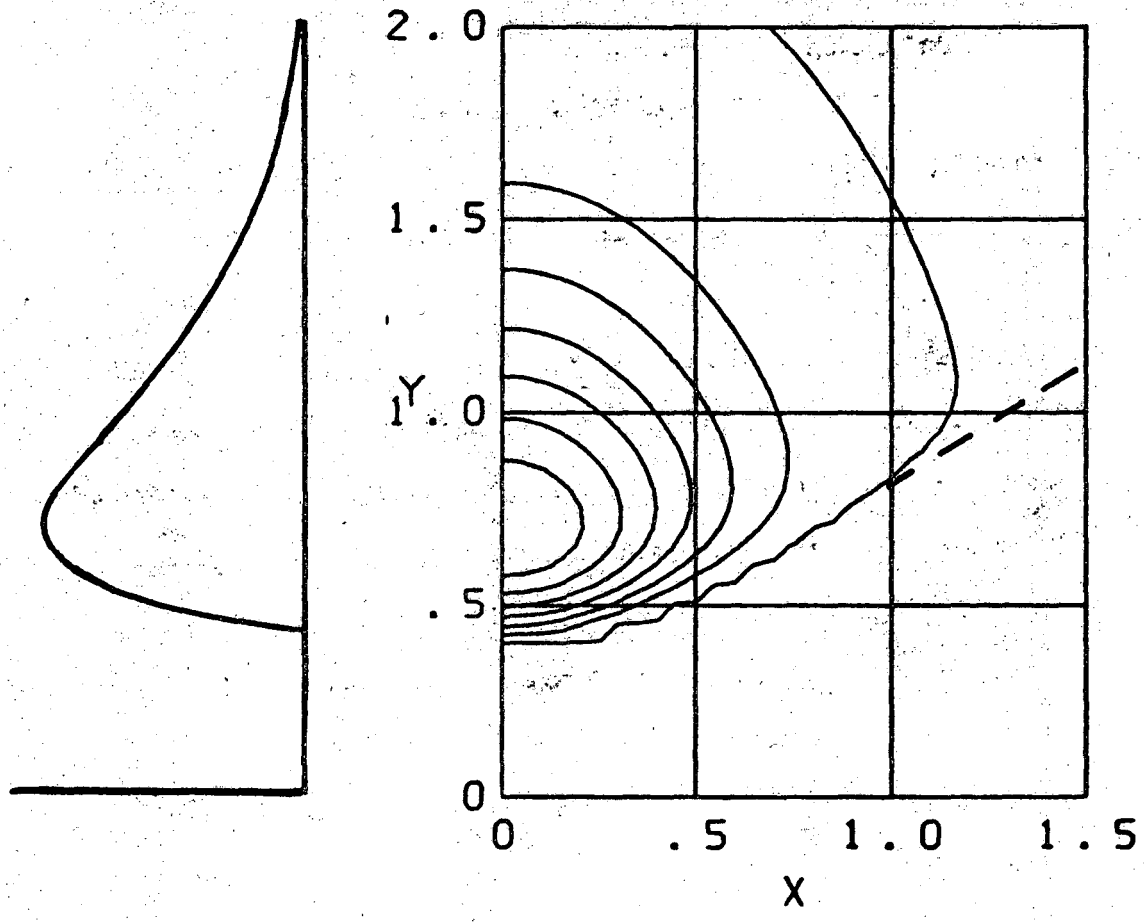

Fig. B-1. Contour lines and cross section of an analytic model for ion distribution $g_0(x,y)$:

$$g_0(x,y) = N[\exp(-x^2/c_{\parallel}^2) - \exp(-x_L^2/c_{\parallel}^2)] \exp(-y^2/c_{\perp}).$$

Ripple is spurious and caused by coarse computation grid. Loss boundary is shown dashed. Contour heights $(0.85g_{0max})(N/6 + 0.01)$ for N = 0, 1, ... 6.

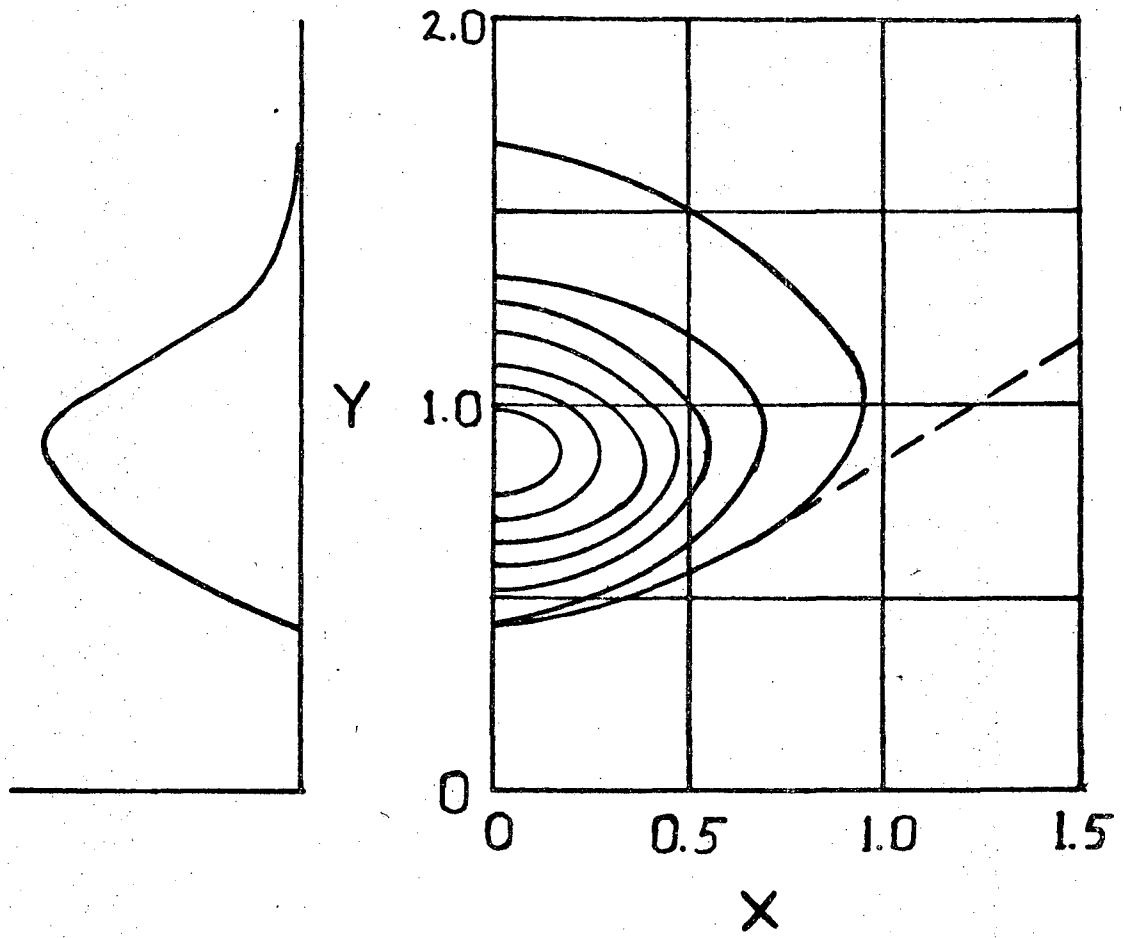

Fig. B-2. Contour lines and cross section of $g_0(x,y)$ as calculated by Marx. Loss boundary shown dashed. Contour heights $(0.85g_{0max})(N/6 + 0.01)$ for N = 0, 1, ··· 6.

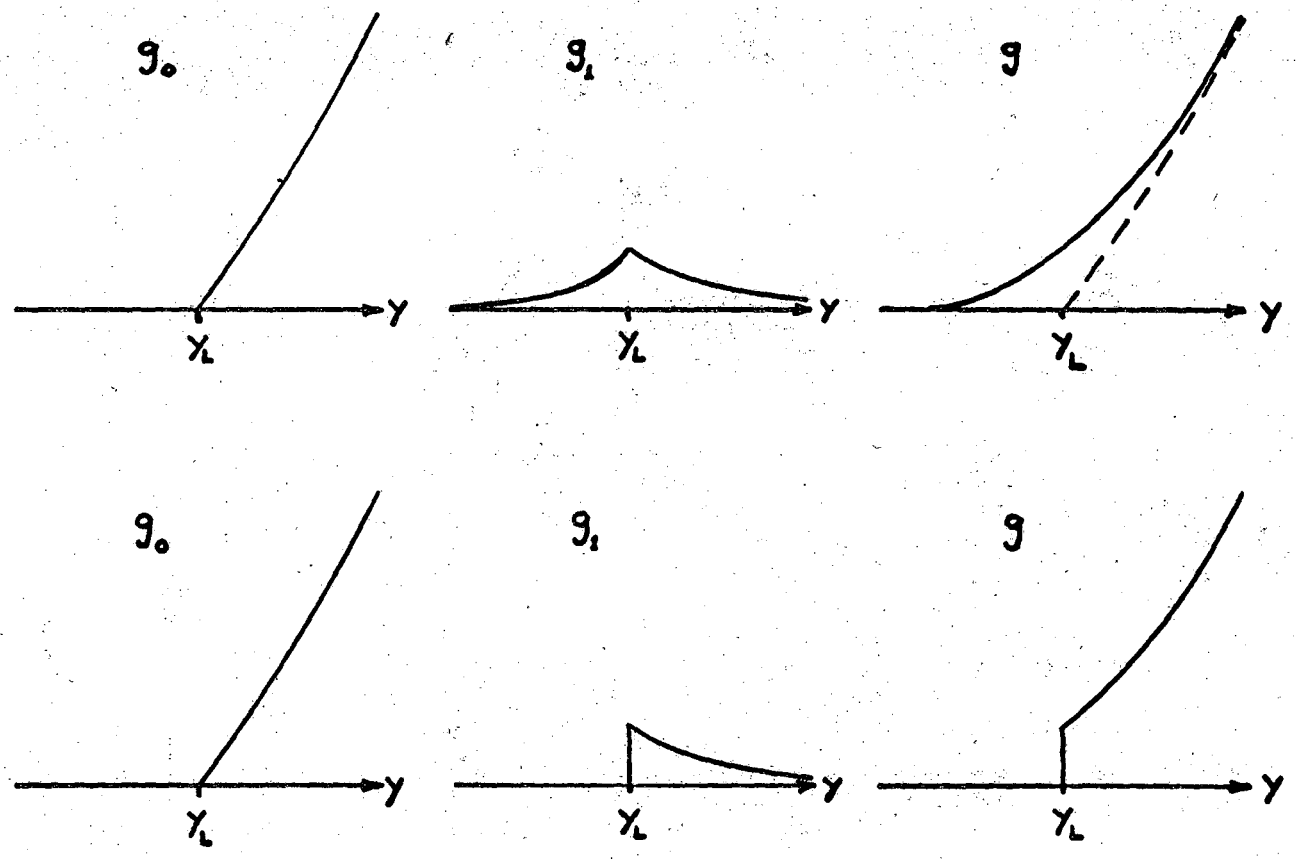

Fig. B-3. Dependence on y (for fixed x) of g_0, g_1, and $g = g_0 + g_1$, near $y = y_L(x)$.

Upper level: $x > 0$. Lower level: $x < 0$.

throat to the loss flux.

Theorem: If $g_1(x,y)$ is zero outside the loss boundary $y_L(x)$ for $x < 0$ and decays outside the loss boundary for $x > 0$ with a decay width κ^{-1} in y^2, and if $\kappa^{-1} \ll y_L^2(x)$ for all x, then

$$\boxed{n(L) \sim (R_L - 1)^{-1/2} F(L) \kappa^{1/2}.} \qquad \text{(B1)}$$

Proof: $F(L) = R_L \int 2\pi y dy \int x dx\, g_1(x,y)$ over the region $x > 0$, $y < y_L(x)$. If the height of g at the loss boundary $y = y_L(x)$ is $C(x)$, then

$$F(L) = \frac{\pi}{2} R_L \int_0^{\infty} d(x^2) C(x) \int_0^{y_L^2(x)} d(y^2) E(y^2), \qquad \text{(B2)}$$

where $E(y^2)$ is any function that decays from unity as y^2 departs from $y_L^2(x)$, with a decay width κ^{-1}. Because of this one has

$$\int_0^{y_L^2(x)} d(y^2) E(y^2) \sim \kappa^{-1},$$

if $\kappa y_L^2 \gg$ everywhere. Next,

$$n(L) = R_L \int 2\pi y dy \int \frac{x dx}{\sqrt{x^2 - x_L^2(y)}}\, g_1(x,y) \qquad \text{(B3)}$$

over the same region. Since $x_L^2(Y)$ and $y_L^2(x)$ represent the same boundary, we rewrite the radicand

$$x^2 - x_L^2(y) = x^2 - (R_L - 1)y^2 + \frac{2}{m_i} e(\phi_0 - \phi_L)$$

as $(R_L - 1)\left[y_L^2(x) - y^2\right]$

with $y_L^2(x) = (R_L - 1)^{-1}\left[x^2 + \frac{2}{m_i} e(\phi_0 - \phi_L)\right]$ and change the order of integration. Letting $t = \sqrt{y_L^2 - y^2}$ we have

$$n(L) = \frac{\pi}{2} R_L (R_L - 1)^{-1/2} \int_0^\infty d(x^2) C(x) \int_0^{y_L} 2dt\, E(y^2). \quad (B4)$$

Since E has decay width κ^{-1} in t^2, one has, for $\kappa y_L^2 \gg 1$,

$$\int_0^{y_L} dt\, E\left[y^2(t)\right] \sim \kappa^{-1/2}, \text{ so that}$$

$$n(L) \sim 2(R_L - 1)^{-1/2} F(L) \kappa^{1/2}.$$

(QED)

We have chosen E to decay with y^2 instead of x^2 so that g will be nonzero in the neighborhood of $x = 0$ and $y < y_L(0)$, representing loss of ions with small parallel velocity by cooling and angle-scattering. The fact that κ^{-1} is the decay width in y^2 rather than normal to $y_L^2(x)$ is reflected in the factor $(R_L - 1)^{-1/2}$.

We note two examples of this theorem: for instance, let

$$\text{(i)}\quad g_1(x,y) = \begin{cases} C(x)e^{-\kappa(y_L^2 - y^2)} & \text{for } y \le y_L(x) \text{ and } x > 0 \\ 0 & \text{for } y \le y_L(x) \text{ and } x < 0 \\ \text{arbitrary} & \text{for } y > y_L(x). \end{cases}$$

For this form of g_1,

$$F(L) = \frac{\pi}{2} R_L \kappa^{-1} \int_0^\infty d(x^2) C(x)$$

and $$n(L) = \pi^{1/2}(R_L - 1)^{-1/2}F(L)\kappa^{1/2}. \qquad (B5)$$

As a second example, let

(ii) $g_1(x,y) = \xi e^{-x^2/c^2}$ for $x > 0$ only on the thin strip $y_L^2(x) - \kappa^{-1} < y^2 \leq y_=^2(x)$; $g_1(x,y) = 0$ elsewhere.

For this form, $F(L) = \frac{\pi}{2} R_L c_\parallel^2 \frac{\xi}{\kappa}$

and $$n(L) = 2(R_L - 1)^{-1/2}F(L)\kappa^{1/2}.$$

Since g_1 is a perturbation on g_0, one expects the height $C(x)$ or ξ to be everywhere small compared with the maximum height of g_0, which is of order $n_0/c_\parallel c_\perp^2$. If it is smaller by a factor of order κ^{-1}, i.e.

if $$\int_0^\infty d(x^2)C(x) \sim \frac{n_0}{c_\parallel c_\perp^2}\frac{1}{\kappa},$$

then $F(L) \propto 1/\kappa^2$ and $n(L)/n_0 \sim \left[F(L)/n_0 c_\parallel\right]^{3/4}$ (and in general, if

$$\int_0^\infty d(x^2)C(x) \propto \kappa^{-p/2},$$

then $$n(L) \propto \left[F(L)\right]^{p+1/p+2},$$

the exponent being between 1/2 for $p = 0$ and 1 for $p = \infty$). The height of g_0 just inside the trapping region, at $y^2 = y_L^2 + \kappa^{-1}$, is of order $S_0\kappa^{-1}$, where S_0 is $\partial g_0/\partial(y^2)$ evaluated at $y = y_L(x)$. If $g_1 \leq g_0$ at $y^2 = y_L^2 + \kappa^{-1}$ and if $g_0 + g_1$ varies smoothly, then at $y^2 = y_L^2$, the height C must be roughly of order $S_0\kappa^{-1}$ or less.

3. Estimate of κ and n(L) from Diffusivity in Velocity Space

A dimensional estimate of κ in terms of the velocity space diffusivity, D, can be made from the dimensional form of the diffusion equation,

$$(\Delta V)^2 \sim Dt.$$

In a transit time of order $2L/c_{\|}$, an ion which began at $s = -L^-$ as barely trapped, statistically wanders into the neighboring "untrapped" region of phase space during its transit to $s = +L^-$. Thus

$$(\Delta V) \sim \left(\frac{2L}{c_{\|}} \bar{D}\right)^{1/2},$$

where $\bar{D}$ is a spatial average of D over a field line. Next, observe that

$$\kappa^{-1} = \Delta(y^2) = 2\langle y_L \rangle \Delta y.$$

Except for $R_L - 1 \ll 1$, $\Delta y \sim \Delta V$. A typical value of y_L, when $R_L - 1 \gtrsim 1$, is $\langle y_L(x) \rangle \sim y_L(c_{\|})$, so we use

$$\langle y_L \rangle \sim c_{\|}(R_L - 1)^{-1/2},$$

assuming $e(\phi_0 - \phi_L) \lesssim T_{\|}$. Thus we have

$$\boxed{\kappa^{-1} \sim 2^{3/2}(R_L - 1)^{-1/2} c_{\|} \left(\frac{L}{c_{\|}} \bar{D}\right)^{1/2}.} \qquad \text{(B6)}$$

If we now write $\bar{D} \sim (c_{\|}^2 + c_{\perp}^2)\nu_0$, where ν_0 is the 90 deg cumulative "collision frequency", and observe that the loss rate $\nu \propto \nu_0$, we can put this expression (B6) into (B5) in the form

$$n(L)/n_0 = R_L(R_L - 1)^{-1/2}(\kappa^{1/2} c_{\|})(L\nu/c_{\|}).$$

We obtain

$$n(L)/n_0 \sim R_L(P\nu/\nu_0)^{1/4}(L\nu/c_\parallel)^{3/4}, \tag{B7}$$

where $P \equiv c_\parallel^2/\, c_\perp^2(R_L - 1)$ and we have assumed $1 + c_\parallel^2/c_\perp^2 \sim 1$. Because ν/ν_0 is unspecified and depends on R_L, we cannot describe the dependence on R_L, but for $R_L - 1 \sim 1$, i.e., intermediate mirror ratios in the range 1.3 to 5, $(\nu/\nu_0)^{1/4} \sim 1$. The salient feature,

$$n(L) \propto (L\nu/c_\parallel)^{3/4},$$

is thus explained.

4. A Slightly Different Model for g_1

One need not take g_1 to decay over a constant width κ^{-1} in y^2 (although the mathematics may be a burden otherwise); other simple models are possible. As an example of a model with constant decay width in y instead of y^2, we show the calculations for the form

$$g_1(x,y) = \begin{cases} S_0(x)(A_1 - B_1)e^{-k(y_L-y)} & \text{for } x > 0 \text{ and } y < y_L(x) \\ 0 & \text{for } x < 0 \text{ and } y < y_L(x) \\ S_0(x)\left[A_1 e^{-a(y-y_L)} - B_1 e^{-b(y-y_L)}\right] & \text{for } y > y_L(x) \end{cases} \tag{B8}$$

with $a > b$ and $A_1 > B_1$, where S_0 is now $\partial g_0/\partial y$ evaluated at $y_L(x) + 0$ $\left[\text{instead of } \partial g_0/\partial(y^2)\right]$ and k^{-1} is the decay width in y instead of in y^2. Figure B-4 shows the qualitative shape of this g_1.

In order to relate the flux F to k (and show the reasonableness of our ordering $C \sim S_0 k^{-1}$), we impose on g_1 the (somewhat artificial) condition[69] that

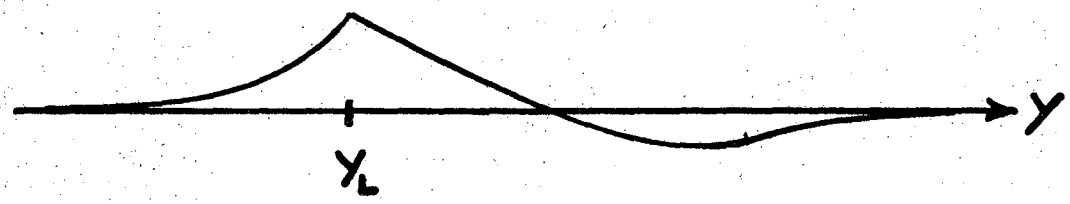

Fig. B-4. $g_1(x,y)$ vs y for fixed $x > 0$, based on Eq. (B8).

(a) $$\int_{-\infty}^{\infty} dx \int_{0}^{\infty} 2\pi y dy\, g_1(x,y) = 0,$$

i.e., that g_1 contributes no correction to the total density

$$\int_{-\infty}^{\infty} dx \int_{0}^{\infty} 2\pi y dy\, g_0(x,y) = n_0.$$

In addition, we requre that the slope of $g_0 + g_1$ be continuous across the loss boundary:

(b) $$\frac{\partial}{\partial y}(g_0 + g_1)\Big|_{y_L+0} = \frac{\partial}{\partial y}(g_0 + g_1)\Big|_{y_L-0},$$

and that g_1 should produce the observable flux $F_i(W)$ at the wall:

(c) $$\int_{-\infty}^{\infty} x dx \int_{0}^{y_L(x)} 2\pi y dy\, g_1(x,y) = F_i(W)/R_W.$$

(Since $F(s)/R_s$ does not vary with s in the absence of scattering, and since g is that distribution which would occur just at the midplane if all scattering took place before the mideplane, at $s < 0$, we can evaluate the first moment integral at $s = 0$.)

Neglecting a^{-1}, b^{-1}, and k^{-1} compared to $y_L(x)$ for all x, condition (a) gives

$$2a^{-1}A_1 - 2b^{-1}B_1 + k^{-1}(A_1 - B_1) = 0, \tag{B9}$$

while condition (b) gives

$$aA_1 - bB_1 + k(A_1 - B_1) = 1. \tag{B10}$$

Condition (c) is the simplest and most important, and gives

$$2\pi k^{-1}(A_1 - B_1)J = F, \tag{B11}$$

where $$J \equiv \int_0^\infty x\,dx\; S_0(x)y_L(x)$$

and $$F \equiv F_i(W)R_W^{-1}$$

is the fictitious flux at s = 0 which gives rise to the known flux $F_i(W)$ at s = W. Combining Eqs. (B9) and (B10), we have

$$k^2 + (a + b)k + \frac{1}{2}ab - \frac{\pi J}{F} = 0.$$

For $a,b \leq k$ this gives

$$k \sim \sqrt{\pi J/F} \tag{B12}$$

(with equality in the limit $a,b \ll k$). This means $A_1 - B_1 = (2k)^{-1}$, so that $C(x) \equiv g_1\left[x,y_L(x)\right] = \frac{1}{2}k^{-1}S_0(x)$, as we assumed.

To relate the density n(L) to the flux $F_i(L)$ we again rewrite the radicand in Eq. (B3)

$$n(L) = R_L\int 2\pi y\,dy\int \frac{x\,dx}{\sqrt{x^2 - x_L^{\,2}(y)}}\; g_1(x,y)$$

as $$(R_L - 1)\left[y_L^{\,2}(x) - y^2\right],$$

with $$y_L^{\,2}(x) \equiv (R_L - 1)^{-1}\left[x^2 + \frac{2}{m_i}\,e(\phi_0 - \phi_L)\right] \tag{B13}$$

and change the order of integration, so that

$$\frac{n_i(L)}{F_i(L)} = (R_L - 1)^{-1/2} \frac{\int_0^\infty xdx\, S_0(x) \int_0^{y_L(x)} \frac{ydy\, e^{-k(y_L - y)}}{\sqrt{y_L^2 - y^2}}}{\int_0^\infty xdx\, S_0(x) \int_0^{y_L(x)} ydy\, e^{-k(y_L - y)}} \qquad (B14)$$

The y-integration in the denominator gives $k^{-1}y_L - k^{-2}(1 - e^{-ky_L})$. And since $ky_L \gg 1$ for all x, we need keep only the first term.[70] The y-integration in the numerator can also be done approximately for $ky_L \gg 1$. We use

$$\int_0^{y_L(x)} \frac{ydy\, e^{-k(y_L - y)}}{\sqrt{(y_L - y)(y_L + y)}} \approx \sqrt{2y_L} \int_0^{\sqrt{y_L}} e^{-kw^2} dw - \frac{3}{2} \frac{1}{\sqrt{2y_L}} \int_0^{\sqrt{y_L}} w^2 e^{-kw^2} dw$$

and replace the upper limits by ∞. Again neglecting $(ky_L)^{-1}$ compared with unity, we get $(\pi/2)^{1/2}(k^{-1}y_L)^{1/2}$ for the integral. Thus

$$\frac{n_i(L)}{F_i(L)} \approx \pi^{1/2}(R_L - 1)^{-1/2}(k/2)^{1/2} \frac{\int_0^\infty xdx\, S_0(x) \sqrt{y_L(x)}}{\int_0^\infty xdx\, S_0(x)\, y_L(x)}, \qquad (B15)$$

which shows the dependence of $n_i(L)/F_i(L)$ on $\kappa^{1/2} = (k/2y_L^{typ})^{1/2}$. [$y_L^{typ}$ is a typical value of $y_L(x)$ defined by the ratio of integrals in Eq. (15).]

Now, if for $g_0(x,y)$ we take the analytic model of Fig. B-1,

$$g_0(x,y) = \begin{cases} N\left[e^{-x^2/c_\parallel^2} - e^{-x_L^2(y)/c_\parallel^2}\right]e^{-y^2/c^2} & \text{for } x < x_L(y) \\ 0 & \text{for } x > x_L(y) \end{cases} \tag{B16}$$

we find

$$S_0(x) \equiv \left.\frac{\partial g_0}{\partial y}\right|_{y_L(x)+0} = \frac{2N}{c_\parallel^2}(R_L - 1)\exp\left[-e(\phi_0 - \phi_L)/T_{eff}\right]y_L(x)e^{-hx^2} \tag{B17}$$

where $P \equiv c_\parallel^2/(R_L - 1)c^2 = \left(\frac{m}{2}c_\parallel^2\right)/T_{eff}$ and $h \equiv (1 + P)c_\parallel^{-2}$. Using the definition (B12) for $y_L^2(x)$, one has then

$$J \equiv \int_0^\infty x\,dx\, S_0(x)y_L(x) = Nc_\parallel^{-2}(1 + h\delta)h^{-2}\exp(-h\delta + \delta/c_\parallel^2)$$

where $\delta \equiv \frac{2}{m_i}e(\phi_0 - \phi_L)$. And the integral in the numerator of (B15) becomes

$$\int_0^\infty x\,dx\, S_0(x)y_L^{1/2}(x) = Nc^{-2}(R_L - 1)^{1/4}e^{\delta/c_\parallel^2}h^{-7/4}\int_{h\delta}^\infty U^{3/4}e^{-U}du,$$

so that

$$\frac{n_i(L)}{F_i(L)} \approx \left(\frac{\pi}{2}\right)^{1/2}(R_L - 1)^{-1/4}\delta^{-1/4}k^{1/2}\rho(h\delta), \tag{B18}$$

where

$$\rho(h\delta) \equiv (h\delta)^{1/4}(1 + h\delta)^{-1}e^{h\delta}\int_{h\delta}^\infty U^{3/4}e^{-U}dU, \tag{B19}$$

related to the incomplete gamma function $\Gamma(7/4,h\delta)$,[71] is shown in Fig. B-5.

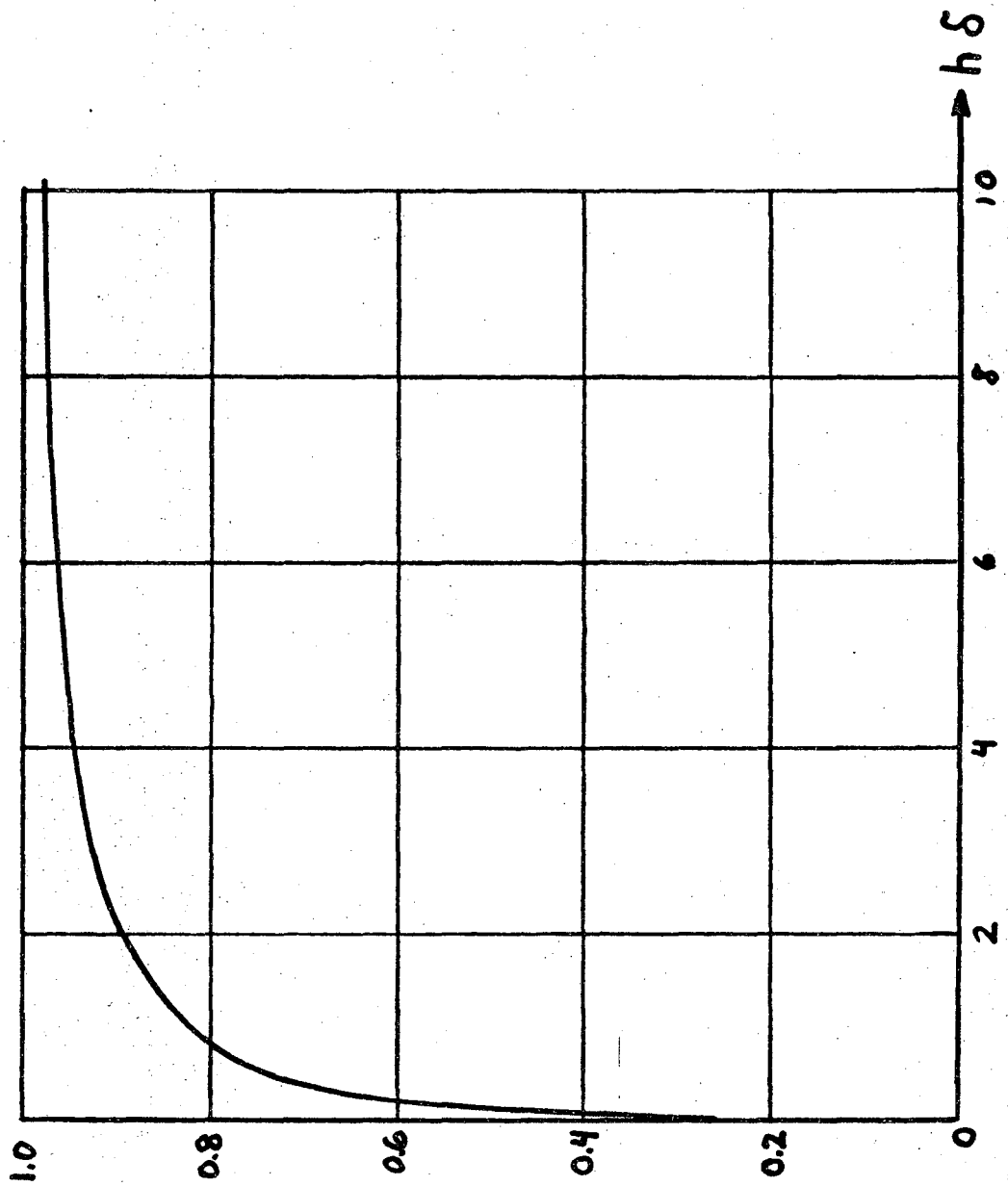

Fig. B-5. $\rho(h\delta)$ vs $h\delta$, from Eq. (B19).

For $h\delta \equiv (1 + P)2e(\phi_0 - \phi_L)/mc_\parallel^2 > 0.2$ (i.e. typically $T_{i\parallel} \lesssim 25\ T_e$), ρ is of order 1/2 to 1. For $h\delta \leq 0.2$, $\rho(h\delta) \approx (h\delta)^{1/4}$; and for $h\delta \gg 1$, i.e. $T_{i\parallel} \ll e(\phi_0 - \phi_L)$ or $R_L - 1 \ll 1$, one has $\rho(h\delta) \approx 1 - \frac{7}{4}(h\delta)^{-1}$. Now if we use the estimate $(\pi J/F)^{1/2}$ for k, and work out the normalization N, we find

$$N = \frac{n_0}{\pi^{3/2}} \frac{(1 + P)^{3/2}}{c_\parallel c_\perp^2} e^{e(\phi_0-\phi_L)/T_{eff}} = \frac{n_0}{\pi^{3/2}} h^{3/2} \frac{c_\parallel^2}{c_\perp^2} e^{h\delta - \delta c_\parallel^{-2}} \qquad (B20)$$

giving

$$J = n_0 \pi^{-3/2} h^{-1/2} c_\perp^{-2} (1 + h\delta)$$

and

$$\frac{n_i(L)}{n_0} = 2^{-1/2}\pi^{3/8} R_L (P\sqrt{1 + P})^{1/4} \left[1 + (h\delta)^{-1}\right]^{1/4} \rho(h\delta) \left(\frac{F}{n_0 c_\parallel}\right)^{3/4}.$$

Since $\left[1 + (h\delta)^{-1}\right]^{1/4} \rho(h\delta) \approx 1$ for all $h\delta$, we can write

$$\boxed{\frac{n_i(L)}{n_0} \approx R_L (P\sqrt{1 + P})^{1/4} \left(\frac{F}{n_0 c_\parallel}\right)^{3/4},} \qquad (B21)$$

with only very weak dependence on $e(\phi_0 - \phi_L)$. Since $F = n_0 L\nu$, the quantity $F/n_0 c_\parallel$ is crudely the ratio of bounce time to loss time, for a typical ion, i.e. Eq. (B7) is recovered.

5. Density at $s > L$

Let the exact ion loss boundary in Fig. B-6 be called $y = y_M(x)$ or $x = x_M(y)$. Let the line $y = y_s(x)$ or $x = x_s(y)$ be

$$y^2 = (R_s - 1)^{-1}\left[x^2 + \frac{2}{m_i} e(\phi_0 - \phi_s)\right]. \qquad (B22)$$

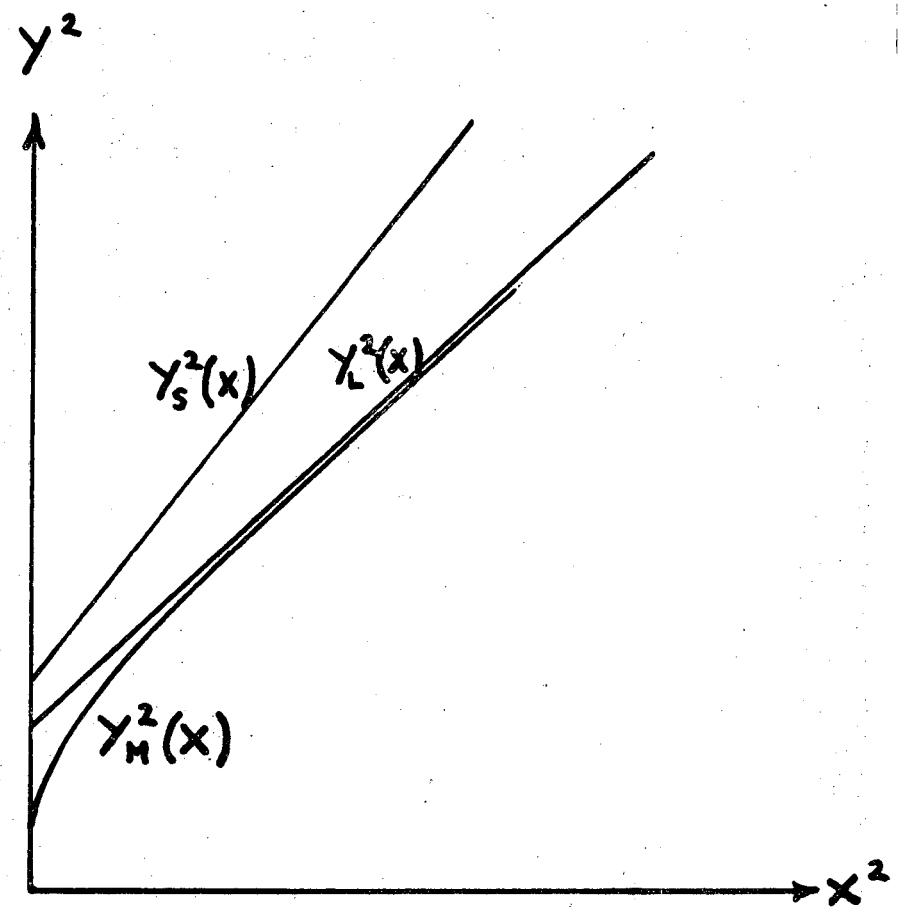

Fig. B-6. Exact loss boundary (curved) and approximate loss boundary [line $y_L^2(x)$] for ions. Also shown is $y_s^2(x) = (R_s - 1)^{-1}[x^2 + 2e(\phi_0 - \phi_s)/m_i]$. [Replacing s by L gives formula for $y_L^2(x)$.]

Then

$$n(s) = R_s \int 2\pi y dy \int \frac{x dx}{\sqrt{x^2 - x_s^2(y)}}\, g_1(x,y)$$

over the region $y < y_M(x)$ becomes

$$n(s) = \pi R_s (R_s - 1)^{-1/2} \int_0^{\infty} dx^2 \int_0^{y_M(x)} \frac{y dy}{\sqrt{y_s^2 - y^2}}\, g_1(x,y). \quad \text{(B23)}$$

For mathematical ease, we return to the model

$$g_1(x,y) = C(x) e^{-\kappa(y_M^2 - y^2)}$$

(where we previously used the approximate boundary y_L^2 instead of the exact y_M^2). Then the y-integration in Eq. (B23) becomes

$$Y = \int_0^{y_M} \frac{y dy}{\sqrt{y_s^2 - y^2}}\, e^{-\kappa(y_M^2 - y^2)}. \quad \text{(B24)}$$

When $s > L$, one has $y_s^2 > y_M^2$ for all x. M(y) is the value of s for which $y^2(dR/ds) + (2e/m_i)(d\phi/ds) = 0$. Expanding R and ϕ about R_L and ϕ_L and letting

$$\psi \equiv \frac{e\phi}{\frac{1}{2} m_i c_\parallel^2}$$

one gets (for y such that M - L is small),

$$M - L \approx -\psi'/R''$$

$$R_M \approx R_L + \frac{1}{2}(c_\parallel^4/y^4)\psi'^2/R''$$

$$\psi_M \approx \psi_L - (c_\parallel^2/y^2)\psi'^2/R''$$

$$x_M^2 - x_L^2 \approx -\frac{3}{2}\left(c_\parallel^2/y^2\right)\psi'^2/R''$$

$$\kappa(y_L^2 - y_M^2) \approx -\frac{3}{2} c_\parallel^4 \kappa\left[x^2 + \frac{2e}{m_i}(\phi_0 - \phi_L)\right]^{-1} \frac{\psi'^2}{R} \equiv \eta(x^2) \qquad \text{(B25)}$$

where prime means d/ds evaluated at s = L. (ψ' and r" are both negative.) Now, writing $y_M^2 - y^2$ in Eq. (B24) as

$$y_M^2 - y^2 \equiv (y_M - y_L^2) + (y_L^2 - y_s^2) + (y_s^2 - y^2)$$

gives

$$Y = e^{\kappa(y_L^2 - y_M^2)}\, e^{\kappa(y_s^2 - y_L^2)} \int_0^{y_M} \frac{y\,dy}{\sqrt{y_s^2 - y^2}}\, e^{-\kappa(y_s^2 - y^2)} \qquad \text{(B26)}$$

where the factors in front of the integral depend only on x and have positive exponents, the first given by Eq. (B25) and the second by Eq. (B22) and Eq. (B22) with s replaced by L :

$$\kappa(y_s^2 - y_L^2) = \zeta x^2 + \theta,$$

$$\zeta \equiv \left(\frac{1}{R_s - 1} - \frac{1}{R_L - 1}\right)\kappa,$$

$$\theta \equiv \frac{2e}{m_i}\left(\frac{\phi_0 - \phi_s}{R_s - 1} - \frac{\phi_0 - \phi_L}{R_L - 1}\right)\kappa. \qquad \text{(B27)}$$

Since $R_s < R_L$ and $\phi_s < \phi_L < \phi_0$ for s > L, it follows that ζ and θ are both positive increasing functions of s. ζ has a second order zero at s = L, while the zero of θ there is first order if $\psi' \neq 0$. η is independent of s. Letting $t \equiv \kappa^{1/2}\sqrt{y_s^2 - y^2}$, Eq. (B26) becomes

$$Y = \kappa^{-1/2} e^u \int_{u^{1/2}}^{\kappa^{1/2} y_s} dt\, e^{-t^2}$$

where $u \equiv (\zeta x^2 + \theta) + \eta(x^2) = \kappa\left[y_s^2(x) - y_M^2(x)\right]$. (See Fig. B-6.) Y is a monotonic decreasing function of u:

$$Y \approx \kappa^{-1/2}\left[\frac{\sqrt{\pi}}{2} - u^{1/2}\right] \qquad \text{for } u \ll 1 \qquad \text{and } \kappa y_s^2 \gg 1, \text{ and}$$

$$Y \backsim \kappa^{-1/2}(\pi\kappa u)^{-1/2} \qquad \text{for } u \gg 1 \qquad \text{and } \kappa y_s^2 \gg u.$$

(In this latter case the upper limit of Y may be replaced by ∞ with an error of only $\exp -\kappa y_s^2$.) The function $u(s,x^2)$ is always positive and has positive $\partial u/\partial s$. For large enough $s - L$, $\partial u/\partial x^2$ is also positive for all x^2, but for small $s - L$, u decreases somewhat before it increases with x^2, the decrease being due to $\eta(x^2) \neq 0$.

The approximation $y_M = y_L$, i.e. $\eta \equiv 0$, gives a reasonably good estimate for n(s) using Eq. (B23), but gives $dn/ds = -\infty$ at $s = L$ because

$$\frac{d}{ds}\int_0^\infty dx^2 C(x^2) Y\left[u(s,x^2)\right] = \int_0^\infty dx^2 C(x^2)\,\frac{dY}{du}\,\frac{\partial u}{\partial s}\,;$$

this is $-\infty$ at $s = L$ because $dY/du = -\infty$ at $u = 0$ while $\partial u/\partial s$ is finite at $s = L$. For a better estimate of n(s) which gives finite dn/ds, one may replace $\eta(x^2)$ by $\bar{\eta} \sim \frac{1}{2}\,\mathrm{Max}(\eta)$. Then Eq. (B23) becomes

$$n(s) \approx \pi R_s (R_s - 1)^{-1/2} \zeta^{-1} \int_\Phi^\infty du\, C\left(\frac{u - \Phi}{\zeta}\right) Y(u)$$

where $\Phi \equiv \theta + \bar{\eta}$. This can be integrated by parts if $C(x^2)$ is of the form $\xi e^{-\mu x^2}$:

$$n_i(s) \approx \pi R_s (R_s - 1)^{-1/2} \frac{\xi}{\pi} \frac{z}{1 - z} \left[z^{-1/2} e^{z\Phi} \int_{\sqrt{z\Phi}}^{\infty} dt\, e^{-t^2} \right.$$

$$\left. - e^{\Phi} \int_{\sqrt{\Phi}}^{\sqrt{\Phi + S_2}} dt\, e^{-t^2} - S_1 e^{-S_2} e^{S_3} \int_{\sqrt{S_3}}^{\infty} dt\, e^{-t^2} \right]$$

where

$$z \equiv \pi/\zeta$$

$$S_2 \equiv \frac{\kappa}{R_L - 1} (\psi_0 - \psi_L) - \bar{\eta} \qquad \left[\Phi + S_2 = \frac{\kappa}{R_s - 1} (\psi_0 - \psi_s) \right]$$

$$S_4 \equiv 1 + \frac{\kappa\kappa/\pi}{R_L - 1}$$

$$S_3 \equiv S_4 \pi (\psi_0 - \psi_s)$$

and $$S_1 \equiv \left(\frac{R_L - 1}{R_s - 1} \right)^{1/2} \left(\frac{\kappa/\pi}{R_L - 1} \right)^{1/2} S_4^{-1/2}.$$

For any χ, the function

$$e^{\chi} \int_{\sqrt{\chi}}^{\infty} dt\, e^{-t^2}$$

decreases from $\pi^{1/2}/2$ at $\chi = 0$ to zero at $\chi = \infty$; the decrease is rapid at first (negative infinite slope) and slow for large χ.

At s = L, z has a second-order pole, while the $\bar{\eta}$ term (electric field at s = L) prevents Φ from having a zero; so the first term in brackets vanishes and the remaining terms go to approximately

$$-e^{\bar{\eta}} \int_{\sqrt{\bar{\eta}}}^{\infty} dt\, e^{-t^2}$$

since S_2 and S_3 are both large and $S_1 \sim 1$ at $s = L$. The coefficient $z/(1 - z)$ is -1 at $s = L$.

As R_s decreases from R_L, a point is reached where $z = 1$. The coefficient $z/(1 - z)$ has a first-order pole, but the square bracket has a first-order zero since $S_1 = 1$ and $\Phi + S_2 = S_3$ there. Next, the point $R_s = 1$ is reached (if $R_W < 1$). Here the factor $(R_s - 1)^{-1/2}$ becomes infinite, but $z = 0$ and $\Phi = \infty$ with $z\Phi = \lambda(\psi_0 - \psi_s)$ finite. The parameters S_2, S_3, S_4 are finite but $S_1 \propto (R_s - 1)^{-1/2}$ is infinite. The second term in brackets vanishes ($\Phi = \infty$) and the result for $n_i(s)$ is finite: at s such that $R_s = 1$,

$$n_i(s) = \pi(\xi/\kappa)\left[\lambda^{-1/2} e^{\lambda(\psi_0-\psi_s)} \int_{\sqrt{\lambda(\psi_0-\psi_s)}}^{\infty} dt\, e^{-t^2}\right.$$

$$\left. - S_4^{-1/2} e^{-S_2} e^{S_3} \int_{\sqrt{S_3}}^{\infty} dt\, e^{-t^2}\right]$$

For $R_s < 1$ the original expression is still correct (if ∞ is replaced by $-i\infty$ in the first integral) but the terms in the bracket are imaginary, as is the factor $(R_s - 1)^{-1/2}$ outside the bracket. The functions Φ and z are negative, and S_1 is imaginary. One can rewrite $n_i(s)$ in terms of $\Phi' = |\Phi|$, $z' = |z|$, $S_1' = S_1$ with $|R_s - 1|$ instead of $R_s - 1$:

$$n_i(s) \approx \pi R_s |R_s - 1|^{-1/2} \kappa^{-1/2} \frac{\xi}{\pi} \frac{z'}{1+z'} \left[(z')^{-1/2} e^{z'\Phi'} \int_{\sqrt{z'\Phi'}}^{\infty} dt\, e^{-t^2} \right.$$

$$\left. + e^{-\Phi'} \int_{\sqrt{\Phi'-S_2}}^{\sqrt{\Phi'}} dt\, e^{+t^2} - S_1' e^{-S_2} e^{S_e} \int_{\sqrt{S_3}}^{\infty} dt\, e^{-t^2} \right].$$

In practically all cases one can take $S_2 \approx \infty$, which corresponds to replacing the upper limit of Y by ∞ (i.e., $\kappa^{1/2} y_s \gg 1$) before doing the integration by parts. Comparing $n_i(s)$ to $n_i(L)$ then,

$$\frac{n_i(s)}{n_i(L)} \approx \frac{R_s}{R_L} \left(\frac{R_L - 1}{R_s - 1} \right)^{1/2} \frac{1}{E(\bar{\eta})} \frac{z}{1-z} \left[z^{-1/2} E(z\Phi) - E(\Phi) \right] \qquad \text{(B28)}$$

for $R_s > 1$, where

$$E(\chi) \equiv \frac{2}{\sqrt{\pi}} e^{\chi} \int_{\sqrt{\chi}}^{\infty} dt\, e^{-t^2}.$$

For $R_s = 1$

$$\frac{n_i(s)}{n_i(L)} \approx \frac{R_s}{R_L} \left(\frac{R_L - 1}{\kappa/\pi} \right)^{1/2} \frac{E\left[\pi(\psi_0 - \psi_s)\right]}{E(\bar{\eta})},$$

and for $R_s < 1$

$$\frac{n_i(s)}{n_i(L)} \approx \frac{R_s}{R_L} \left(\frac{R_L - 1}{|R_s - 1|} \right)^{1/2} \frac{1}{E(\bar{\eta})} \frac{|z|}{1+|z|} \left[|z|^{-1/2} E(|z||\Phi|) + \frac{1}{\sqrt{\pi}} \int_0^{\sqrt{|\Phi|}} dt\, e^{t^2} \right].$$

For convenience, we repeat the definitions

$$z \equiv \left[\frac{\kappa}{\pi} \left(\frac{1}{R_s - 1} - \frac{1}{R_L - 1} \right) \right]^{-1}, \text{ with } \pi \sim c_{\|}^{-2} \text{ and } \kappa \gg c_{\|}^{2}$$

$$\Phi \equiv \kappa c_{\|}^2 \left(\frac{\psi_0 - \psi_s}{R_s - 1} - \frac{\psi_0 - \psi_L}{R_L - 1} \right) + \bar{\eta} ,$$

$$\bar{\eta} \equiv \frac{3}{4} \kappa c_{\|}^2 (\psi_0 - \psi_L)^{-1} \psi'^2 |R''|^{-1} , \quad \text{(prime = d/ds at s = L)}$$

and $\psi \equiv e\phi/(\frac{1}{2} m_i c_{\|}^2)$, subscripted as necessary.

A plot of Eq. (B28) vs R_s and ϕ_s is shown in Fig. B-7 for typical parameters $R_L = 3$, $\varphi_0 - \varphi_L = 4$, $T_e/T_{i\|} = 1/2$, $\kappa d_{\|}^2 = 10$, $\bar{\eta} = 0.2$. The Fortran program used in making the plot (IONS) is given in Appendix F.

To obtain the behavior of $n_i(s)$ for s fairly far from L, we expand Eq. (B28) for $z \ll 1$, $\Phi \gg 1$, and $z\Phi \ll 1$, and keep only the leading term, $z^{-1/2}$, for the expression in brackets. (This ordering is the proper one if $\theta \ll \kappa c_{\|}^2$, i.e., if $T_e \ll \frac{1}{2} m_i c_{i\|}^2$). Then writing

$$F(L) = R_L L n_0 \nu ,$$

$$\nu \approx c_{\|}^{-2}$$

and $$\kappa^{1/2} z^{1/2} (R_s - 1)^{-1/2} = \left(\frac{R_L - 1}{R_L - R_s} \right)^{1/2} c_{\|}^{-1},$$

we have

$$\boxed{\frac{n(s)}{n_0} \sim \left(\frac{R_L - 1}{R_L - R_s} \right)^{1/2} \frac{R_s L \nu}{c_{\|}} ,} \qquad \text{(B29)}$$

for s sufficiently large. To compare this with Eq. (20) of the main text, simply note that for this model

$$T_{\perp}^{\text{Loss}} \sim T_{\|} (R_L - 1)^{-1}.$$

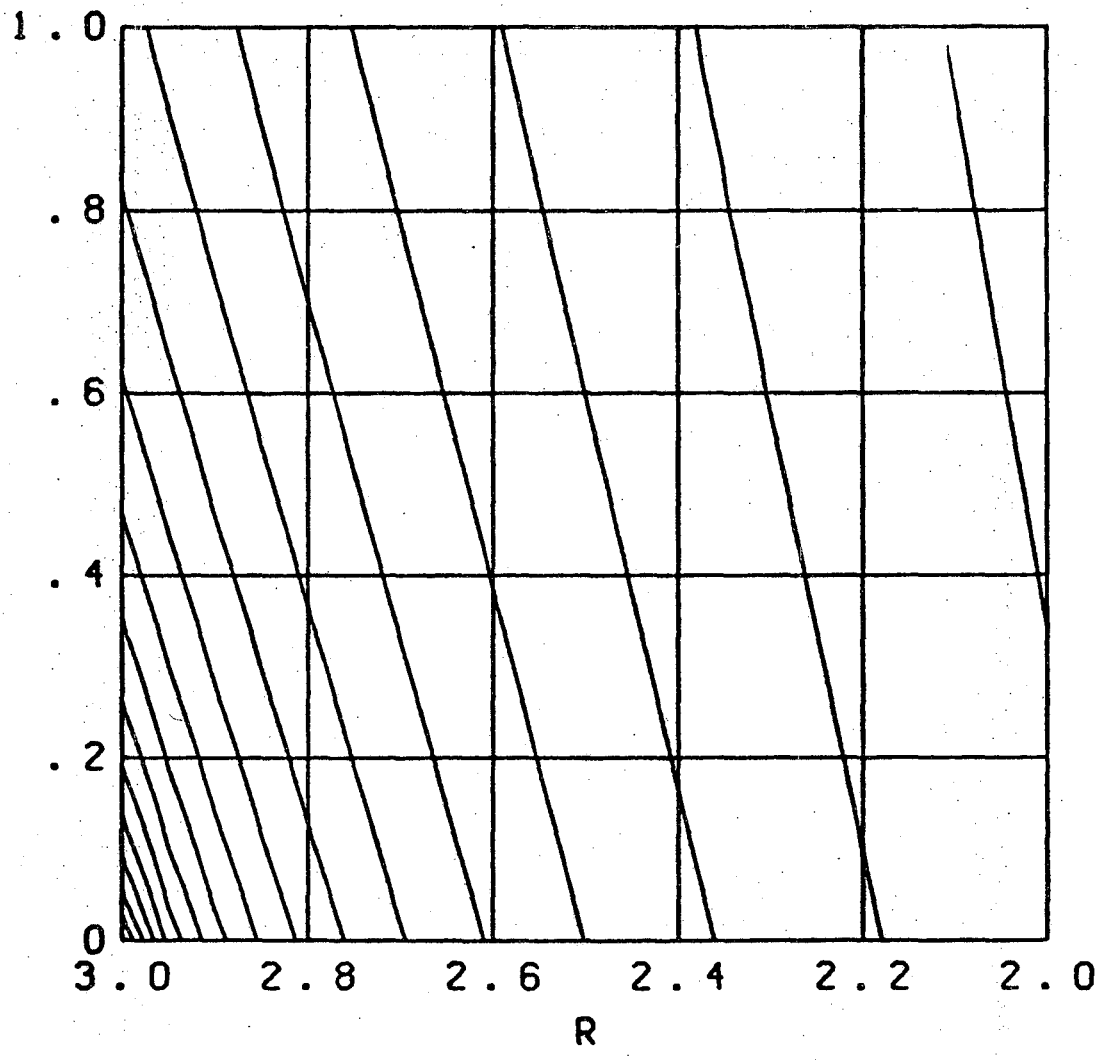

Fig. B-7. Contours of relative ion density in region II. Equating this to electron density from Appendix C gives a curve of $\varphi_L - \varphi$ vs R.

6. Small Mirror Ratio

Here we examine $P \equiv (c_{\|}^2/c_{\perp}^2)(R_L - 1)^{-1}$ when $R_L - 1 \ll 1$. The quantities $c_{\|}^2$ and $c_{\perp}^2$ come from the model

$$g_0(x,y) = N\left[e^{-x^2/c_{\|}^2} - e^{-x_L^2(y)/c_{\|}^2}\right] e^{-y^2/c_{\perp}^2} \qquad \left[x^2 < x_L^2(y)\right].$$

They are asymptotic "tail temperatures" in the confinement region. The actual temperatures $T_{\|} = 2\langle\epsilon_{\|}\rangle$ and $T_{\perp} = \langle\epsilon_{\perp}\rangle$ may be calculated from g_0:

$$T_{\|} = \frac{m}{2} c_{\|}^2 (1 + P)^{-1};$$

$$T_{\perp} = \frac{m}{2} c_{\perp}^2 (1 + \omega P)(1 + P)^{-1},$$

with $\omega \equiv (T_e/T_{\|})(\varphi_0 - \varphi_L) + 5/2$. Note that $T_{\|} < \frac{m}{2} c_{\|}^2$ and $T_{\perp} > \frac{m}{2} c_{\perp}^2$. When $R_L - 1 \ll 1$, P can be large without limit, and the approximation $T_{\|} = \frac{m}{2} c_{\|}^2$, $T_{\perp} = \frac{m}{2} c_{\perp}^2$ (made frequently in the main text) fails. One may write

$$P = P'(1 - \omega P)^{-1}, \qquad \text{where } P' = (T_{\|}/T_{\perp})(R_L - 1)^{-1}.$$

(P' remains finite as $R_L - 1 \to 0$, while P becomes infinite.)

But the limit $R_L - 1 \to 0$ is not strictly applicable in this paper because of the initial requirement $\chi\nu\tau \ll 1$ (where τ is a typical bounce time and ν the inverse loss time). ν is related to the scattering rate ν_0 by $\nu/\nu_0 = \lambda(R_L - 1)^{-1}$ with some constant $\lambda \sim 1$, when $R_L - 1 \ll 1$. Thus even if $c_{i\|}$ stays finite as $R_L - 1$ and $T_{\|}$ go to zero, we have the limitation

$$(R_L - 1)^{3/2} \gg \lambda(L\nu_0/v),$$

where $m\upsilon^2/2 = T_\perp$. Since $L\nu_0/\upsilon$ is usually quite small (say 10^{-3}) this is not a serious restriction on the values of R_L one might wish to consider. If $c_\parallel$ is held constant as $R_L - 1$ and $T_\parallel$ become small, the condition $\nu\tau \ll 1$ imposes a practical upper limit on P:

$$P \ll \frac{c_\parallel^2}{c_\perp^2}\left(\frac{L\nu_0}{\upsilon}\right)^{-2/3} .$$

For $c_\parallel^2/c_\perp^2 \simeq 0.1$ and $L\nu_0/\upsilon \sim 10^{-4}$ this means that in Eq. (B21)

$$(P\sqrt{1+P})^{1/4} \lesssim 2.$$

7. Symbols Peculiar to This Appendix

a, A_1, b, B_1 = parameters in the model (B8) for $g_1(x,y)$.

$c_\parallel$, $c_\perp$ = $(2T_{\parallel,\perp}/m_i)^{1/2}$ ordinarily, but when using quantities derived from (B16) for g_0,

$c_\parallel$, $c_\perp$ = asymptotic "thermal speed" parameters in g_0. For $R_L - 1 \gtrsim 1$ the difference in definition is negligible. For $R_L - 1 \ll 1$, see final part of this appendix.

$C(x)$ or $C(x^2)$ = height of $g(x,y)$ at the loss boundary $y = y_L(x)$ [or $x = x_L(y)$].

D = velocity space diffusivity, in some average sense (averaged over velocities where the distribution function is large).

$\bar{D}$ = spatial average of D over a typical bounce orbit.

$E(y^2)$ = any function that decays from unity as y^2 decreases from $y_L^2(x)$.

F = $F_i(s)/R_s$ for any s. F is independent of s for $s \geq L$.

$h = (1 + P)c_{\|}^{-2}$. See P.

$J = \int_0^\infty x\,dx\, S_0(x)y_L(x)$.

k = decay width, in y, of the model (B8) for $g_1(x,y)$.

N = normalization of $g_0(x,y)$ in model (B16). Value given in Eq. (B20).

p = arbitrary exponent in $\int_0^\infty d(x^2)C(x) \propto \kappa^{-p/2}$.

$P = (c_{\|}^2/c_{\perp}^2)(R_L - 1)^{-1}$

$\mathcal{r}$ = parameter in $C(x) \propto e^{-\mathcal{r}x^2}$, $\mathcal{r} \sim c_{\|}^{-2}$.

$S_0(x)$ = slope of g_0 at $y_L(x)$. $S_0 = \partial g_0/\partial y$ or $\partial g_0/\partial(y^2)$.

S_1, S_2, S_3, S_4 = functions defined on page 133.

t, u, U, w = various temporary integration variables.

Y = integral defined by Eq. (B24).

$z = \mathcal{r}/\zeta$. See $\mathcal{r}$, ζ.

$\delta = (2e/m_i)(\phi_0 - \phi_L)$

$\zeta = \kappa\left[(R_s - 1)^{-1} - (R_L - 1)^{-1}\right]$

η = small quantity measuring electric field at the mirror: $\eta = \frac{3}{2}\kappa c_{\|}^4\left[x^2 + \frac{2e}{m_i}(\phi_0 - \phi_L)\right]^{-1}\psi'^2|R''|^{-1}$, where ' means d/ds at s = L and where $\psi \equiv e\phi/(m_i/2)c_{\|}^2$. $\bar{\eta}$ is an average of η, or order 1/2 Max(η).

$$\theta = \frac{2e}{m_i}\left(\frac{\phi_0 - \phi_s}{R_s - 1} - \frac{\phi_0 - \phi_L}{R_L - 1}\right)\kappa .$$

κ = decay width in y^2 of $g_1(x,y)$.

ξ = amplitude of $C(x)$ in $C(x) = \xi e^{-\mathcal{r}x^2}$ for some $\mathcal{r} \sim c_{\|}^{-2}$.

$\upsilon = (2T_\perp/m_i)^{1/2}$.

$\varphi = e\phi/T_e$ as elsewhere in this paper.

$\Phi = \theta + \overline{\eta}$. See θ, η.

$\psi = e\phi/(m_i/2)c_\parallel^2$, subscripted like ϕ where necessary.

$\omega = 5/2 + (T_e/T_{i\parallel})(\varphi_0 - \varphi_L)$.

C. Model Calculations of External Electron Density as a Function of Potential

1. Model for g(x,y)

For the electrons we take g(x,y) to be a Maxwellian multiplied by a function H(x,y) such that H ≈ 1 in the confinement region and H ≈ 0 in the loss region, with a smooth transition between them:

$$g(x,y) = N e \exp\left(-x^2/c_{\|}^2\right) \exp\left(-y^2/c_{\perp}^2\right) H(x.y).$$

It is convenient to take for H the form

$$H(x,y) = \begin{cases} 1 - (1-\xi)e^{-\kappa'(x_1^2 - x^2)/c_{\|}^2} \\ \xi e^{-\kappa(x^2 - x_1^2)/c_{\|}^2} \\ 0 \end{cases} \begin{array}{l} \text{for } x^2 < x_1^2(y^2) \\ \text{for } x^2 > x_1^2(y^2) \text{ and } x > 0 \\ \text{for } x^2 > x_1^2(y^2) \text{ and } x < 0, \end{array}$$

where

$$x_1^2(y^2) \equiv \begin{cases} (R_L - 1)y^2 + \frac{2e}{m}(\phi_0 - \phi_L) \\ (R_W - 1)y^2 + \frac{2e}{m}\phi_0 \end{cases} \text{ for } y^2 \gtrless y_0^2, \qquad \text{(C1)}$$

(see Fig. C1) with $y_0^2 \equiv (\frac{2e}{m}\phi_L)/(R_L - R_W)$. We take $\xi < 1$, $\kappa' \gtrsim 1$, $\kappa \gtrsim 1$ and note that for smooth slope $\kappa' = \xi\kappa(1-\xi)^{-1}$. Figures 10 and 11 show g and H vs x for $\xi = 0.1$, $\kappa' = 1, 2$. The parameter ξ is the value of H at the escape velocity x_1; κ' measures the abruptness of the damping at $x < x_1$; κ measures the abruptness of the decay for $x > x_1$. The region of integration in x,y for $n_e(L)$ is $x^2 > x_L^2(y^2)$ where

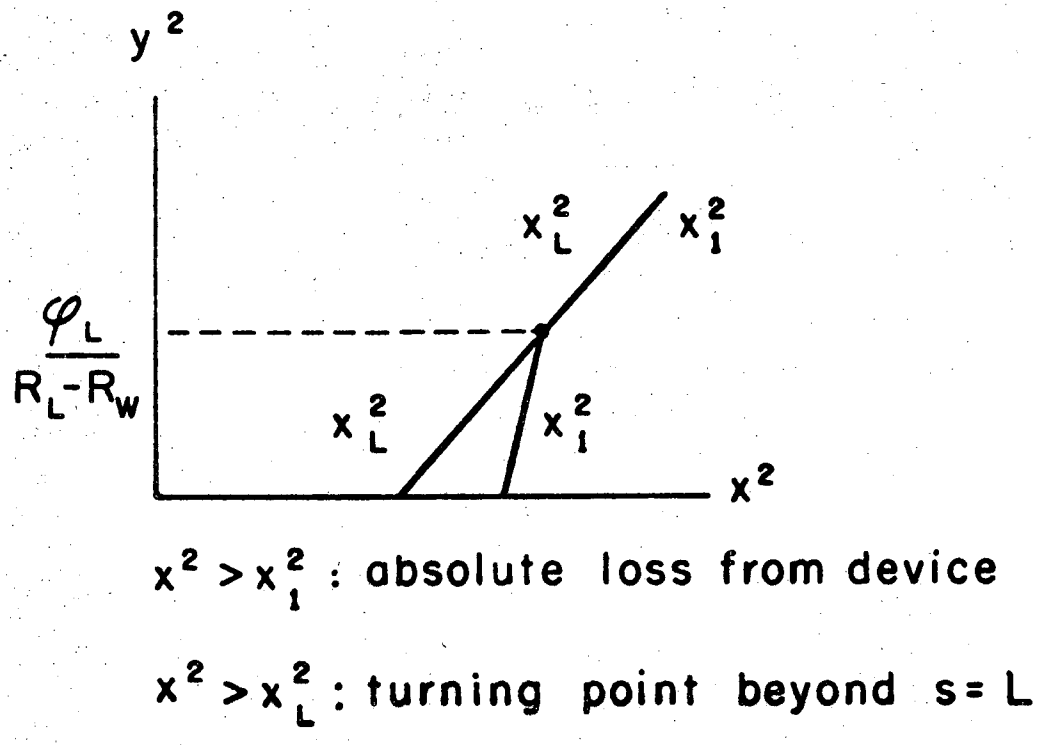

Fig. C-1. Approximate electron loss boundaries in midplane energy space.

$$x_L^2(y^2) \equiv (R_L - 1)y^2 + \frac{2e}{m}(\phi_0 - \phi_L).$$

Then

$$n_e(L) = NR_L \int_0^\infty 2\pi y dy\, e^{-y^2/c_\perp^2}$$

$$\times \left\{ \int_{x_L^2}^{x_1^2} \frac{d(x^2)}{\sqrt{x^2 - x_L^2}} e^{-x^2/c_\parallel^2} \left[1 - (1 - \xi) e^{-\kappa'(x_1^2 - x^2)/c_\parallel^2} \right] \right.$$

$$\left. + \frac{1}{2} \int_{x_1^2}^\infty \frac{d(x^2)}{\sqrt{x^2 - x_L^2}} e^{-x^2/c_\parallel^2} \left[\xi e^{-\kappa(x^2 - x_1^2)/c_\parallel^2} \right] \right\} \qquad (C2)$$

2. Evaluation of Integrals

To do these integrals by parts, first transform from x,y to t,u as follows:

$$c_\parallel t = \sqrt{x^2 - x_L^2} \qquad ; d(x^2)/\left(\sqrt{x^2 - x_L^2}\right) = 2c_\parallel dt$$

$$c_\parallel u = \sqrt{x_1^2 - x_L^2} = \sqrt{(2e\phi_L/m) - (R_L - R_W)y^2} \; ; \; 2ydy = -(R_L - R_W)^{-1} c_\parallel^2 2udu.$$

x from x_L to ∞ maps into t from 0 to ∞.

y from 0 to y_0 maps into u from $\phi^{1/2}$ to 0, where $\phi \equiv \frac{2}{m} e\phi/c_\parallel^2$.

y from y_0 to ∞ will be done separately. Then

$$e^{-x^2/c_\parallel^2} e^{-\kappa'(x_1^2 - x^2)/c_\parallel^2} = e^{-x_L^2/c_\parallel^2} e^{-(b+1)u^2} e^{-bt^2}$$

and

$$e^{-x^2/c_\parallel^2} e^{-\kappa(x^2 - x_1^2)/c_\parallel^2} = e^{-x_L^2/c_\parallel^2} e^{+(k-1)u^2} e^{-kt^2},$$

where $b \equiv \kappa' - 1$ and $k \equiv \kappa + 1$.

So the x-integrations in the curly bracket of Eq. (C2) become

$$c_\parallel e^{-x_L^2/c_\parallel^2}\left\{2\int_0^u dt\, e^{-t^2} - 2(1-\xi)e^{-(b+1)u^2}\int_0^u dt\, e^{bt^2} + \xi e^{(k-1)u^2}\int_u^\infty dt\, e^{-kt^2}\right\}.$$

If we take $\xi < 1$, $\kappa > 1$, and $\kappa' \geq 1$, all parentheses are intrinsically positive. Next let

$$a + 1 \equiv \frac{R_L - 1}{R_L - R_W}\left[1 + \frac{c_\parallel^2}{c_\perp^2(R_L - 1)}\right]$$

and

$$\phi_0 \equiv \frac{2}{m}\, e\phi_0/c_\parallel^2 = e\phi_0/T_\parallel.$$

Then

$$e^{-y^2/c_\perp^2}\, e^{-x_L^2/c_\parallel^2} = e^{-\phi_0}\, e^{-a\phi}\, e^{(a+1)u^2},$$

so

$$n_e(L) = N\pi c_\parallel^3 \frac{R_L}{R_L - R_W} e^{-\phi_0}\, e^{-a\phi}\int_0^\phi d(u^2) e^{(a+1)u^2}\left\{2\int_0^u dt\, e^{-t^2} - 2(1-\xi)e^{-(b+1)u^2}\int_0^u dt\, e^{bt^2} + \xi e^{(k-1)u^2}\int_u^\infty dt\, e^{-kt^2}\right\}$$

$$+ N\pi R_L \xi \int_{y_0^2}^\infty d(y^2) e^{-(y^2/c_\perp^2 + x_L^2/c_\parallel^2)}\int_0^\infty c_\parallel dt\, e^{-kt^2}. \qquad (C3)$$

We do the first three double integrals by parts:

$$I_1 = \int UdV = UV\Big|_0^{u=\sqrt{\phi}} - \int VdU;$$

$$U = \int_0^u dt\, e^{-t^2}, \qquad dU = e^{-u^2}\, du;$$

$$dV = 2d(u^2)e^{(a+1)u^2}, \qquad V = \frac{2}{a+1}\, e^{(a+1)u^2};$$

so

$$I_1 = \frac{2}{a+1}\, e^{a\phi}\left[e^{\phi}\int_0^{\sqrt{\phi}} dt\, e^{-t^2} - e^{-a\phi}\int_0^{\sqrt{\phi}} du\, e^{au^2}\right].$$

Similarly the second double integral is

$$I_2 = -\frac{2(1-\xi)}{a-b}\, e^{a\phi}\left[e^{-b\phi}\int_0^{\sqrt{\phi}} dt\, e^{bt^2} - e^{-a\phi}\int_0^{\sqrt{\phi}} du\, e^{au^2}\right].$$

For I_3, $\qquad U = \int_0^u dt\, e^{-kt^2}, \qquad dU = -e^{ku^2}\, du;$

$$dV = \xi e^{(k+a)u^2} d(u^2), \qquad V = \frac{\xi}{k+a}\, e^{(k+a)u^2};$$

$$I_3 = \frac{\xi}{k+a}\, e^{a\phi}\left[e^{k\phi}\int_{\sqrt{\phi}}^{\infty} dt\, e^{-kt^2} + e^{-a\phi}\int_0^{\sqrt{\phi}} du\, e^{au^2} - \frac{1}{2}\left(\frac{\pi}{k}\right)^{1/2} e^{-a\phi}\right].$$

Finally, $e^{-(y^2/c_\perp^2 + x_L^2/c_\parallel^2)} = e^{-(\phi_0-\phi)}\, e^{-(a+1)(R_L-R_W)(c_\parallel^{-2})y^2}$, so that

$$I_4 = e^{-(\phi_0-\phi)}\int_{y_0^2}^{\infty} d(y^2) e^{-(a+1)(R_L-R_W)(c_\parallel^{-2})y^2} \cdot c_\parallel \int_0^{\infty} dt\, e^{-kt^2}$$

$$= \frac{c_\parallel\, e^{-(\phi_0-\phi)}\, e^{-(a+1)(R_L-R_W)(c_\parallel^{-2})y_0^2}}{(a+1)(R_L-R_W)} \cdot \frac{1}{2}\left(\frac{\pi}{k}\right)^{1/2}$$

$$= \frac{c_{\|}^3 e^{-\phi_0}}{R_L - R_W} \frac{e^{-a\phi}}{a+1} \frac{1}{2} \left(\frac{\pi}{k}\right)^{1/2} .$$

Note that, with their respective coefficients in (C3), I_1 alone gives the density due to a Maxwellian cutoff abruptly at x_1, I_2 is the damping correction (always negative) for ST particles; I_3 is the "tail" of SF electrons with $y < y_0$, i.e. decelerated in region II but still lost; I_4 is due to electrons with $y > y_0$, accelerated out from $s = L$ by the predominance of magnetic forces. We expect I_3 and I_4 to be much smaller than $I_1 + I_2$ for reasonably large ϕ, because the "tail" is small (height $\propto \xi$) and short ($\kappa \gg 1$) for reasonable loss flux.

Treating $I_3 + I_4$ as a small correction to be dealt with subsequently, we have

$$n_e(L) \approx N\pi c_{\|}^3 \frac{R_L}{R_L - R_W} \frac{2}{a+1} e^{-\phi_0} \left\{ \left[e^{\phi} \int_0^{\sqrt{\phi}} dt\, e^{-t^2} - e^{-a\phi} \int_0^{\sqrt{\phi}} dt\, e^{at^2} \right] - (1-\xi)\left(\frac{a+1}{a-b}\right) \left[e^{-b\phi} \int_0^{\sqrt{\frac{a}{b}\phi}} dt\, e^{bt^2} - e^{-a\phi} \int_0^{\sqrt{\phi}} dt\, e^{at^2} \right] \right\} .$$

From Fig. 11 one can see that, for $x_1^2(0) \equiv \phi_0 c_{\|}^2 \geq 4\, c_{\|}^2$ (i.e. $e\phi_0 \geq 4\, T_{e\|}$) and $\kappa' \geq 1$, the normalization N differs by at most a percent or two from that of an ordinary Maxwellian:

$$N = n_0 \pi^{-3/2} c_{\parallel}^{-1} c_{\perp}^{-2} .$$

And for isotropy, where $c_{\parallel} = c_{\perp}$,

$$\frac{R_L}{R_L - R_W} \frac{1}{a + 1} = 1.$$

For this case, then,

$$\boxed{\frac{n_e(L)}{n_0} \approx e^{-\phi_0} \, \mathrm{EST}(\phi_L, a_L, b, \xi),} \tag{C4}$$

with $\phi_L \equiv e\phi_L/T_e$ and $a_L \equiv R_W/(R_L - R_W)$, and

$$\mathrm{EST}(\phi, a, b, \xi) \equiv \frac{2}{\sqrt{\pi}} \left\{ \left[e^{\phi} \int_0^{\sqrt{\phi}} dt \, e^{-t^2} - e^{-a\phi} \int_0^{\sqrt{\phi}} dt \, e^{at^2} \right] - (1 - \xi) \left(\frac{a + 1}{a - b} \right) \left[e^{-b\phi} \int_0^{\sqrt{\phi}} dt \, e^{bt^2} - e^{-a\phi} \int_0^{\sqrt{\phi}} dt \, e^{at^2} \right] \right\} . \tag{C5}$$

3. Various Approximations

For $a\phi$, $b\phi \lesssim 3$, a power series representation,

$$e^{-\gamma\phi} \int_0^{\sqrt{\phi}} dt \, e^{\gamma t^2} = \phi^{1/2} \sum_0^{\infty} \frac{2^n}{(2n + 1)!!} (-\gamma\phi)^n$$

(with γ = a, b, or -1) converges reasonably. As an approximation to Eq. (C5) one has (for the isotropic case)

$$\mathrm{EST}(\varphi, a, b, \xi) = \frac{2}{\sqrt{\pi}} \phi^{1/2} \sum_0^{\infty} \frac{2^n \phi^n}{(2n + 1)!!} \left\{ \left[1 - (-a)^n \right] + (1 - \xi) \left(\frac{a + 1}{a - b} \right) (-1)^n \left[a^n - b^n \right] \right\} . \tag{C6}$$

The n = 0 term in the sum is zero; the n = 1 term is $\frac{2}{3}(a + 1)\xi\phi$, which is small of order ξ; the first "large" term is the n = 2 term,

$$\frac{4}{15}(a + 1)\left[(b + 1) - \xi(a + b)\right]\phi^2$$

and for n = 3,

$$\frac{-8}{7 \times 5 \times 3}(a + 1)\left[(a - 1) + b(a + b) - \xi(a^2 + b^2 + ab)\right]\phi^3 .$$

We shall see shortly that it is not unreasonable to take $\xi = 0.1$, $a = 2$ to 3, and $b = 0$. For these values we have Table CI. Crudely then, if one expects $\xi \ll \phi \lesssim 1$,

$$\frac{n_e(L)}{n_0} \sim 0.3e^{-\phi_0}(a + 1)\left[(b + 1) - \xi(a + b)\right]\phi^{5/2}, \qquad (C7)$$

for a not too large. (Recall that $a + 1 = R_L/(R_L - R_W)$ and $b + 1 = \kappa'$.) For $b \neq 0$ the dominance of the n = 2 term ($\phi^{5/2}$ approximation) is less; for a = 2 and $\xi = 0.1$ the coefficients of ϕ^n in the sum, when b = 0.5, 1.0, are listed in Table CII.

For $a\phi \gtrsim 3$ (e.g. for $R_L - R_W \ll 1$) but $b\phi \lesssim 1$, we use the asymptotic form[72]

$$e^{-a\phi}\int_0^{\sqrt{\phi}} dt\, e^{at^2} \approx \left[\frac{\phi^{1/2}}{2a\phi}\; 1 + \frac{1}{2a\phi} + \frac{3}{4(a\phi)^2} + \cdots\right]$$

so that, again for the isotropic case,

Table CI. Terms in the series expansion of $EST(\varphi,a,b,\xi)$ for $b = 0$.

	I_1 term $1 - (-a)^n$		I_2 term $(1 - \xi)\frac{a+1}{a-b}(a^n - b^n)(-1)^n$		$\frac{2^n}{(2n+1)!!}$	Coef. of φ^n in Σ	
	a=2,	3	a=2,	3		a=2,	3
n = 1	3	4	- 2.7	- 3.6	$\frac{2}{3}$	0.20	0.27
n = 2	-3	- 8	5.4	10.8	$\frac{4}{15}$	0.64	0.75
n = 3	9	28	-10.8	-32.4	$\frac{8}{7 \times 15}$	-0.14	-0.34
n = 4	-15	80	21.6	96	$\frac{16}{63 \times 15}$	0.11	0.27

Table CII. Coefficients of φ^n in the sum Eq. (C6) when b = 0.5, 1.0.

	b = 0.5	b = 1.0
n = 1	0.20	0.20
2	1.00	1.36
3	-0.396	-0.755
4	0.233	0.415

(a = 2)

$$\mathrm{EST}(\phi, a, b, \xi) \approx \frac{2}{\sqrt{\pi}}\phi^{1/2}\left\{\sum_0^\infty \frac{2^n\phi^n}{(2n+1)!!}\left[1 - (1-\xi)\left(\frac{a+1}{a-b}\right)(-1)^n b^n\right]\right.$$
$$\left. - \frac{1}{2a\phi}\left[1 - (1-\xi)\left(\frac{a+1}{a-b}\right)\right]\left[1 + \frac{1}{2a\phi} + \frac{3}{4(a\phi)^2} + \cdots\right]\right\} \quad (C8)$$

in which the last line is a small correction. The "exact" form of Eq. (C5) and the approximate forms of Eqs. (C7) and (C8) are shown in Figs. 12 and 13 for several values of a, b.

The correction terms involving I_3 and I_4 are

$$n_e^{SF}(L) = \xi n_0 \frac{e^{-\phi_0}}{\sqrt{\pi}}\left\{\frac{a+1}{k+a}\left[e^{-a\phi}\int_0^{\sqrt{\phi}} dt\, e^{at^2} + e^{k\phi}\int_{\sqrt{\phi}}^\infty dt\, e^{-kt^2}\right]\right.$$
$$\left. + \frac{1}{2}\frac{k-1}{k+a}\left(\frac{\pi}{k}\right)^{1/2} e^{-a\phi}\right\}.$$

For $a \geq 1$, the first function in square brackets reaches a maximum of less than 0.55 at $\phi < 1$. The second function is always less than $0.89k^{-12}$ and behaves like $\frac{1}{2}k^{-1}\phi^{-1/2}$ for $\phi \gtrsim 2k^{-1}$. The coefficient of $e^{-a\phi_0}$ in the last term is always less than 0.27 for $k \geq 1$ and $a \geq 1$. Thus, for all ϕ,

$$\frac{n_e^{SF}(L)}{n_0} < \xi e^{-\phi_0} \qquad \text{for } k, a \geq 1,$$

compared with $n_e^{ST}(L)/n_0 = e^{-\phi_0}\mathrm{EST}(\phi_L, a_L, b, \xi)$ in Fig. 7 , so that this correction is only important for $\phi \lesssim 0.2$ for any $k, a \geq 1$. (For $k = 10$ and $a = 2$, n_e^{SF}/n_0 has a maximum of $0.16\xi e^{-\phi_0}$ at $\phi = 0$, dropping

to about $0.14\xi e^{-\phi_0}$ at $\phi = 0.2$; and $n_e^{SF} = n_e^{ST}$ at $\phi \sim 0.12$. By the time ϕ is as large as 0.2, $n_e^{ST} \gtrsim 3n_e^{SF}$.)

4. Equation for the Loss Flux

We have said that we expect $\xi < 1$ and $k \gg 1$. Some insight into appropriate sizes for ξ and k is gained from the equation for electron flux at s = W based on this model g(x,y):

$$F_e(W) = \frac{N\pi}{2} R_W \int_0^\infty d(y^2) e^{-y^2/c_\perp^2} \int_{x_1^2(y^2)}^\infty d(x^2) e^{-x^2/c_\parallel^2} \left[\xi e^{-\kappa(x^2 - x_1^2)/c_\parallel^2} \right]. \qquad (C9)$$

Letting $u \equiv c_\parallel^{-2}(x^2 - x_1^2)$ the integral over x^2 becomes

$$\xi c_\parallel^2 e^{-x_1^2/c_\parallel^2} \int_0^\infty du\, e^{-ku}, \quad \text{where } k = \kappa + 1 \text{ as before.}$$

Then, using the definitions of x_1^2, ϕ, and ϕ_0,

$$F_e(W) = \frac{N\pi}{2} R_W c_\parallel^2 \frac{\xi}{k} \left[e^{-\varphi_0} \int_0^{y_0^2} d(y^2) e^{-\beta_W y^2} + e^{-(\varphi_0 - \varphi)} \int_{y_0^2}^\infty d(y^2) e^{-\beta_L y^2} \right]$$

where $\beta_W \equiv c_\perp^{-2} + (R_W - 1)c_\parallel^{-2}$

and $\beta_L \equiv c_\perp^{-2} + (R_L - 1)c_\parallel^{-2}$.

Now using $y_0^2 \equiv c_\parallel^2 \varphi/(R_L - R_W)$ to define

$$a_W + 1 = \beta_W y_0^2/\varphi = \frac{R_W - 1}{R_L - R_W}\left[1 + \frac{c_\parallel^2}{c_\perp^2(R_W - 1)}\right]$$

and

$$a_L + 1 = \beta_L y_0^2/\varphi = \frac{R_L - 1}{R_L - R_W}\left[1 + \frac{c_\parallel^2}{c_\perp^2(R_L - 1)}\right] \equiv a + 1,$$

we have

$$F_e(W) = \frac{N\pi}{2}\frac{R_W}{R_L - R_W} c_\parallel^4 e^{-\varphi_0}\frac{\xi}{k}\left[\frac{1 - e^{-(a_W+1)\varphi}}{a_W + 1} + \frac{e^{-a_L\varphi}}{a_L + 1}\right].$$

Then, again using $N = n_0\pi^{-3/2}c_\parallel^{-1}c_\perp^{-2}$, we have for the isotropic case $c_\parallel = c_\perp = c_e$,

$$\boxed{F_e(W) = \frac{\xi}{k} n_0 c_e \frac{1}{2\sqrt{\pi}} e^{-\varphi_0}\left[1 - \frac{1}{a + 1} e^{-a\varphi}\right],} \qquad (C10)$$

where we have used $a \equiv a_L = a_W + 1 = R_W/(R_L - R_W)$ for isotropy. For $a\varphi \gtrsim 2$ this result depends only weakly on φ. Compare this with the ion flux $F_i(W) = (R_W L\nu/c_{i\parallel})n_0 c_{i\parallel}$, where the parenthesis is typically of order $10^{-3.5}$: $F_e = F_i$ gives

$$\frac{\xi}{k} = 2\sqrt{\pi}\, e^{\varphi_0}\frac{c_{i\parallel}}{c_e}\left[1 + \frac{1}{a + 1} e^{-a\varphi}\right]^{-1} \frac{R_W L\nu}{c_{i\parallel}}.$$

For protons with $T_\parallel = 10\ T_e$ and for $\varphi_0 = 5$, $2\sqrt{\pi}\, e^{\varphi_0} c_{i\parallel}/c_e \approx 40$, so that $\xi/k \sim 0.01$ typically. Thus if, for instance, $\xi = 0.1$ and $k = 10$ this can be satisfied. If we now choose $\kappa' = \kappa\xi/(1 - \xi)$ so that the slope of g is continuous, then ξ/k becomes (using $k \equiv \kappa + 1$) just

ξ^2/κ', showing that if the "damping" of g is not too abrupt (say $\kappa' \lesssim 2$) then ξ is in fact small. If the ion loss of the ratio $T_{i\|}/T_e$ is enhanced by a factor of ten, the smallness of ξ begins to break down. The actual realistic values for κ' and ξ can be determined only from the detailed nature of the scattering process.

5. Extension to s > L

The preceding analysis does not require that L be the point of maximum B; only the values of a and φ would be changed if L had been some other point s. The region of integration in (C2), however, may not have the simple form

$$x^2 > (R_s - 1)y^2 + \frac{2}{m} e(\phi_0 - \phi_s)$$

for some general point s as it does for s = L. A look at Fig. 2 will verify this. Fortunately, most of the alterations occur in the region $y \approx y_0$, and if $\varphi_0 \sim 5$ and $\varphi \sim 1$, y_0 is large enough so that there are only a few electrons in this part of velocity space. The contribution to $n_e(L)$ from values of the integration variable y larger than some y_1, for $0 < y_1 < y_0$, is found by replacing $u^2 = \varphi$ by

$$u^2 = \varphi^* \equiv \varphi(1 - y_1^2/y_0^2)$$

in the limits of the $d(u^2)$ integration in Eq. (C3). Thus the ratio

$$\frac{n_e^{ST} \text{ due to } y > y_1}{n_e^{ST}} = e^{-a\varphi y_1^2/y_0^2} \cdot \frac{EST(\varphi^*,a,b,\xi)}{EST(\varphi,a,b,\xi)}$$

$$\sim e^{-a\varphi y_1^2/y_0^2} (1 - y_1^2/y_0^2)^{5/2}$$

for $a\varphi \lesssim 2$ (or less than this if $y_1 > 0.9\, y_0$). For $y_1^2/y_0^2 = 1/2$ this ratio is about 1/16, if $a = 2$ and $\varphi \sim 1$. So for points $s > L$ but not too near W, $n_e(s)/n_0$ is given by Eq. (C4) with a_L replaced by $a_s \equiv R_W/(R_s - R_W)$ and $\varphi_L \equiv e\phi_L/T_e$ replaced by $\varphi_s \equiv e\phi_s/T_e$:

$$n_e(s)/n_0 \approx e^{-\varphi_0} \mathrm{EST}(\varphi_s, a_s, b, \xi),$$

again ignoring the SF particles (terms I_3 and I_4).

Let us now look more carefully at the region of integration for $s > L$. Particles contributing to $n_e(s)$ are those which are not turned around at any $s' < s$, i.e. those to the right of all lines $\epsilon_{s'}(\epsilon_\perp)$ for $s' < s$ in Fig. 2. (Recall that $\epsilon_\parallel = \frac{m}{2} x^2$, $\epsilon_\perp = \frac{m}{2} y^2$. In constructing Fig. 2, we have assumed that $d\phi/ds < 0$ at all s--including $s = L$, where $dR/ds = 0$.) In general, part of the exact integration boundary is the envelope of the preceding $\epsilon_{s'}$ lines

$$\epsilon_\parallel = \epsilon_{s'}(\epsilon_\perp) \equiv (R_{s'} - 1)\epsilon_\perp + e(\phi_0 - \phi_{s'}),$$

and thus its shape depends on the final answer, ϕ_s

The lines $\epsilon_\parallel = \epsilon_s(\epsilon_\perp)$ and $\epsilon_\parallel = \epsilon_{W+}(\epsilon_\perp)$ intersect at

$$\epsilon_\perp = \frac{e\phi_s}{R_s - R_w}.$$

If $d\phi/ds < 0$ at L where $dR/ds = 0$, then as s increases beyond L, this value of $\epsilon_\perp$ first decreases, then increases again (an effect related to the fact that the maximum of $U = \mu B - e\phi$ is at a value of s slightly larger than L if $\mu \neq 0$.) For s near L, so that $e\phi_s/(R_s - R_W) < e\phi_1/(R_1 - R_W)$, the triangle

$$\epsilon_s(\epsilon_\perp) < \epsilon_\parallel < \epsilon_{W+}(\epsilon_\perp), \qquad 0 < \epsilon_\perp < \frac{e\phi_s}{R_s - R_w}$$

is thus a good approximation to the region of integration for the ST particles (integrals I_1 and I_2). For s nearer to W, where $e\phi_s/(R_s - R_W) > e\phi_L/(R_L - R_W)$, the upper portion $\epsilon_\perp > e\phi_L/(R_L - R_W)$ (i.e. $y > y_0$) of the triangle should not be part of the integration region, and using the technique just discussed for evaluating the contribution from y greater than some y_1 we can subtract it off. The remainder, according to Fig. 2, is a much better approximation to the exact integration region. A still better approximation is obtained by subtracting off all of $y > y_1$, where y_1 in the intersection of $x_s(y)$ and $x_L(y)$,

$$\frac{m}{2} y_1^2 = \frac{e(\phi_L - \phi_s)}{R_L - R_s}$$

(see Fig. C-2):

$$\frac{n_e^{ST}(s)}{n_0} \approx e^{-\varphi_0} \left\{ EST(\varphi_s, a_s, b, \xi) - \exp\left[- \frac{R_W}{R_L - R_s} (\varphi_L - \varphi_s) \right] EST\left[\varphi_S - (\varphi_L - \varphi_s) \frac{R_s - R_W}{R_L - R_s}, a_s, b, \xi \right] \right\}$$

where EST is understood to be zero if its first argument is negative. The correction term increases from zero at some $s \lesssim W$ to a finite value at $s = W^-$. The worst case is obviously $s = W^-$, where $\phi_s = \phi_W$ and $R_s = R_W$, i.e. the left and right boundaries of the integration region for n_e^{ST} are the parallel lines

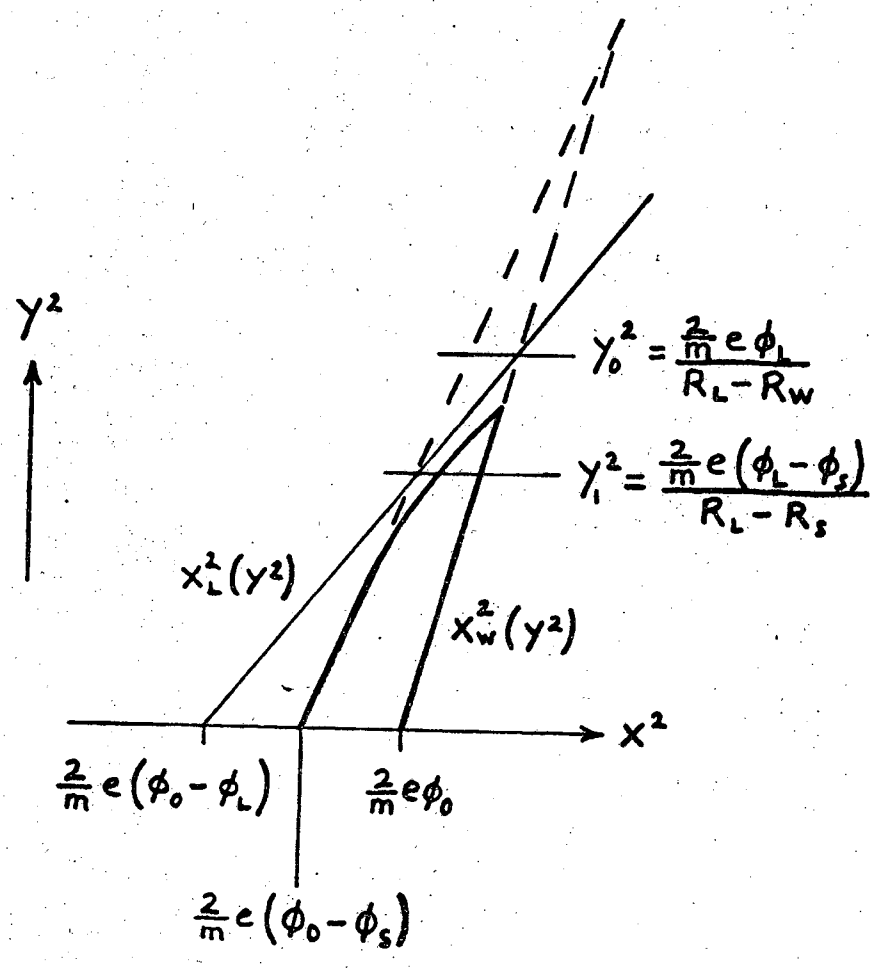

Fig. C-2. Exact integration region for ST electrons at s (heavy curve). Approximate integration region (dashed triangle) truncated at y_0^2 or y_1^2.

$$\epsilon_{\|} = (R_W - 1)\epsilon_{\perp} + e(\phi_0 - \phi_W)$$
$$\epsilon_{\|} = (R_W - 1)\epsilon_{\perp} + e\phi_0 \ .$$

For this case $a_s = \infty$, we have

$$\boxed{\frac{n_e^{ST}(W)}{n_0} = e^{-\varphi_0}\left[1 - e^{-a_L(\varphi_L - \varphi_W)}\right] EST(\varphi_W, \infty, b, \xi).} \qquad (C12)$$

We note in passing that

$$EST(\varphi, \infty, b, \xi) = \frac{2}{\sqrt{\pi}}\varphi^{1/2}\left\{\xi + \sum_1^{\infty} \frac{2^n\varphi^n}{(2n+1)!!}\left[1 - (1 - \xi)(-b)^n\right]\right\} \qquad (C13)$$

and the correction due to SF particles is $(4k\varphi)^{-1}$ times the ξ term in this expression, i.e. negligible except for $\varphi \lesssim \xi$.

When formula (B2) is generalized to an arbitrary point s, the contribution from the SF electrons may also be corrected by extending the y^2 integration only up to $y^2 = y_0^2$ in Fig. C-2. And since the contribution of those particles above y_0^2 is negligible, we can write an expression analogous to Eq. (C12) for $n_e^{SF}(W)$:

$$\boxed{\frac{n_e^{SF}(W)}{n_0} = \left[1 - e^{-a_L\varphi_L}\right] \frac{1}{2}\xi k^{-1/2} e^{k\varphi_W} \operatorname{erfc}\sqrt{k\varphi_W}\, e^{-\varphi_0}} \qquad (C14)$$

where the expression to the right of the square bracket is just the previous form of $n_e^{SF}(L)$ with φ_L changed to φ_W and a_L changed to a_W ($a_W \equiv 0$).

6. Comparison with Simpler Models

Now we compare the entire damped-Maxwellian model with first the ordinary Maxwellian and second a simple dimensional model.

If g is an undamped Maxwellian for $x > x_1$ (particles leaving the device) but still zero for $x < -x_1$ (no SF particles returning from $s > L$ to $s < L$), then we have $\kappa = 0$, $k = 1$, and $\xi = 1$ in Eq. (C1) and subsequently. The term involving I_2 is zero. For this case, then,

$$\frac{n_e^{ST}(L)}{n_0} = \frac{2}{\sqrt{\pi}} e^{-\varphi_0} \left[e^{\varphi} \int_0^{\sqrt{\varphi}} dt\, e^{-t^2} - e^{-a\varphi} \int_0^{\sqrt{\varphi}} dt\, e^{at^2} \right]$$

and

$$\frac{n_e^{SF}(L)}{n_0} = \frac{1}{\sqrt{\pi}} e^{-\varphi_0} \left[e^{-a\varphi} \int_0^{\sqrt{\varphi}} dt\, e^{at^2} + e^{\varphi} \int_{\sqrt{\varphi}}^{\infty} dt\, e^{-t^2} \right]. \qquad (C15)$$

If particles are also supplied in the returning tail so that the entire distribution is Maxwellian, then the region of integration for the SF particles is doubled. The terms involving a then cancel to give the usual result

$$\frac{n_e(L)}{n_0} = e^{-(\varphi_0 - \varphi)}$$

The "damping" of the Maxwellian, thus replaces

$$\frac{n_e(L)}{n_0} = e^{-\varphi_0} e^{\varphi_L}$$

with $$\frac{n_e(L)}{n_0} = e^{-\varphi_0} EST(\varphi_L, a_L, b, \xi).$$ (See Fig. 13.)

A simple dimensional estimate of n(s), for s near L, may be got by expanding $g(x,y)$ in $x^2 - x_1^2$ near $y = 0$ and assuming $g(x_1,y) = 0$

(i.e. neglecting the SF particles). For simplicity, we take $c_{\parallel} = c_{\perp} = c_e$ and $c_e > y_0$ (see Fig. C-2) so that exponential decay of g and y^2 can be neglected over the integration region for n(s). For s near L, the integration region consists of the two triangles in x^2, y^2 (one for $x > 0$ and one for $x < 0$);

$$x_s^2 < x^2 < x_1^2, \qquad y^2 < y_0^2 \equiv \frac{c_e^2 \varphi_s}{R_s - R_W}$$

(for s = L, see Fig. C-1). The area of these is $c_e^4 \varphi_s^2 (R_s - R_W)^{-1}$. We write $g(x,y) = (x_1^2 - x^2)S_0$, where $S_0 = -\partial g/\partial(x^2)$ evaluated at $x = x_1$ and $y = 0$. Then

$$n(s) = \frac{\pi}{2} R_s \int d(y^2) \int d(x^2) \frac{g(x,y)}{\sqrt{x^2 - x_s^2}}$$

becomes

$$n(s) \sim R_s c_e^4 \varphi_s^2 (R_s - R_W)^{-1} \left\langle \frac{x_1^2 - x^2}{\sqrt{x_2 - x_s^2}} \right\rangle S_0,$$

where $\langle\ \rangle$ means an average over the integration region. But, crudely,

$$\left\langle \frac{x_1^2 - x^2}{\sqrt{x^2 - x_s^2}} \right\rangle \sim c_e \varphi_s^{1/2},$$

and for a rough guess (an underestimate, actually) at S_0, we calculate it from a Maxwellian:

$$S_0 = \frac{n_0}{\pi^{3/2}} \frac{e^{-\varphi_0}}{c_e^5} .$$

Thus we have

$$\frac{n(s)}{n_0} \sim \pi^{-3/2} \frac{R_s}{R_s - R_w} \varphi_s^{5/2} e^{-\varphi_0} \qquad \text{(C16)}$$

(for s near L), which should be compared with Eq. (C7).

D. Comparison with Existing Theory for ϕ_s

In this appendix we discuss an equation due to Newcomb[29] as presented by Kaufman:[74]

$$-\frac{ed\phi(s)}{dB(s)} \approx \frac{T_{e\|}(s)}{2B(s)}\left[\langle v_\perp^2 / v_\|^2\rangle_i - \langle v_\perp^2/v_\|^2\rangle_e\right], \qquad (D1)$$

where the local values of these averages, at s, are to be used. We first recapitulate the derivation, then discuss the result. Let the functional S(A) of any function $A(s,\mu,H)$ be defined by

$$S(A) \equiv \sum_{\text{species } a} B\int_0^\infty d\mu \int_{\mu B+q_a\phi}^\infty dH\left[2m_a(H - \mu B - q_a\phi)\right]^{1/2} \times \frac{\partial - F_a(\mu,H)}{\partial H} A_a(s,\mu,H). \qquad (D2)$$

where $F_a(\mu,H)$ is the midplane distribution function, f_a, of species a except for a constant normalization factor $F_a(\mu,H) = 2\pi/m_a^2\left[f_a(v_\|,v_\perp)\right]$ with $v_\| = v_\|(\mu,H)$ and $v_\perp = v_\perp(\mu)$. This functional is linear; and for any constant function $A_a = C_a(s)$,

$$S(C) = \sum_a C_a \int_0^\infty d(\mu B)\int_0^\infty d\left[2m_a(H - \mu B - q_a\phi)\right]^{1/2} F_a(\mu,H)$$

$$= \sum_a C_a n_a,$$

where we have simply integrated by parts.

To calculate dS(A)/ds, one must consider the s-dependence of

(a) the factor B before the integral

(b) the B and ϕ in the limit of integration

(c) the B and ϕ in the integrand, and

(d) A in the integrand.

The contribution of (b) is identically zero since the integrand is zero at the limit of integration. For dS(A)/ds we have then

$$\frac{dS(A)}{ds} = \frac{1}{B}\frac{dB}{ds} S(A) - \frac{1}{2B}\frac{dB}{ds} S\left(\frac{\mu B}{H - \mu B - q\phi} A\right) - \frac{1}{2\phi}\frac{d\phi}{ds} S\left(\frac{q\phi}{H - \mu B - q\phi} A\right) + S\left(\frac{\partial A}{\partial s}\right) \quad (D3)$$

From quasineutrality, $S(q) = 0$; so with $A = q$ we have from Eq. (D3)

$$-\frac{d\phi(s)}{dB(s)} = \frac{S(qv_\perp^2/v_\parallel^2)}{2BS(q^2/mv_\parallel^2)} . \quad (D4)$$

The functionals S(A) are dimensionally and qualitatively like an average of A multiplied by the density, summed over species:

$$S(q^2/mv_\parallel^2) \sim ne^2/T_{e\parallel}(s) + ne^2/T_{i\parallel}(s) \quad (D5)$$

and

$$S(qv_\perp^2/v_\parallel^2) \sim ne\left[\langle v_\perp^2/v_\parallel^2\rangle_i - \langle v_\perp^2/v_\parallel^2\rangle_e\right] \quad (D6)$$

evaluated at s. Thus

$$-\frac{ed\phi(s)}{dB(s)} \sim \frac{\bar{T}_\parallel(s)}{2B(s)}\left[\langle v_\perp^2/v_\parallel^2\rangle_i - \langle v_\perp^2/v_\parallel^2\rangle_e\right]$$

with $\bar{T}_{\|}(s) = \dfrac{T_{e\|}T_{i\|}}{T_{e\|} + T_{i\|}}$ evaluated at s.

Crudely, $v_\perp^2/v_\|^2 \sim T_\perp(s)/T_\|(s)$. At the mirror, $T_{i\|}$ is very small since only the SF ions are creeping over the barrier. $T_{e\|}$ is not so small if ϕ continues to decrease in region II. So, using $T_\perp(s)/B(s) = T_\perp(0)/B_0$, Eq. (D1) becomes

$$-\frac{ed\phi}{dB} \sim \frac{T_{i\perp}}{2B_0}$$

near the mirror. $T_{i\perp}$ indicates the usual midplane temperature. The right side is finite as $dB/ds \to 0$, so $d\phi/ds \to 0$ at the mirror.

In region II we see that Eq. (D1) predicts increasing, rather than decreasing, ϕ; the right side does not change sign. But this equation is not correct in region II, as we now show. $S(1) = \sum_a n_a$ holds only when the region $H > \mu B + q\phi$ is filled with particles governed by $F(\mu,H)$, as a look at the lower limit of the H integration in S shows. The more general lower limit to be used in the definition (D2) of S is

$$H_a' = \sup_{s' \le s} \left[\mu B(s') + q_s \phi(s')\right] \tag{D7}$$

as in Eq. (5) of the main text, in the language of midplane velocities x and y. But with this change in the integration limit, it is still not true that $\frac{1}{2} S(1) = n$, or $S(q) = 0$. Instead,

$$n_a = S_a(1) - B\int_0^\infty d\mu \left[2m_a(H_a' - \mu B - q_a\phi)\right]^{1/2} F_a(\mu,H_a') \tag{D8}$$

where H_a' is the expression (D7), a function of μ but not s. (This new expression is obtained upon integrating (D2) by parts with the new lower limit of H-integration. The subtraction represents the fact that the low-$v_\parallel$ part of phase space at s in region II is empty if there are only SF particles there.) So if

$$\sup_{s'\le s}\left[\mu B(s') + q\phi(s')\right] \neq \mu B(s) + q\phi(s),$$

as in region III for the ions, then Eq. (D4) is incorrect, even though Eq. (D3) is still correct. The contribution (b) from the limit of integration is again zero, but now for a different reason: the limit

$$\sup_{s'\le s}\left[\mu B(s') + q\phi(s')\right]$$

for the ions is independent of s.

Furthermore, if $d\phi/ds < 0$ at the mirror, instead of 0 as implied by Eq. (D1), then for ions the maximum of $\mu B + q\phi$ occurs at $s = M(\mu) \le L$. This means that even <u>at</u> $s \approx L$, the more general lower limit must be used. Consequently, Eq. (D1) also fails near the mirror, and there is no physical requirement that $d\phi/ds$ be zero there.

From Eq. (D8) and quasineutrality we have $S(q) = X(q)$ instead of $S(q) = 0$, where

$$X(A) = \sum_a B \int_0^\infty d\mu \left[2m_a(H_a' - \mu B - q_a\phi)\right]^{1/2} F_a(\mu, H_a') A_a(s, \mu, H_a') \qquad (D9)$$

with H_a' given by Eq. (D7). H_a' is a function of μ.

If one plans to use Eq. (D3), there can now be special problems evaluating the left hand side, if $H' - \mu B - q\phi \neq 0$ over only part of

the μ-integration range for species a. If it is zero for all μ for both species, there is no problem because $X(q) \equiv 0$. If it is nonzero for all μ for both species, we have

$$\frac{dS(q)}{ds} = \frac{1}{2B}\frac{dB}{ds} X\left(q\frac{\mu B}{H' - \mu B - q\phi} + 2q\right) + \frac{1}{2\phi}\frac{d\phi}{ds} X\left(\frac{q^2\phi}{H' - \mu B - q\phi}\right). \quad (D10)$$

But if for some a, $H_a' - \mu B - q_a\phi \neq 0$ for some $\mu > \mu_0(s)$, but $H_a' - \mu B - q_a\phi \equiv 0$ for $\mu < \mu_0(s)$, the coefficients of the X's in Eq. (D10) cannot be factored out. The terms of (D10) are separately infinite, having nonintegrable singularities in the integrands because $(H_a' - \mu B - q_a\phi)^{1/2}$ departs from zero linearly at $\mu = \mu_0(s)$. The situation is analogous to

$$\int_0^\infty d\mu \frac{\mu x - y}{\sqrt{(\mu x - y)^2 + h(\mu)0\left[(\mu x - y)^4\right]}}$$

for an arbitrary function $h(\mu)$, where, for x and y positive, one cannot write the expression as

$$x\int_0^\infty \frac{\mu d\mu}{\sqrt{(\text{above})}} - y\int_0^\infty \frac{d\mu}{\sqrt{(\text{above})}}$$

The proper nonsingular version of Eq. (D10)

$$\frac{dS(q)}{ds} = \sum_a Bq_a\sqrt{m_a/2}\int_0^\infty d\mu\left[(H_a' - \mu B - q_a\phi)\left(\mu\frac{dB}{ds} + q\frac{d\phi}{ds}\right)^{-2}\right]^{-1/2} \times F_a(\mu, H_a')$$

is too unwieldy to give a useful expression for $(d\phi/ds)(dB/ds)^{-1}$

when substituted into Eq. (D3).

If $d\phi/ds \neq 0$ at $s = L$ where $dB/ds = 0$, then the maximum of $\mu B + q\phi$ lies outside the mirror for electrons (for those μ large enough that there is a maximum) and inside the mirror for the ions. Thus X_i gies problems for at least some range of $s < L$ and X_e gives problems for a certain distance beyond L. If for some s, $\mu B + q\phi \leq \mathrm{Sup}(\mu B + q\phi)$ for all μ, or if one simply ignores the electron density at the largest value of μ for which $\mu B - e\phi = \mathrm{Sup}(\mu B - e\phi)$, then one can get a useful expression. For $s > L$, the first condition is satisfied by the ions. Ignoring large-μ electrons then, we have, from Eqs. (D3) and (D10)

$$\frac{d\phi}{dB} \approx \frac{1}{2B}\left[\frac{X_i(ev_\perp^2/\Delta_\parallel^2) - S(qv_\perp^2/v_\parallel^2)}{-X_i(e^2/m\Delta_\parallel^2) + S(e^2/mv_\parallel^2)}\right] \tag{D11}$$

in region II, where

$$\frac{m_a}{2}\Delta_{\parallel a}^2 \equiv H_a' - \mu B - q_a\phi$$

is the minimum parallel kientic energy of species a at s. H_a' is given by Eq. (D7). F_i is zero when $\Delta_\parallel^2 < 0$. F_a is an average of F_a on the forward and backward velocity sheets. Like S, X is always non-negative. X(A) is dimensionally and qualitatively like an average over μ of $A\Delta_\parallel$ times a mean value of F at the loss boundary. Since the ion spread in parallel energy for a given μ is small in region II, the X_i's nearly cancel the S_i's. The result is

$$\frac{ed\phi}{dB} \sim \frac{T_{e\perp}}{2B_0} = \text{const.} > 0,$$

for s sufficiently far from L in region II.

E. ATYPICAL SPECIAL CASES

1. Simplification when B(s) Has No Maximum Inside the Device

In the case $W < L$ (or L undefined) there is no region II outside the confinement region. Density at the wall can be evaluated from the loss rate just as $n_i(L)$ was evaluated previously. The loss boundary in midplane energy space becomes simply

$$\epsilon_{\parallel} = (R_W - 1)\epsilon_{\perp} - q\phi_0.$$

In some short-mirror experiments, for example DCX 1.5,[75] this is the geometry. The meaningful "mirror ratio" for such devices is just R_W. Theorem 3 remains valid, so that there cannot be a denser external plasma without strong two-stream instability.

The magnetosphere is another mirror-confinement situation with no local maxima of B in the region accessible to particles. At the ionosphere (the "ends": $s = W$) it also differs from the situation assumed thus far, in that the gravitational field produces an upward-directed ambipolar electric field there (i.e., $\partial\phi/\partial s \geq 0$), and this allows the plasma density there to be greater than in the rest of the magnetosphere. (The second premise of theorem 3 is violated.) But because the ionosphere layer is thin compared with the magnetosphere dimensions, this dense, collision-dominated layer can be considered part of the "wall", i.e., to be at $s = W^+$, with a suitable reformulation of conditions at the "sheath". (Because the ionosphere is free to emit electrons, it can have little if any sheath drop.) Only the region outside the plasmapause[76] has electron temperature high enough to give significant plasma potential.[77] As with some ion-injection

experiments[19], it is not clear that the equilibrium source rates of ions and electrons are equal; and because R_W is large (of order 100), the ion loss times are much longer than corresponding 90 deg scattering times. But in any case, if the ring current belt[78] has an equatorial density of order 1 cm^{-3} and Debye length of order 20 meters (3×10^{-6} earth radii),[79] then because λ_D varies only as $n^{-1/2}$, there is no doubt that the plasma condition is satisfied at all s. Hence the ring current belt is not isolated from the ionosphere, in the sense of section IIA.

2. Hot-Electron Plasma

When $T_e \gg T_i$, the dimensionless plasma potential $\varphi_0 \equiv e\phi_0/T_e$ is reduced because scattering rates are smaller at higher temperatures, and φ_0 is determined by equating electron and ion loss rates. For $T_e/T_i \sim (m_i/m_e)^{1/3}$, the value of φ_0 necessary to maintain equal loss fluxes becomes very small, as mentioned in section IB. In this case one cannot generally have nearly-isotropic electrons, and the "damped Maxwellian" model of section IIIB is no longer a good one; the electron loss region reaches nearly to the origin in velocity space. Typically in hot-electron laboratory plasmas,[80] $T_{e\perp} \gg T_{e\parallel}$ because of electron heating by gyroresonance, and this is consistent with good confinement. There is usually a large contribution of cold electrons to f_e near $v = 0$. As a further difference, often the ions in such experiments are mostly untrapped (SF), maintaining quasineutrality by virtue of their low T_i and thus long transit times. Since usually no attempt is made to heat the ions, they may be collisional, i.e., $\nu_i L/c_i \gg 1$. Electron scattering may be primarily due to neutral

atoms.[81]

When $T_e/T_i > (m_i/m_e)^{1/3}$, ϕ_0 is negative[82] and scales with T_i, so that the shapes of the loss regions and distributions for ions and electrons are just interchanged from the usual case with $T_i \gg T_e$. Fokker-Planck calculations, both initial value problems and steady state ones, have been reported by Lieberman[81] for typical hot-electron plasma, ignoring the plasma potential and external regions.

To see what happens in the external region when ϕ_0 is negative, consider as an example the case where the ions are collisional, i.e., the ion loss region in midplane velocity space is filled by the Maxwell tail as if there were no loss boundary. The ion density at s = L is then

$$n_i(L) = n_i^{ST}(L) + n_i^{SF}(L),$$

with

$$\frac{n_i^{ST}(L)}{n_0} = \frac{2}{\sqrt{\pi}} e^{-|\psi_0|}\left[e^{|\psi|}\int_0^{\sqrt{|\psi|}} dt\, e^{-t^2} - e^{-a|\psi|}\int_0^{\sqrt{|\psi|}} dt\, e^{at^2}\right] \tag{E1}$$

$$\frac{n_i^{SF}(L)}{n_0} = \frac{1}{\sqrt{\pi}} e^{-|\psi_0|}\left[e^{-a|\psi|}\int_0^{\sqrt{|\psi|}} dt\, e^{at^2} + e^{|\psi|}\int_{\sqrt{|\psi|}}^{\infty} dt\, e^{-t^2}\right]$$

where $\psi_0 \equiv e\phi_0/T_i$, $\psi \equiv e\phi_L/T_i$, and $a = a_L = R_W(R_L - R_W)^{-1}$. These equations are taken over directly from Eq. (C14) for electrons, and it is assumed that rgion II is collisionless so that no SF ions return to region I. The electron density at s = L is

$$n_e(L) = n_e^{SF}(L) + n_e^{c}(L),$$

with

$$n_e^{SF}(L) \sim n_0^H R_L P^{1/4} (L\nu/c_e)^{3/4}$$

and

$$n_e^c(L) \sim F_0^c R_L \left[(2/m_e)(\phi_L - \phi_0)\right]^{-1/2} \qquad \text{(E2)}$$

as given in Eqs. (19) and (21) for ions; P and ν now refer to electrons [ν is the loss rate and $P \equiv (c_\parallel^2/c_\perp^2)(R_L - 1)^{-1}$]; F_0^c is the effective source flux of cold electrons. The electrons, however, are quickly accelerated out from s = L because of their low mass and their magnetic moment, so that the density $n_e^{SF}(s)$ decreases rapidly with s for s > L. In order that the ion density may decrease similarly, $\varphi(s)$ increases rather sharply with s to its maximum value, at which $n_i^{ST} = 0$ and $n_i = n_i^{SF}$. If this maximum is reached at some $s_1 < W$ and n_e^{SF} continues to decrease rapidly beyond s_1, n_i^{SF} may not be able to decrease correspondingly (note that $n_i^{SF} \sim \frac{1}{2} n_0 e^{-|\psi_0|}$ when $\psi = 0$) unless the gradient of ϕ reverses, accelerating out ions and (more importantly) making a trapping well for cold electrons entirely in region II. The situation is somewhat like that discussed at the end of section V. If cold electrons can collect in this new depression in $-\psi$ (Fig. E-1), it need not be very deep because now

$$n_e = n_e^{SF} + n_e^c + n_e^{TII}$$

where TII refers to cold particles trapped entirely within region II (superscript c refers to particles without magnetic moment, streaming through region II). The new contribution n_e^{TII} can be quite large for a given depth of the potential depression, since the escape time of cold particles from such a depression scales with the energy-scattering

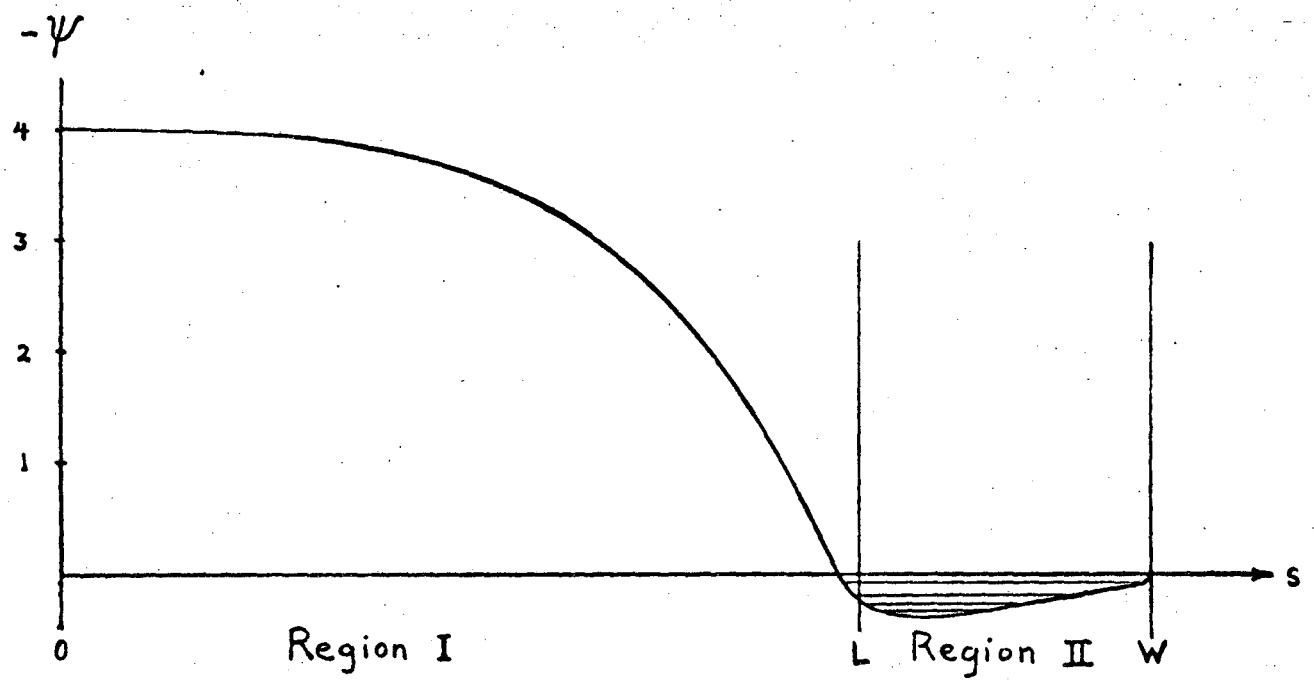

Fig. E-1. Potential energy, -ψ, for low-magnetic-moment ions in a hot- electron plasma. Hypothetical -ψ vs s, showing possible trapping of cold ions in region II.

time.

If the electrons trapped in this depression have temperature $T_W \ll T_i$, and if sufficient background gas is available to supply such electrons, then ϕ stays within a few times T_W of its maximum value, ϕ_1, as s increases. Thus $\phi_W \approx \phi_1$; the availability of very cold electrons "clamps" ϕ at roughly its maximum value for all s outboard of the maximum. But if the ions are so cold that $T_i \sim T_W$, then the scale of $\phi(s)$ is of order T_W and the depression is not a negligible feature. And since the maximum of ϕ in this case is no longer at the wall as assumed in referring to potentials in Eq. (E1) to the wall, one must change $|\psi_0|$ to $|\psi_0 - \psi_1|$ and $|\psi_L|$ to $|\psi_L - \psi_1|$ in Eq. (E1), if the wall is still defined as the zero of potential. (ψ_1 is the dimensionless potential $e\phi/T_i$ at s_1, i.e. the maximum value of ψ.)

3. Small Mirror Ratio

Decreasing temperature and decreasing mirror ratio both increase the particle loss rate (except in the case where the loss rate is governed by transit time). Let ν be the loss rate of that species which scatters slowest. (When discussing both species at once, we will use "<" to refer to this species and ">" to refer to the faster-scattering species.) When $R_L - 1 \sim 1$, ν is of order $\nu_0/\ln R_L$, where ν_0 is the cumulative 90-degree scattering rate, and transit times are assumed much faster than $\ln R_L/\nu_0$. But as $R_L - 1 \to 0$, ν increases to the inverse transit time, $v_\parallel/L$. By contrast, the faster-scattered species is contained largely by the plasma potential and its loss rate is sensitive to R_L only through the dependence of ϕ_0 on R_L (except, of course, when ϕ_0 becomes very small). In order that the loss rates

always be equal, $|\phi_0|$ must decrease(and then increase, if ϕ_0 begins at some negative value for moderate $R_L - 1$), as $R_L - 1 \to 0$, until the situation is just that of plasma in a box ($dB/ds \equiv 0$), where most of the potential ϕ_0 appears at the sheath and $n(s) \approx n_0$ for all $s < W^-$. Then

$$e\phi_0/T_e \sim \ln (\bar{v}_{e\|}/\bar{v}_{i\|}),$$

independent of scattering rates (and almost always positive) instead of

$$e\phi_0/T_> \sim \ln[\nu_0(>)/\nu_0(<)]$$

as in the case of moderate mirror ratios[17] and short bounce times. (For nonrelativistic Coulomb scattering, $\nu_0 \propto m^{-2}\bar{v}^{-3}$.) In the mirror-free limit, the time required to scatter into the velocity-space loss region is zero, and the loss time is just the transit time. In this limit the collisionless model is not a very good one; the distribution of the slower scattering species is all "tail." (In the notation of section III G, $k^{-1} = T$.) The isotropy factor P in Eqs. (28) through (31) becomes large, as discussed at the end of Appendix B. In the hot-electron plasma, if one assumes that electron lifetime is given by

$$\nu_<^{-1} = \nu_{0e}^{-1} \ln R_L + L/\bar{v}_{e\|},$$

while ion lifetime, for zero plasma potential, is

$$\nu_>^{-1} = \nu_{0i}^{-1} \ln R_L + L/\bar{v}_{i\|}.$$

Then, if ions fill the Maxwell tail, ϕ_0 increases to zero when R_L decreases to

$$R_L \sim \exp\left[\frac{L\nu_{0i}}{\bar{v}_{i\|}}\left(\frac{\nu_{0e}}{\nu_{0i} - \nu_{0e}}\right)\right].$$

(The exponential argument is usually small if T_e/T_i is very large.) For smaller R_L, ϕ_0 is positive and scales with T_e, just as if the electron scattering rate were largest.

F. FORTRAN PROGRAMS

A relatively trivial FORTRAN program, XTRNL, was run to calculate the relative ion density $n_i(s)/n_i(L)$ vs R_s and $\varphi_L - \varphi_s$, and the relative electron density $n_e(s)/n_e(L)$ (ST + SF electrons) vs R_s and $\varphi_L - \varphi_s$, for typical parameters, and to compare the two functions to find $\varphi_L - \varphi_s$ vs R_s from quasineutrality. In the same program but independent of this calculation, the model ion velocity distribution function, Eq. (B16), was tabulated. This was contour-plotted by CALCOMP, as was the relative ion density. Trivial subroutines IONPLOT and FIPLOT (not shown here) invoked the University of California Graphical Display System (GDS) to drive the CALCOMP. The program was run on a CDC-6400 and took 4.4 sec to compile and 11.9 sec to execute. Since the plot routines are not instructive, we list the grid size and contour spacing here:

IONPLOT [Plotting $n_i(s)/n_i(L)$]

Grid size in both r and $\varphi_L - \varphi$: 0.05

Contour interval: 0.05

$n_i(s)/n_i(L)$ from 1.0 (at $s = L$ and $\varphi = \varphi_L$) down to about 0.18 (for $R = R_W = 2$ and $\varphi = 1$)

FIPLOT [Plotting Eq. (B16)]

Grid size in both $x \equiv v_\parallel/c_\perp$ and $y \equiv v_\perp/c_\perp$: 0.05

Contours: 7, given by (0.85 FIMAX)(N/6 + 0.01), N = 0, 1, ··· 6.

(FIMAX is the maximum height of the function.)

The results of IONPLOT are shown in Fig. B-7, page 137; those of FIPLOT, in Fig. B-1, page 114. A plot of the computed potential $\varphi_L - \varphi_s$

vs R is shown in Fig. F-1, and illustrates the approach to linear dependence of the parallel electric field on B as discussed in Appendix **B** (on p. 166) and on p. 29 of the main text. Values of the density along the curve $\varphi_L - \varphi_s$ vs R are used in Fig. 9 to compare with a simple approximate formula Eq. (20) .

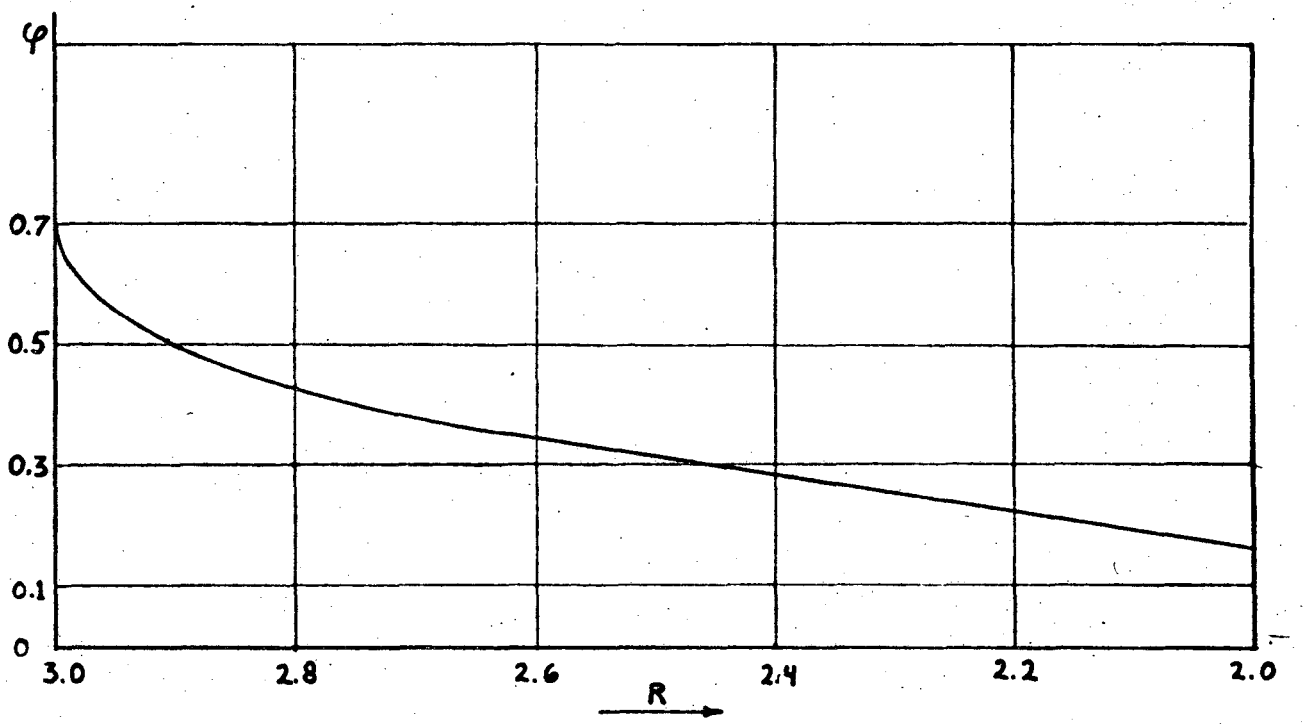

Fig. F-1. Potential vs R outside the mirror (computer result for $R_W = 2$, $R_L = 3$). $\varphi \equiv e\phi_0/T_e$ assumed 0.7 at $R = R_L$.

```
RUN FORTRAN COMPILER VERSION 2.3 B.1

                      PROGRAM XTRNL(OUTPUT,TAPE99)
000003                CALL SECOND(X)
000005                PRINT 5,X
000013                CALL IONS
000014                CALL SECOND(X)
000016                PRINT 5,X
000024                CALL FION
000025                CALL SECOND(X)
000027                PRINT 5,X
000035                CALL ELECTRN
000036                CALL SECOND(X)
000040                PRINT 5,X
000046                CALL POTNTL
000047                CALL SECOND(X)
000051                PRINT 5,X
000057              5 FORMAT(* TIME USED IS*F10.3)
000057                STOP
000061                END
```

```
      FUNCTION ERF(X)
C            ERROR FUNCTION                                    C3 BKY* ERF
C
C  ERF=2/SQRT(PI)*INTEGRAL OF EXP(-T*T) FROM 0 TO X.
C  USING AN APPROXIMATION DUE TO HASTINGS. ABSOLUTE ERROR ABOUT 3E-7
C
      DIMENSION A(6)
      DATA A/.0000430638,.0002765672,.0001520143,.0092705272,.0422820123
     1,.0705230784 /
      Y = ABS(X)
      T = A(1)*Y
      DO 10 I=2,6
      T = (T + A(I))*Y
   10 CONTINUE
      T=1./(T+1.)
      ERF=1.-T**16
      IF (X.LT.0) ERF = -ERF
      RETURN
      END
```

```
FORTRAN COMPILER VERSION 2.3 R.1

      REAL FUNCTION E(Q)
      EINF(Q)=(1./(SQRT(3.14159*Q)))*SUMN
      IF(Q)7,4,4
    4 IF(Q- 8.)5,9,9
    5 E=EXP(Q)*(1.-ERF(SQRT(Q)))
      GO TO 10
C     GET TO 7 IF Q NEGATIVE
    7 E=1.
      GO TO 10
    9 GO TO 316
  316 TOPN=1.
      BOTN=1.
      SUMN=1.
      DO 317 N=1,10
      TOPN=(2.*N-1.)*TOPN
      BOTN=-2.*BOTN*Q
      TN=TOPN/BOTN
      SUMN=SUMN+TN
  317 CONTINUE
      E=EINF(Q)
   10 RETURN
      END
```

```
      REAL FUNCTION DAWSON(A,U)
      COMMON/ACOM/ACOM
      EXTERNAL EXPAT2
      AU=A*U
      IF(U)318,318,310
  310 IF(AU-10.0)311,311,314
  311 N=0
      ACOM=A
      CALL QUAD(0.0,SQRT(U),AREA1,AREA2,RELERR,N,EXPAT2)
C     QUAD IS A BINARY DECK WHICH INTEGRATES EXPAT2 FROM 0. TO SQRT(U)(
C     GIVING AREA2 AS VALUE OF INTEGRAL.
C     EXPAT2 MUST BE GIVEN BY A REAL FUNCTION SUBROUTINE OF ONE VARIABLE
      DAWSON=(2./SQRT(3.1416))*EXP(-AU)*AREA2
      GO TO 319
  314 IF(A)311,315,316
  315 DAWSON=(2.0/SQRT(3.1416))*SQRT(U)
      GO TO 319
  316 TOPN=1.
      BOTN=1.
      SUMN=1.
      DO 317 N=1,10
      TOPN=(2.*N-1.)*TOPN
      BOTN=2.*AU*BOTN
      TN=TOPN/BOTN
      SUMN=SUMN+TN
  317 CONTINUE
      SERIES=SUMN
      DAWSON=(2.0/SQRT(3.1416))*(.5/(A*SQRT(U)))*SERIES
      GO TO 319
  318 DAWSON =0.0
  319 RETURN
      END
```

```
      SUBROUTINE IONS
      COMMON/F/F(21,21)
      COMMON/R/RL,RW,DELT
      REAL NEDECAY
C     CONSTS.RL,RW,WIDTH,DELT,DELTAL,P,TEMP=TE/TI PARALLEL
C     R IS INDEP VBL, RW .LT. R .LT. RL
C     Y IS DEP VBL OF XTRNL PROB., Y .GT. 0.0, USUALLY .LT. 1.0
C     Y= MAX POTL - POTL(R)
C     IF DELTAL=DELT, MAX POTL IS POTL(RL)
C     FOR THIS PROBLEM, Y IS PHY(L)-PHY(S), AND DELTAL =DELT
C     PHY =SMALL SCRIPT PHY IN APPENDIX B. PHI=CAPITAL PHI.
C     P IS CALLED ETA-BAR IN APPENDIX B
C     IN THESIS NOTATION, S2=(PSI(0)-PSI(L))/(RL-1)*KAPPA,-(ETA BAR)
C     PSI=TE/TI(PARALLEL)*PHY
C     (PSI SCALED TO TI, PHY SCALED TO TE)
C     F(I,J) IS RELATIVE ION DENS AT POINT R, YJ DEFINED
C     BY R=RL-.05*(I-1.)*(RL-RW)
C     AND YJ=.05*(J-1.)
C     ARITHMETIC STATEMENT FUNCTIONS FOLLOW
      DECAY(Z,PHI,S1,S2,S3)=(Z/(1.-Z))*(E(Z*PHI)/SQRT(Z)-E(PHI)
     ++EXP(-S2)*(E(PHI+S2)-S1*E(S3)))
C     BECAUSE S2 IS LARGE, THE CONTINUATION LINE IS NEGLIGIBLE
C     CAN SHOW Z=1. IMPLIES S1=1. AND PHI+S2=S3.
      NEDECAY(Z,PHI,S1,S2,S3)=(Z/(1.+Z))*(E(Z*PHI)/SQRT(Z)+DAWSON(G,PHI)
     +-EXP(-S2)*(DAWSON(G,PHI-S2)+S1*E(S3)))
C     BECAUSE S2 IS LARGE, THE CONTINUATION LINE IS NEGLIGIBLE
C     G STANDS FOR 1.0
      DECAY1(Z,PHI)=(0.5-PHI)*E(PHI)+SQRT(PHI/3.1416)
      DECAYLG(Z,PHI)=(Z/(1.-Z))*((1./SQRT(Z))*E(Z*PHI)-E(PHI))
```

```
C       DEFINITION...
C       DAWSON(A,U)=2/SQRT(PI)*EXP(-AU)*INTEGRAL(0,SQRT(U)) EXP(A*T*T)DT
C       COMPARE DAWSON(1,Q) WITH E(Q)...
C       E(Q)=2/SQRT(PI)*EXP(Q)*INTEGRAL(SQRT(Q),INF) OF EXP(-T*T)DT
C       DECAY IS USED WHEN Z IS POSITIVE (R LARGER THAN UNITY)
C       NEDECAY IS USED WHEN Z IS NEGATIVE (R SMALLER THAN UNITY)
C       NEITHER IS USED WHEN R=1., SINCE BOTH ARE ZERO BUT COEF B2=INF)
C       DECAY1 IS USED WHEN Z=1., BECAUSE DECAY IS PECULIAR THERE
C       DECAYLG IS USED WHEN Z IS LARGE, JUST TO AVOID WORK.
C       SPECIFY CONSTS NOW
        RL=3.0
        RW=2.0
        WIDTH=0.1
        DELT=4.0
        DELTAL=4.0
        P=0.2
        TEMP=0.5
C       WITH THESE CONSTS, AS R GOES FROM 3 TO 2,ZI
C       GOES FROM INF TO 0.2 AND PHI FROM 0.2 TO (15.2 WHEN YJ=1 )
        G=1.0
        A=WIDTH*(RL-1.)
        S1L=1./SQRT(1.+A)
        S2=TEMP*DELT/A-P
        S3L=(1.+1./A)*DELT*TEMP
        S4=1.+1./A
        XNORM=1./(E(P)-EXP(-S2)*(E(P+S2)-S1L*E(S3L)))
        PRINT 86,XNORM
   86   FORMAT(1X,*XNORM= *,E10.4)
C       WITH THESE VALUES OF CONSTS, A=.2, S1L=.9(APPROX), S2=9.8,S3L=12,
C       AND S4=6.
C       WITH THESE CONSTS, THE EXP(-S2)*... PART OF XNORM IS SMALL.
C       APPROXIMATELY, XNORM =1./E(.2)=1.4
C       P+S2=TEMP*DELT/A
```

```
C      BEGIN CALCULATION OF F(R,Y)
   10 DO 80  I=1,21
      R=RL-.05*(I-1)*(RL-RW)
      IF(ABS(RL-R)-.001)15,15,13
   13 IF(ABS(R-1.)-.001)25,25,14
   14 IF(R-1.)35,25,20
   20 B2=(R/RL)*SQRT((RL-1.)/ABS(R-1.))*XNORM
   21 ZI=WIDTH/(1./(R-1.)-1./(RL-1.))
C      ZI IS INFINITE WHEN R=RL (15), AND ZERO WHEN R=1. (25)
C      ZI IS NEGATIVE FOR R .GT. RL OR R .LT. 1.
      IF(ZI.LT.(0.0).AND.R.GE.(1.))GO TO 55
   30 IF(ABS(ZI-1.0)-.001)45,45,40
   40 ZI=ABS(ZI)
      IF(ZI.EQ.0.0)GO TO 25
      S1=SQRT((RL-1.)/ABS(R-1.))*S1L
      PRINT 96,R,ZI,PHI,B2
   96 FORMAT(1X,*R=*,F6.2,*ZI=*,E10.4,*PHI=*,E10.4,*     B2=*,E10.4)

C      FROM HERE TO STATEMENT 79 = CALCULATION OF F(R,Y) IN ORDINARY CASE
   50 DO 79 J=1,21
      YJ=(J-1)*.05
      S3=(1.+1./A)*(DELT+YJ)*TEMP
      TH =(1./WIDTH)*((DELT+YJ)/(R-1.)-DELTAL/(RL-1.))*TEMP
C      TH IS NEGATIVE WHEN R .LT. 1., AND INFINITE WHEN R=1.
C      TH IS ZERO WHEN R=RL AND YJ=DELTAL-DELT, AND
C      IF DELTAL=DELT, THEN YJ MUST BE NEGATIVE TO GET ANY OTHER
C      ZERO OF TH FOR R .LT. RL.
      PHI=ABS(TH*P)
   70 F(I,J)=B2*DECAY(ZI,PHI,S1,S2,S3)
      IF(I.GT.2)GO TO 79
      ETEST=E(PHI)
      PRINT 26,ETEST,R,YJ
   26 FORMAT(1X,*ETEST  *E10.4,*      R    *,F5.2,*     YJ    *F4.2)
   79 CONTINUE
      GO TO 80
```

```
C      CALCULATION OF F(R,Y) IN PECULIAR CASES Z=INF,1,0,NEG
C      FIRST CASE. R NEAR MIRROR. R=RL)
   15  ZI=9999.
       B2=(R/RL)*SQRT((RL-1.)/(R-1.))/E(P)
       DO 19 J=1,21
       YJ=(J-1)*.05
       PHI=(1./WIDTH)*((DELT+YJ)/(R-1.)-DELTAL/(RL-1.))*TEMP +P
   18  F(I,J)=B2*DECAYLG(ZI,PHI)
   19  CONTINUE
C      END OF FIRST CASE
       GO TO 80

C      SECOND CASE. ZI=1.  R IS NEAR, BUT NOT AT, RL
   45  DO 49 J=1,21
       YJ=(J-1)*.05
       PHI=(1./WIDTH)*((DELT+YJ)/(R-1.)-DELTAL/(RL-1.))*TEMP +P
       PHI=ABS(PHI)
       F(I,J)=B2*DECAY1(ZI,PHI)
   49  CONTINUE
C      END OF SECOND CASE
       GO TO 80

   55  PRINT 56,R,ZI
C      ZI IS NEGATIVE, R EXCEEDS RL
   56  FORMAT(17H Z IS NEGATIVE,R=,F6.3,5H  ZI=,E10.3)
       ZI=0.0
C      THIRD CASE. ZI=0.  (R=1.)
   25  DO 29 J=1,21
       YJ=(J-1)*.05
C      S1 IS NOT USED SINCE IT IS SINGULAR. DITTO B2. S2 IS IN CONSTS.
       S3=(1.+1./A)*(DELT+YJ)*TEMP
       F(I,J)=(E((DELT+YJ)*TEMP)-EXP(-S2)*E(S3)/SQRT(S4))*XNORM*SQRT(A)*
      +(R/RL)
   29  CONTINUE
C      END OF THIRD CASE
       GO TO 80
```

```
C       FOURTH CASE. R .LT. 1., BUT NOT TOO NEAR 1.
   35   S1=SQRT((RL-1.)/ABS(R-1.))*S1L
C       S2 IS DEFINED IN CONSTS.
        B2=(R/RL)*SQRT((RL-1.)/ABS(R-1.))*XNORM
        ZI=WIDTH/(1./(R-1.)-1./(RL-1.))
        ZI=ABS(ZI)
        DO 39 J=1,21
        YJ=(J-1)*.05
        S3=(1.+1./A)*(DELT+YJ)*TEMP
        TH =(1./WIDTH)*((DELT+YJ)/(R-1.)-DELTAL/(RL-1.))*TEMP
        PHI=ABS(TH+P)
        F(I,J)=B2*NEDECAY(ZI,PHI,S1,S2,S3)
   39   CONTINUE
C       END OF FOURTH CASE
   80   CONTINUE

   81   PRINT 76,(K,K=1,21,2),(I,(F(I,J),J=1,21,2),I=1,21)
   76   FORMAT(60X,*ARRAY F*//1X,*COL*,11I11//(1X,*R*,I2,11F11.4))
        PRINT 16,(K,K=2,20,2),(I,(F(I,J),J=2,20,2),I=1,21)
   16   FORMAT(60X,*ARRAY F*//1X,*COL*,10I11//(1X,*R*,I2,10F11.4))
C       J GOES ACROSS, I GOES DOWN
        CALL IONPLOT
  100   RETURN
        END
```

FORTRAN COMPILER VERSION 2.3 B.1

```
      SUBROUTINE ELECTRN
      COMMON/R/RL,RW,DELT
      COMMON/ELEC/ELEC(21,21)
      DIMENSION ST(21,21),SF(21,21)
C     ARITH STATEMENT FUNCTIONS FOLLOW
      EST(A,U)=EXP(U)*ERF(SQRT(U)) - DAWSON(A,U)
     +-(1.-XEE)*(1.+A)/(A-B)*(DAWSON(B,U)-DAWSON(A,U))
      ESF(A,U)=XEE*((1.+A)/(CK+A)*.5*(DAWSON(A,U)+E(CK*U)*.5/SQRT(CK))
     ++0.5*((CK-1.)/(CK+A))*SQRT(1./CK)*EXP(-A*U))
      SST(A,U)=EXP(U)*ERF(SQRT(U)) -DAWSON(A,U)
     ++(1.-XEE)*(1.+A)*(DAWSON(A,U)-DAWSON(A-.01,U))*100.0
C     NOTATION...EST(A,U) IS EST(PHY,A,B,XEE) IN THESIS
C     A=A, U=PHY. (ORDER OF FIRST 2 VARIABLES INTERCHANGED.)
C     SST IS SPECIAL VALUE OF EST FOR CASE A=B
C     SEE SUBROUTINE IONS FOR DEFINITION OF DAWSON
C     CK IS CALLED K IN APPENDIX C.
C     SPECIFY CONSTS FOR ELECTRONS
      B=0.0
      XEE=0.1
      CK=10.0
      PHY0=4.7
      BNORM=1.0
      AL=RW/(RL-RW)
      PHYCFL=PHY0-DELT
      PRINT 4036
```

```
C     CALCULATION OF ELEC(I,J) IN ORDINARY CASES
      DO 400 I=1,21
      R=RL-.05*(I-1)*(RL-RW)
      IF(R-RW)335,345,330
  335 R=RW
  345 AI=9999.
      GO TO 350
  330 AI=RW/(R-RW)
      IF(AI-B)350,355,350
  350 DO 399 J=1,21
      YJ=.05*(J-1)
      UJ=PHYOFL-YJ
      IF(UJ)365,365,360
  365 UJ=0.0
  360 IF(RL-R)375,375,380
  380 UPR=UJ-YJ*(R-RW)/(RL-R)
      IF(UPR)375,375,390
  390 CORRST=EXP(-RW*YJ/(RL-R))
  391 CORRSF=CORRST
      ST(I,J)=EST(AI,UJ)-CORRST*EST(AI,UPR)
      SF(I,J)=ESF(AI,UJ)-CORRSF*ESF(AI,UPR)
C     ST,SF ARE THE ST,SF ELECTRN DENSITIES EXCEPT FOR FACTOR EXP(-PHYO)
      ELEC(I,J)=BNORM*(ST(I,J)+SF(I,J))/(ST(1,1)+SF(1,1))
      GO TO 399
  375 R=RL
  395 GO TO 385
  385 UPR=0.0
      CORRST=0.0
      GO TO 391
  399 CONTINUE
      GO TO 400
```

```
C       NOW THE CASE AI=B
  355 DO 999 J=1,21
      YJ=.05*(J-1)
      UJ=PHYOFL-YJ
      IF(UJ)965,960,960
  965 UJ=0.0
  960 IF(RL-R)975,975,980
  980 UPR=UJ-YJ*(R-RW)/(RL-R)
      IF(UPR)995,995,990
  990 CORRST=EXP(-RW*YJ/(RL-R))
      GO TO 991
C       IF UPR IS NEGATIVE OR ZERO NOW
  995 GO TO 985
  975 R=RL
  985 UPR=0.0
      CORRST=0.0
  991 CORRSF=CORRST
      ST(I,J)=SST(AI,UJ)-CORRST*SST(AI,UPR)
      SF(I,J)=ESF(AI,UJ)-CORRSF*ESF(AI,UPR)
      ELEC(I,J)=BNORM*(ST(I,J)+SF(I,J))/(ST(1,1)+SF(1,1))
  999 CONTINUE
C       END OF THE CASE AI=B
  400 CONTINUE
 4000 PRINT 4006,(K,K=1,21,2),(I,(ST(I,J),J=1,21,2),I=1,21)
 4006 FORMAT(60X,*ARRAY ST*//1X,*COL*,11I11//(1X,*R*,I2,11E11.4/))
      DENSL=ST(1,1)+SF(1,1)
 4010 PRINT 4016,DENSL
 4016 FORMAT(1X,*DENSITY AT L*,4X,E12.4/)
      PRINT 4036
 4020 PRINT 4026,(K,K=5,15),(I,(SF(I,J),J=5,15),I=1,21)
 4026 FORMAT(60X,*ARRAY SF*//1X,*COL*,11I11//(1X,*R*,I2,11E11.4/))
      PRINT 4036
```

```
      DO 4030 M=1,3
      IF(M-2)4021,4022,4023
4022  AOUT=0.1
      GO TO 4024
4023  AOUT=0.3
4024  DO 4029 N=1,21
      UN=.1*(N-1)
      TEST=EST(AOUT,UN)
      PRINT 4116,UN,TEST
4116  FORMAT(1X,*UN*,5X,2E11.4)
4029  CONTINUE
      GO TO 4030
4021  AOUT=0.0
      DO 4032 N=1,21
      UN=.1*(N-1)
      TEST=SST(AOUT,UN)
      PRINT 4116,UN,TEST
4032  CONTINUE
4030  CONTINUE
      PRINT 4036
4036  FORMAT(1H1)
      RETURN
      END
```

```
      SUBROUTINE POTNTL
      COMMON/R/RL,RW,DELT
      COMMON/F/F(21,21)
C     SEE SUBROUTINE IONS
      COMMON/ELEC/ELEC(21,21)
C     SEE SUBROUTINE ELECTRN
      DIMENSION CHARGE(21,21)
      PRINT 406
  406 FORMAT(1X,*Y OF R*/)
C     ROUTINE TO FIND J, GIVEN I, SUCH THST F(I,J)=ELEC(I,J)
  401 DO 500 I=1,21
      R=RL-.05*(I-1)*(RL-RW)
      DO 499 J=1,21
      YJ=.05*(J-1)
      CHARGE(I,J)=F(I,J)-ELEC(I,J)
      IF(J-1)499,499,430
  430 SIGND=(CHARGE(I,J))*(CHARGE(I,J-1))
      IF(SIGND)460,499,499
  460 PRINT 466,R,YJ,F(I,J),F(I,J-1)
  466 FORMAT(1X,F7.3,F7.3,E12.4,E12.4)
C     SIGN OF CHARGE HAS CHANGED ON CHANGING J. THIS MEANS A ROOT.
      GO TO 499
  499 CONTINUE
  500 CONTINUE
      GO TO 501
  501 RETURN
      END
```

```
      SUBROUTINE FION
C     CALCULATES THE ION DISTRIBUTION OF EQUATION B-16
C     ALL VELOCITIES SCALED TO SQRT OF 2*TI(PERP)/M
      DIMENSION FI(41,41)
      COMMON/FIMAX/FIMAX
      RL=3.
      DELT=2.6
      DATA CPAR2/.3333/
      DATA TRATIO/.125/
C     CPAR2 IS TI(PAR)/TI(PERP)
C     TRATIO IS TE/TI(PERP)
      Z=CPAR2/(RL-1.)
  710 DO 780 I=1,41
      YI=.05*(I-1)
      XL2=(RL-1.)*YI*YI-(DELT*TRATIO)
      IF(XL2)725,725,720
  720 DO 779 J=1,41
      XJ=.05*(J-1)
      BRACKET=EXP(-XJ*XJ/CPAR2)-EXP(-XL2/CPAR2)
      IF(BRACKET)735,730,730
  730 FI(I,J)=BRACKET*EXP(-YI*YI)
      GO TO 779
  735 FI(I,J)=0.0
  779 CONTINUE
      GO TO 780
  725 DO 729 J=1,41
      XJ=.05*(J-1)
      FI(I,J)=0.0
  729 CONTINUE
  780 CONTINUE
  781 PRINT 786,(K,K=1,21,2),(I,(FI(I,J),J=1,21,2),I=1,41)
  786 FORMAT(1H1,*ARRAY FION*//1X,*J    *,11I11//(1X,*I *,I2,11E11.4))
      FIMAX=1./(1.+Z)*(1.+1./Z)**(-Z)*EXP(-DELT*TRATIO/(RL-1.))
      PRINT 796,FIMAX
  796 FORMAT(1X,*FIMAX *,E11.4,//)
  790 CALL FIPLOT(FI)
      RETURN
      END
```

G. SYMBOLS USED IN THE MAIN TEXT

a = $R_W/(R - R_W)$, function of position at which $R = B/B_0$ is evaluated. (Generalized form for anisotropy, p. 145.)

a_L = $R_W/(R_L - R_W)$

a_i = ion gyroradius in Sec. IIB.

A = atomic weight, Sec. IIA.

b = $\kappa - 1$ measures extent to which the electron loss erodes the trapped electron distribution just inside trapping region.

$\bar{b}(R_L, \varphi_0)$ = function derived from BenDaniel calculations, typically $\bar{b} \sim 1$.

B = magnetic field strength.

c $\approx$ thermal speed $(2T/m)^{1/2}$ at midplane. Exact value of c is defined as a parameter in the analytic form of $g(x,y)$. c is subscripted as follows:

$c_\parallel$, $c_\perp$ = parameters for species being considered.

c_e = electron parameter, when $c_{e\parallel} = c_{e\perp}$.

sub c = "cold", referring to cold particles.

sub cx = "charge exchange"

$C(x)$ = height of the ion distribution $g(x,y)$ at the loss boundary $y = y_L(x)$.

D = velocity space diffusivity, averaged over velocity space near the loss boundary

e = magnitude of electron charge.

sub e = referring to electrons

$EST(\varphi,a,b,\xi)$ = function giving dimensionless electron density vs φ. b and ξ are parameters of the "damping" of $g_e(x,y)$.

$\mathcal{E}$ = energy in waves due to saturated instability.

f = usual distribution function $f(\vec{v})$.

$f(s;v_{\|},v_{\perp})$ = same thing, at spatial point s.

$F(s)$ = flux of escaping particles, per unit area normal to field line, evaluated at point s.

F = value of $\int 2\pi\, y\,dy\, x\,dx\, g(x,y)$ at midplane which would give the observed $F(s)$ at large s if the dynamics were collisionless.

$\mathcal{J}$ = energy loss flux

g = modified midplane distribution function, see Sec. IIB.

$g(x,y)$ = same.

$G(x,y)$ = Maxwellian in midplane velocity space x,y.

H = total energy (Sec. IIB).

$H(x,y)$ = damping factor multiplying Maxwellian.

sub i = referring to ions

I (Roman numeral) refers to spatial region between mirrors. II refers to region outside mirrors.

j = integer

J = action integral

k = inverse decay width of $g_e(x,y)$, as in Appendix C. $k \equiv \kappa + 1$ $\left[\kappa = \text{decay width of } H(x,y)\right]$.

k = wave vector, in Ch. IVB.

L = distance along field line from midplane to mirror.

m = particle mass.

$M(\mu)$ = distance from midplane to point of highest potential energy, for a given magnetic moment μ. Understood to depend on species. For most μ, $M(\mu) \approx L$.

n = number density, particles/cm^3.

N = normalization of distribution function

P = $(c_{\|}^2/c_{\perp}^2)(R_L - 1)^{-1}$, referring usually to ions.

q = particle charge

Q = coefficient in $n_i(W) = Q(Lv/c_{i\|})$, Sec. IIA.

r = coordinate(s) normal to s.

R = B/B_0. $R_L = B_L/B_0$, $R_s = B_s/B_0 = B/B_0$, $R_W = B_W/B_0$. For any s, $B_s \equiv B(s)$.

s = arclength coordinate along field line, measured from midplane.

$\sup_{s'<s}$ = maximum value, over the range of s' consistent with s'<s.

ST : referring to particles streaming through region I but trapped within the device.

SP : referring to particles streaming through region I and not trapped within the device.

T = temperature at midplane, in energy units (subscripted as necessary with e, i, $\|$, $\perp$).

$T(s)$ = effective temperature at spatial point s.

u = dummy integration variable.

U = $U(s,\mu) = \mu B + q\phi$, potential for parallel motion.

v = velocity.

V = Vlasov transformation of velocity distribution at point s into velocity distribution at s = 0.

W = value of s at the end wall (midplane-wall distance).

sub W = evaluated at wall.

sub W^- = evaluated about a Debye length from the wall ($R_W = R_{W^-}$, but ϕ and n vary rapidly in the sheath).

sub x referring to electrons born in region II or at the end walls. Such electrons are called x-electrons.

x = parallel velocity at midplane.

y = perpendicular velocity at midplane.

α = parameter in Sec. IVA describing extent to which "x" electrons from the wall are trapped and thermalized for long times in the device.

α = magnetic field coordinate in Ch. V.

β = magnetic field coordinate in Ch. V.

β = fraction of "x" electrons trapped for longer than one transit time through the device.

γ = dimensionless constant of order unity in Sec. IVA.

δ : $\delta v_{\|}$, $\delta v_{\perp}$, $\delta \epsilon_{\|}$, $\delta \epsilon_{\perp}$ = width of some peak feature on the velocity distribution.

Δ (operator) = change in parameters from the case where "x" electrons are absent.

ϵ = kinetic energy at midplane. $\epsilon_{\|}$ = energy of parallel motion. $\epsilon_{\perp} = \mu B$ = energy of gyromotion (drift motion ignored).

κ = decay constant in velocity space for the "damping" function $H(x,y)$ outside the loss boundary. κ' = decay constant for $H(x,y)$ inside the loss boundary. $k \equiv \kappa + 1$; $b \equiv \kappa' - 1$.

λ = wavelength.

λ_D = Debye length.

Λ = plasma parameter $4\pi n\lambda_D^3$.

μ = magnetic moment.

ν = loss rate. ν_0 = collision rate (for cumulative 90-degree scattering). ν_{cx} = loss rate due to charge exchange. ν_p = loss rate of "p" (main plasma) electrons; ν_x = loss rate of "x" electrons. ν_{esc} = escape time of cold particles from a simple potential well. ν^* = ionization rate.

ξ = height of electron mock-distribution $g_e(x,y)$ at the loss boundary, divided by height of the corresponding Maxwellian there.

π = 3.1416.

ρ = phase-space density (f/B) in $\alpha\beta s\vec{v}$ space (Ch. V).

σ = cross section (Ch. V).

τ = bounc time

ϕ = electrostatic potential. Subscript indicates where evaluated, e.g. $\phi_L = \phi(L)$, $\phi_s = \phi(s)$, $\phi_W = \phi(W^-)$.

φ = $e\phi/T_e$, dimensionless potential. Similarly subscripted.

Φ = see list of simbols at end of Appendix B.

ψ = $e\phi/T_i$ for, e.g., hot electron plasma, where ϕ scales with T_i.

ω = wave frequency (angular), Sec. IVB.

REFERENCES AND FOOTNOTES

1. D. J. BenDaniel, Plasma Potential in a Magnetic Mirror System, J. Nucl. Energy Pt. C 3, 235 (1961).

2. R. F. Post, Equilibrium Ambipolar Potentials in a Mirror Machine, Phys. Fluids 4, 902 (1961).

3. W. B. Kunkel and J. U. Guillory, Jr., Interchange Stabilization by Incomplete Line-Tying, in Proceedings of the 7th International Conference on Ionization Phenomena in Gases (Gradevinska Knjiga, Belgrade, 1966), Vol. II, p. 702.

4. B. Lehnert, Short Circuit of Flute Disturbances at a Plasma Boundary, Phys. Fluids 9, 1367 (1966).

5. G. E. Guest and C. O. Beasley, Cold Plasma Effects in Finite-Length Plasmas, Phys. Fluids 9, 1798 (1966).

6. R. C. Harding (Lawrence Radiation Laboratory, Livermore), private communication.

7. H. L. Berk, C. W. Horton, M. N. Rosenbluth, and R. N. Sudan, Plasma Wave Reflection in Slowly Varying Media, Phys. Fluids 10, 2003 (1967).

8. H. L. Berk, Boundary Conditions for Convective Wave Instabilities in Mirror Machines, University of California Lawrence Radiation Laboratory Report UCID-15591, 1969 (unpublished).

9. Or even quasi-steady state: true steady state in the presence of particle losses requires a source, such as neutral injection, to maintain the plasma. In the absence of such a source the problem can be treated as quasi-steady if the loss rate is sufficiently small.

10. T. G. Northrop, The Adiabatic Motion of Charged Particles (J. Wiley and Sons, Inc., New York, 1963), p. 61.

11. Such deviations may be due, for example, to Ioffe bars[12] or other minimum-B windings.

12. Y. B. Gott, M. S. Ioffe, and V. C. Telkovsky, Some New Results on Confinement in Magnetic Traps, Nucl. Fusion Suppl., Pt. 3, 1045 (1962).

13. H. Persson, Electric Field Parallel to the Magnetic Field in a Low-Density Plasma, Phys. Fluids 9, 1090 (1966).

14. It is assumed that no electrostatic field is applied from outside; hence if ions and electrons are supplied in small equal numbers inside the trapping region of velocity space, charge neutrality is satisfied with ϕ = constant.

15. J. Killeen and K. D. Marx, The Solution of the Fokker-Planck Equation for a Mirror-Confined Plasma, in Methods in Computational Physics (Academic Press, New York, 1970), Vol. 9, p. 421.

16. L. Spitzer, Physics of Fully Ionized Gases, 2nd Ed. (J. Wiley and Sons, Inc., New York, 1967), p. 133.

17. A. N. Kaufman, Ambipolar Effects in Mirror Losses, Conference on Controlled Thermonuclear Reactions, Gatlinburg, Tenn., AEC Report TID-7520 (Pt. 2), p. 387.

18. R. F. Post, Summary of UCRL Pyrotron (Mirror Machine) Program, in Proceedings of the Second United Nations Conference on Peaceful Uses of Atomic Energy (United Nations, Geneva, 1958), Vol. 32, p. 245.

19. T. K. Fowler and M. Rankin, J. Nucl. Energy Pt. C 4, 311 (1962).

20. M. N. Rosenbluth, W. M. MacDonald, and D. L. Judd, Fokker-Planck Equation for an Inverse-Square Force, Phys. Rev. 107, 1 (1957).

21. W. M. MacDonald, M. N. Rosenbluth, and Wong Chuck, Relaxation of a System of Particles with Coulomb Interactions, Phys. Rev. 107, 350 (1957).

22. J. E. Roberts and M. L. Carr, End-Losses from Mirror Machines, University of California Lawrence Radiation Laboratory Report UCRL-5651-T, April 1960.

23. G. F. Bing and J. E. Roberts, End-Losses from Mirror Machines, Phys. Fluids 4, 1039 (1961).

24. D. J. BenDaniel and W. P. Allis, Scattering Loss from Magnetic Mirror Systems--I and II, J. Nucl. Energy Pt. C 4, 31 and 77 (1962).

25. D. L. Fisher, B. McNamara, and D. W. Mason, Calculations of Plasma Loss and Plasma Potential in Mirror Machines, in Proceedings of the International Conference on Plasma Confined in Open-Ended Geometry, Gatlinburg, Tenn., 1967, Oak Ridge National Laboratory Report CONF-671127, p. 280.

26. J. Killeen and A. H. Futch, Numerical Solution of the Fokker-Planck Equations for a Hydrogen Plasma Formed by Neutral Injection, J. Computational Phys. 2, 236 (1968).

27. K. D. Marx, Solution of a Spatially Dependent Fokker-Planck Equation for Mirror-Confined Plasmas (Ph. D. Thesis), University of California, Davis, 1968.

28. R. F. Post, Velocity-Space Instabilities in the Mirror Machine, Risö Report 18, 1960, p. 209.

29. W. A. Newcomb (Lawrence Radiation Laboratory, Livermore), private communication.

30. H. Grad, The Guiding Center Plasma, New York University Report NYO-1480-50, MF 48, 1966.

31. Under some circumstances where charge exchange is the dominant loss mechanism, one may not neglect the density of loss-component ions, since their escape time is long. See Ref. 19.

32. We assume $e\phi_c$ in Eq. (46) of that paper should be $|e\phi_c|$, making some of Eq. (45) redundant.

33. J. Berkowitz, H. Grad, and H. Rubin, Magnetohydrodynamic Stability, in Proceedings of the Second United Nations Conference on Peaceful Uses of Atomic Energy (United Nations, Geneva, 1958), Vol. 31, p. 177.

34. M. V. Babykin, P. P. Gavrin, E. K. Zavoysky, L. I. Rudakov, and V. A. Skoryupin, Stability of a Turbulently Heated Plasma During Adiabatic Compression, Zh. Eksperim. i Teor. Fiz. 47, 1631 (1964) [English transl.: Soviet Phys.-JETP 20, 1096 (1965)].

35. M. N. Rosenbluth and R. F. Post, High Frequency Electrostatic Plasma Instability Inherent to "Loss-Cone" Particle Distributions, Phys. Fluids 8, 547 (1965).

36. This loss time refers really to the lifetime in the device, not just to the time required to scatter into the loss region in phase space. The lifetime is the loss time plus about one transit time out from the midplane after such scattering occurs. Because transit times are long for barely untrapped particles, this may not be a small correction.

37. Assuming equal source rates.

38. T. Consoli, Etudes Theoretiques et Experimentales sur les Interactions Ondes et Plasma a la Resonance Cyclotron dans un Miroir Magnetique, in Proceedings of the 8th International Conference on Phenomena in Ionized Gases (IAEA, Vienna, 1968), p. 239.

39. S. Chandrasekhar, Stochastic Problems in Physics and Astronomy, Rev. Mod. Phys. 15, 1 (1943).

40. G. Ecker and W. Kröll, Lowering of the Ionization Energy for a Plasma in Thermodynamic Equilibrium, Phys. Fluids 6, 62 (1963).

41. R. F. Post et al., Preliminary Report of Direct Recovery Study, University of California Lawrence Radiation Laboratory Report UCID-15650, May 1970.

42. J. U. Guillory and W. B. Kunkel, Role of End Regions in the Steady State of Mirror-Confined Plasmas, Plasma Phys. 12, 529 (1970).

43. P. C. T. deBoer, Filling Rate of the Tail of the Velocity Distribution Function, Phys. Fluids 10, 2485 (1967).

44. Y. Itikawa and O. Aono, Energy Change of a Charged Particle Moving in a Plasma, Phys. Fluids 9, 1259 (1966).

45. C. Roque, The Scattering of Charged Particles in a Weakly Unstable Plasma, Phys. Fluids 11, 247 (1968).

46. Ya. B. Fainberg and V. D. Shapiro, Quasilinear Theory of Instabilities Caused by Injection of an Electron Beam into a Semi-Infinite Plasma, Zh. Eksperim. i Teor. Fiz. 47, 1389 (1964) [English Transl.: Soviet Phys.-JETP 20, 937 (1965).

47. A. Bers, Computer Simulation of the Beam-Plasma Interaction, NASA-SP-153, pp. 217-235.

48. T. K. Allen, R. A. Bailey, and K. G. Emeleus, The Appearance of Some Oscillating Discharges, Brit. J. Appl. Phys. 6, 320 (1955).

49. J. R. Apel, Nonlinear Effects and Turbulent Behavior in a Beam-Plasma Instability, Phys. Fluids 12, 640 (1969).

50. H. L. Berk and D. L. Book, Plasma Wave Regeneration in Inhomogeneous Media, Phys. Fluids 12, 649 (1969).

51. V. Kopecky and J. Preinhaelter, Transformation and Absorption of Waves in an Inhomogeneous Beam-Plasma System, Plasma Phys. 11, 333 (1969).

52. R. E. Aamodt and W. E. Drummond, Wave-Wave Scattering of Beam and Plasma Oscillations, Phys. Fluids 8, 171 (1965).

53. R. Z. Sagdeev and A. A. Galeev, Nonlinear Plasma Theory (W. A. Benjamin, Inc., New York, 1969), Section II-5, p. 67.

54. A. N. Kaufman and T. Nakayama, Interactions of Waves and Particles in an Inhomogeneous One-Dimensional Plasma, Phys. Fluids 13, 956 (1970).

55. C. F. Kennel and F. Engelmann, Velocity Space Diffusion from Weak Plasma Turbulence in a Magnetic Field, Phys. Fluids 9, 2377 (1966).

56. T. M. O'Neil and J. H. Malmberg, Transition of the Dispersion Roots from Beam-Type to Landau-Type Solutions, Phys. Fluids 11, 1754 (1968).

57. I. B. Bernstein and F. Engelmann, Quasi-Linear Theory of Plasma Waves, Phys. Fluids 9, 937 (1966).

58. A. I. Akhiezer, I. A. Akhiezer, R. V. Polovin, A. G. Sitendo, and K. N. Stepanov, Collective Oscillations in a Plasma (Pergamon Press, New York, 1967), p. 81.

59. The scattering terms may include a Boltzmann collision integral to describe scattering from neutrals.

60. R. V. Meghreblian and D. K. Holmes, Reactor Analysis (McGraw-Hill Book Company, New York, 1960), p. 179.

61. W. D. MacMillan, The Theory of the Potential (Dover Publications, Inc., New York, 1958), p. 62

62. W. E. Drummond and M. N. Rosenbluth, Anomalous Diffusion Arising from Microinstabilities in a Plasma, Phys. Fluids 5, 1507 (1962).

63. E. G. Harris, Plasma Instabilities Associated with Anisotropic Velocity Distributions, J. Nucl. Energy Pt. C 2, 138 (1961).

64. L. Hall, W. Heckrotte, and T. Kammash, Ion Cyclotron Electrostatic Phys. Rev. 139A, 1117 (1965).

65. F. H. Coensgen, W. F. Cummins, W. E. Nexsen, Jr., and A. E. Sherman, Boundary Condition Effects in a Magnetic Mirror Compression Experiment, Phys. Fluids 9, 187 (1966).

66. A. F. Kuckes, Interchange Instability in a Hot Electron, Phys. Fluids 9, 2239 (1966).

67. F. R. Scott, T. H. Jensen, and C. B. Wharton, Flute Characteristics of and Microwave Emission from a Plasma in a Mirror, in Plasma Physics and Controlled Nuclear Fusion Research (IAEA, Vienna, 1966) Vol. II, p. 463.

68. D. Bohm, in The Characteristics of Electrical Discharges in Magnetic Fields, ed. by A. Guthrie and R. K. Wakerling (Mc-Graw Hill Book Company, New York, 1949), Ch. 3.

69. Requiring exact instead of approximate normalization of $g_0 + g_1$ is not physically necessary (see, for example, the analogous calculation

for electrons in Appendix C).

70. $ky_L \gg 1$ simply means that $g(x,y)$ drops off rapidly in velocity space outside the loss boundary, falling to $e^{-1}g(x,y_L(x))$ over a velocity small compared with $(2e\phi_0/m_i)^{1/2}$.

71. P. J. Davis, Gamma Function and Related Functions, in Handbook of Mathematical Functions, M. Abramowitz and I. A. Stegun, eds. (National Bureau of Standards, Washington, D. C., 1964), p. 263.

72. B. D. Fried and S. D. Conte, The Plasma Dispersion Function (Academic Press, Inc., New York, 1961).

73. This is a better approximation provided $(\phi_L - \phi_s)/(R_L - R_s) < \phi_s/(R_s - R_W)$. When $(\phi_L - \phi_s)/(R_L - R_s) > \underset{s'<s}{\text{Min}}\left[\phi_{s'}/(R_{s'} - R_W)\right]$, it is still not as good an approximation as using the "Min" for a cutoff, but the value of this "Min" is unknown.

74. A. N. Kaufman, University of California, Berkeley, private communication.

75. R. J. Colchin, J. L. Dunlap, and H. Postma, Plasma Containment in DCX 1.5, in International Conference on Plasma Confined in Open-Ended Geometry, Gatlinburg, 1967, CONF-671127, p. 46.

76. D. L. Carpenter, Whistler Evidence of a "Knee" in the Magnetospheric Ionization Density Profile, J. Geophys. Research 71, 711 (1966).

77. K. I. Gringauz, Rocket and Satellite Measurements of the Ionospheric and Magnetospheric Particle Temperature, in Solar-Terrestrial Physics, J. W. King and W. S. Newman, eds. (Academic Press, Inc., New York, 1947)

78. L. A. Frank, On the Extraterrestrial Ring Current During Geomagnetic Storm, J. Geophys. Research 72, 3753 (1967).

79. C. S. Liu, Low Energy Electrostatic Instabilities in the Magnetosphere (Ph.D. Thesis), University of California Lawrence Radiation Laboratory Report UCRL-18121, March 1968.

80. M. A. Lieberman and A. J. Lichtenberg, Plasma Density Measurement by Cavity Perturbation in High Density Plasma, Phys. Fluids 12, 2109 (1969).

81. M. A. Lieberman, Solution of Fokker-Planck Equation for Mirror-Confined, Hot-Electron Plasma, Phys. Fluids 13, 782 (1970).

82. The exact condition for negative ϕ_0 depends on the scattering mechanism. The criterion given is for Coulomb scattering.

TECHNICAL INFORMATION DIVISION
LAWRENCE RADIATION LABORATORY
UNIVERSITY OF CALIFORNIA
BERKELEY, CALIFORNIA 94720